THE ROLE OF GLYCOSYLATION ON FC γ RECEPTOR IIIA / CD16A STRUCTURE AND FUNCTION

by

PAUL GARRETT KREMER

(Under the Direction of Adam W. Barb)

ABSTRACT

Antibodies have become a popular treatment for a wide variety of diseases. Within the body, certain immune cells express Fcγ receptors (FcγRs), that bind to the Fc region of antibodies, and initiate cell activation. In response, the immune cells will release cytotoxic granules that destroy the opsonized target. This process, antibody-dependent cell-mediated cytotoxicity (ADCC), is primarily mediated by natural killer, although macrophages, neutrophils and monocytes may also perform ADCC to an extent. ADCC response is triggered by antibody binding and subsequent signaling through a single receptor, CD16a. Several recent immunotherapies have investigated the potential of CD16a-expressing NK cells as a new disease treatment. Additionally, the most common therapeutic antibody class IgG1, binds to CD16a. Despite the significance of CD16a connecting antibody binding to cytotoxic response, relatively little is known about its structure and function. Herein, we detail the structure and function of CD16a as well as propose a model for its binding to Fc. We show how CD16a glycosylation changes its structure and regulates ADCC. The role of glycans is often overlooked. Even the concept that glycosylation had any impact on CD16a affinity was a recent discovery. The deep level of involvement that glycosylation has on CD16a highlights the importance of these modifications on protein function. The tools we used to study them, including our novel NMR

labeling approach, provide researchers with techniques that will allow them to study glycans in-depth. Another significant discovery is the CD16a affinity directly correlates with ADCC. Several clinical trials are investigating “high affinity” NK cells as a treatment for multiple different diseases. Although, the high affinity is referring to the cells being V158 homozygotes. We have achieved higher affinity than V158, and provide evidence to suggest that further improving CD16a affinity will lead to higher ADCC. The contents of this work provide a compelling case for CD16a engineering for therapeutic use.

INDEX WORDS: Fcγ receptor IIIa, CD16a Antibody Dependent Cell-mediated Cytotoxicity, N-Glycosylation, Natural killer cells

THE ROLE OF GLYCOSYLATION ON FC γ RECEPTOR IIIA / CD16A STRUCTURE AND FUNCTION.

by

PAUL GARRETT KREMER

B.A., Ripon College, 2019

A dissertation submitted to the Graduate Faculty of The University of Georgia in Partial Fulfillment of the Requirements for the Degree

DOCTOR OF PHILOSPHY

ATHENS, GEORGIA

2024

THE ROLE OF GLYCOSYLATION ON FC γ RECEPTOR IIIA / CD16A STRUCTURE AND FUNCTION.

by

PAUL GARRETT KREMER

Major Professor:	Adam Barb
Committee:	Kelley Moremen
	Fikri Avci
	Camillo Perez

Electronic Version Approved:

Ron Walcott
Vice Provost for Graduate Education and Dean of the Graduate School
The University of Georgia
August 2024

ACKNOWLEDGEMENTS

I would like to thank everyone who helped me get to this point in my career. There are too many to name individually, but I would like to name a few people. First of all, I would like to thank Dr. Adam Barb for being the best mentor that I could ask for. Indeed, I have selfishly asked him for more, and he has always delivered. Your abundant availability and quick turnaround times were beyond anything I could hope for, allowing me to move at my own pace. I cannot fully express my gratitude for all that you have done for me.

I would like to thank my current and former lab members for their help and advice. You all saved me a lot of troubleshooting experiments and made the lab space a fun environment. I hope that my future lab mates as good to me as you all were.

I would like to thank Dr. William Lanzilotta for his time and knowledge of crystallography. I was not a member of Bill's lab, nor was he on my committee, but nonetheless, Bill was always available to help me interpret screens or shoot some crystals. Thank you for your patience and help over these past few years.

I would like to thank Angie Stockton for always helping me with any administrative task. She was always on top of every deadline and looking out for each and every BCMB graduate student. I would also like to thank Dr. Zachary Wood for his exceptional job as graduate coordinator, for making a journal club always fun, and for the wonderful opportunities for graduate students to get feedback on their science. These experiences were helpful parts in shaping the scientist I am today.

I would like to thank Dr. Colleen Byron for giving me my first academic research experience and confirming my love for scientific research. My current and former committee

members Dr. Kelley Moremen, Dr. Fikri Avci, Dr. Jarrod Mousa, and Dr. Camillo Perez for their excellent advice and guidance.

I would like to thank my best friends Alex Davis and Chris Esselman for all of the good times had in and around Athens. I will miss our many hiking adventures, weekends hanging out, and other shenanigans we did together. You both made it very tempting to stay around for another few years to stay in your company, and it is hard to go.

Lastly, I would like to thank my family for their constant support of me. Even if I seemed annoyed by your many questions about my studies, I always appreciated that you cared. Thank you for welcoming me back home anytime I wanted a break from the busy life of a graduate student.

TABLE OF CONTENTS

Page

LIST OF TABLES

Page

LIST OF FIGURES

Page

CHAPTER 1

INTRODUCTION

Purpose

Natural killer cells are a critical component of the immune system and a main expresser of antibody receptor FcγRIIIa/CD16a. Many native and therapeutic antibodies utilize this receptor to clear target diseases. Efforts to improve antibody-dependent cell-mediated cytotoxicity (ADCC) have targeted antibody engineering, but relatively little about CD16a is known. Structure and functional understanding of CD16a and NK cells as a whole will improve antibody therapies and open the door for CD16a engineering for immunotherapy. This chapter will discuss the nature and function of natural killer cell cytotoxicity, the use of NK cells in immunotherapies, and the nature of the post-translational modification, glycosylation, on CD16a.

Natural Killer Cells

The immune system is generally separated into the adaptive and innate systems. The hallmark of the adaptive immune system is its ability to adapt its response specific to the target, mediated primarily through antibody-producing B cells and robust T cells. While highly effective, adaptive immune response can be slow to respond to stimulus. In many cases, the innate immune system is capable of immediate action. These responses are carried out by a variety of cells and include many functions, commonly activating additional immune responses through cytokine signaling. One such innate immune cell, Natural killer (NK) cells, are highly cytotoxic and strong producers of inflammatory cytokines, such as INF-γ. NK cells were first characterized in the 1970's by their defining morphology of large granules in the cytoplasm, characteristic of cytotoxic cells (1). Named for their ability to lyse target cells without prior activation, termed

“natural killing”, they are effective in neutralizing many targets including tumor cells and viral pathogens (2). While highly robust, NK cell response is limited to the innate repertoire of germline-encoded activating and inhibitory NK receptors.

NK development begins in the bone marrow from the common lymphoid progenitor (CLP) that also gives rise to B cells and T cells. What influences CLP differentiation are the present signaling molecules, for NK cells this is thought to be IL-15 (3). IL-15 induces the expression of several transcription factors that are known to be critical for NK cell development (4). During NK development, young NK cells are exposed to healthy host cells that serve to train NKs cell to avoid attacking healthy host tissue, termed licensing (5). A fully licensed NK cell expresses Ly49 receptor and CD56, both markers of NK maturation (6).

Human NK cells are functionally categorized by their expression of CD56 and CD16. The $CD56^{dim}CD16^{bright}$ subset accounts for the vast majority of circulating human NK cells and is characterized by having greater perforin and granzyme than $CD56^{bright}$ cells (7,8). Due to the high expression of CD16, $CD56^{dim}CD16^{bright}$ cells are able to efficiently mediate antibody-dependent cell- mediated cytotoxicity (ADCC), unlike $CD56^{bright}CD16^{dim}$ cells. In this process, NK cells are activated through binding of CD16 to the Fc region of antibodies. ADCC activation triggers the release of cytotoxic granzyme and perforin toward the bound immunogen. While poor at ADCC, $CD56^{bright}CD16^{dim}$ cells are more efficient at cytokine production, expressing as much as 20-30-fold more INF-γ compared to $CD56^{dim}CD16^{bright}$ cells (9). These cells also express different adhesion molecules and chemokine receptors leading to different migratory patterns, especially within secondary lymphoid organs (10). Within the follicular region of lymph nodes, it was observed that over 3/4ths of NK cells are $CD56^{bright}CD16^{dim}$, although the

total number of NK cells here are low (11,12). Similarly, the tonsils (12) and uterus (13) also saw increased presence of $CD56^{bright}CD16^{dim}$ cells.

NK cell receptors

While NK cells are known for their interaction with antibodies through ADCC, they express several antibody-independent receptors that elicit cytotoxic response. NKG2D is a C-type lectin receptor that activates cytotoxic response from NK cells and T cells. It binds to MIC molecules which are normally absent from normal cells, but present on many types of cancer cells, stressed cells and infected cells (14). Tumor cells evade NKG2D response through ligand shedding or exosomal release, triggering immune suppression (15). At the cellular surface, NKG2D associates with DAP10, which begins the intracellular signaling cascade upon NKG2D activation (16). NKG2D activates NK cell cytotoxicity without the presence of antibody.

Another important type of NK cell receptor is Killer cell immunoglobulin-like receptors (1). There are 14 identified human KIR's which may be activating or inhibitory to NK cell function (17). The ligands of KIR's are class 1 HLA molecules, which play a critical role in NK cell licensing during development (18). They further function in mature NK cells to inhibit NK response to a host cell or activate NK response due to HLA downregulation. Structurally, the inhibitory KIR's contain a long, cytoplasmic tail containing ITIMs, whereas activating KIR's have a short cytoplasmic tail that associates with DAP12 for ITAM signaling (18).

One of the defining characteristics of NK cells is their typical expression of CD16a. This transmembrane receptor features two extracellular immunoglobulin-like domains and a short cytoplasmic tail. CD16a functions as an activating receptor that binds to the crystallizable fragment (Fc) region of IgG1 and IgG3 antibodies with low affinity (19). It belongs to a class of

receptors that bind to Fc with different affinity and subclass preference, called Fc γ receptors (FcγR). FcγRs are expressed on many different immune cells in the body, with some immune cells displaying multiple different FcγR's. CD16a is not unique to NK cells, it is also expressed on other immune cells such as macrophages, monocytes and neutrophils (20). It has been suggested that CD16a may mediate cell killing in an antibody independent manner called spontaneous cytotoxicity (21).

NK Cell activation pathway

NK cell functionality is regulated by a series of activating and inhibitory surface receptors. The inhibitory signals function as checks to suppress premature cellular activation. Thus, activation is achieved when the strength of the activating signals is greater than that of the inhibitory signals. One common inhibitory signal for NK cells is the recognition of HLA molecules, which are expressed by most cells of the human body (22). The inhibitory signals these receptors, such as KIRs, provide inhibitory signals that counteract cellular activation and function to keep NK cells from attacking healthy tissues.

Some activating receptors, including CD16a, are unable to initiate a signaling cascade alone, instead they need to associate with the signaling adapter molecules. CD16a has been found to associate with CD247 (TCRζ) or FcεR1γ (23) (24), each with the ability to initiate signaling through tyrosine residues on the cytoplasmic tail of the protein (Figure 1.1). Referred to as immunoreceptor tyrosine-based activation motifs (ITAM's), these integral membrane proteins associate with and signal for many immunoreceptors across different cell types, such as T cell receptors (TCR) (24,25). Specifically, for CD16a, key acidic residues in an intracellular tail motif drive association with these signaling molecules (26). When CD16a engages an

antibody, tyrosine residues on the ITAM become phosphorylated by kinases. Many CD16a molecules need to be engaged in a local area in order to overcome innate suppression, and activate downstream proteins in a signaling cascade. This concept is the immune synapse and applies to many other activating receptors including the T-cell receptor (27). FcεR1γ is initially phosphorylated by Syk kinases and CD247 by ZAP70 (28,29). The subsequent cascade signals trigger transcription factors, proteins, and other physical changes to prepare for ADCC.

An essential component of the CD16a signaling pathway is the reorganization of the actin cytoskeleton (30). This relocates microtubule organizing centers (MTOC) near the site of activation between the host and target cells (31). Lytic granules containing perforin and granzyme are transported across microtubules towards the synapse by dynein motor proteins (32,33). The granules fuse with the plasma membrane through a SNARE complex and release their contents into the synaptic cleft (34). LFA-1 adhesion at the synapse aids granular diffusion towards the target cell (35). The neutral pH of the extracellular space activates perforin allowing it to bind to the membrane of the target cell (36). The presence of Ca2+ triggers the formation of perforin oligomers that form pores on the membrane. These pores can range from 13-20 nM in diameter and can coalesce into larger pores with the recruitment of more oligomers (37,38). Expelled granzyme enters the target cell through the newly formed pores and triggers cell death through a variety of mechanisms, dependent on the granzyme subtype. The most studied granzyme, granzyme B, is a serine protease with a wide specificity. It has also been shown to cleave caspace-3 and caspace-7 subsequently including apoptosis through the caspase pathway (39,40). Additionally, granzyme B also cleaves Bid, triggering apoptosis through the mitochondrial proteins Bax and Bak(41). The other granzyme proteins have different protease

specificity and pathway activation allowing cytotoxic activates toward a variety of targets including tumors, microbes and virally-infected cells (42-44). The diverse cytotoxic nature of NK cells makes them effective protectors of immunity.

Despite the proximity to released perforin and granzymes, NK cells remain functional and resistant to their effects. Any escaped or internalized granzyme B is thought to be neutralized by granzyme B inhibitor, SB9 (45). As an additional defense measure, NK cells externalize CD107a at the immune synapse to line the plasma membrane with protein, reducing the ability of perforin to bind to the cell's phospholipids (46). Cathepsin B was found to have a similar mechanism and function for inhibiting perforin as CD107a (47). The presence of redundant defensive pathways that ensure the cell survives its cytotoxic activity.

The CD16a activation pathway is ended by ADAM17 cleavage. This surface metalloprotease cleaves CD16a between residues 195 and 196. Interestingly, the S197P mutation disrupts ADAM17 cleavage of CD16a and results in higher ADCC likely due to continuous activation (48,49). The kinetics of this cleavage are quite high, occurring within minutes (50,51). In addition to CD16a, ADAM17 cleaves LFA-2 assisting in the detachment of the activated NK cell (52,53).

NK cell immunotherapies

Researchers are interested in utilizing NK cells for immunotherapy after the recent successes of T-cell immunotherapy. Many T-cell therapies genetically modify T-cells to express engineered receptors that are specific for a target antigen, called chimeric antigen receptors (CARs). While a promising treatment option, there are multiple limitations of CAR-T-cell treatments, many of which NK cells may be able to address. NK cells can be allogenically

transferred while sparing graft versus host disease in contrast to the need of T-cells to be autologously transplanted or HLA donor matched (54) (55). Without the need to HLA match the patient, NK cell therapies provide “off-the-shelf” availability that offer a cheaper platform and more readily available platform for cellular immunotherapy. In this regard, researchers have begun preclinical testing of several CAR-NK cell lines to promising results (56-58). CAR-T cells also have limited success as treatments for solid tumors (59). Meanwhile, multiple NK cell treatments for solid tumors have reached clinical trials (NCT02100891) (NCT04319757) (NCT03940820), in addition to showing increased migration and infiltration of tumors (60,61). While T-cells lack CD16a expression, it is a hallmark of mature NK cells (62). High affinity CD16a NK cells (HaNK) are beginning to reach clinical trials as treatments for multiple different diseases (NCT03874026)(NCT03027128)(NCT05618925). Rather than utilizing a single-target CAR, HaNK cells direct cytotoxic activity towards antibody-coated cells. This allows the same HaNK cell line to be used to treat many different diseases, differing specificity by the antibody used. The term “high affinity NK cell” is misleading because the cell has not been engineered for higher specificity, rather NK cells of the higher affinity V158 allotype are selectively used (63). Engineering CD16a affinity beyond that of the V158 allotype are expected to increase success of HaNK cell treatments.

Glycosylation

More than 50 % of proteins are estimated to be modified by glycans, covalently linked sugar chains (64). N-glycans form an N-glyosidic linkage to the side chain amine nitrogen of asparagine in proteins. However, a N-glycan will only be added the sequon N-X-S/T, where X is any amino acid except proline. All N-glycans share a common core sequence of two N-

acetylglucosamine (GlcNAc) residues followed by one mannose residue that then forms two branches with a single mannose each (Figure 1.2). What sugars follow determines the type of N-glycan, either oligomannose, complex, or hybrid. Oligomannose N-glycans only extend with other mannose residues, while complex type branches continue with other sugars first initiated by GlcNAc. Finally, hybrid types contain one branch in style of oligomannose and one branch in style of complex N-glycans. In addition, complex N-glycans become may contain more than two branches and contain other modifications such as core fucosylation. Together, these characteristics lead to the vast heterogeneity N-linked glycans.

The complex process of eukaryotic N-glycosylation begins on the endoplasmic reticulum (ER), where sugars are added to dolichol phosphate. Eventually, it will take the form of the N-glycan precursor, $Glc_3Man_9GlcNAc_2$-P-P-Dol (65,66). The fully synthesized glycan then associates with high affinity to oligosaccharyltransferase A (42) which is complexed to a translocon. As a protein is cotranslationally expressed, OSTA will add this glycan to viable sequons on the nascent polypeptide. Once the protein is folded and within the lumen of the ER, OSTB may postranslationally modify N-glycan sequons (67). While OST-mediated N-glycosylation is highly efficient, there are many cases of sequons remaining unmodified. Suggested reasons include sequon residues, spacing of sequons and proximity to the c-terminal (68). Nevertheless, within the ER, glycosidases remove terminal sugars from the $Glc_3Man_9GlcNAc_2$ glycans leaving a majority of them in the form of $Man_8GlcNAc_2$, before the protein is transferred to the Golgi (66). Here, the terminal mannose residues are removed until the glycans are $Man_5GlcNAc_2$ (66). For the remainder of the journey through the Golgi, many different enzymes will add and remove sugars from glycans. The nature of the glycosylation

pathway creates a diverse array of glycans such that the glycans of two identical proteins processed at the same time can be different.

The extracellular domain of CD16a is only 20 KDa, yet it contains five N-glycans. Mass spectrometry analysis on primary human NK cells has shown that each of these five glycans are predominantly highly processed, complex-type glycans and that the N162 site has broad heterogeneity (69). It is quite remarkable that one N-glycan site displays such heterogeneity considering that proteins follow the same glycan processing pathway, with the same glycan machinery. This effect is also observed with primary samples, indicating possible clinical significance (70). Investigation on the impact of CD16a glycan heterogeneity on affinity found that smaller, less processed glycoforms have greater affinity than larger, more processed glycoforms (19). Further, removal of the N162 glycan nearly eliminated any difference in affinity, suggesting that the composition of the N162 site plays a role in ligand affinity, although the mechanism is unknown.

There exists a gap in knowledge of how these differences in glycosylation impact the function of CD16a. It was recently shown that CD16a glycan composition affects affinity, and that humans have large heterogeneity of their CD16a glycome. It is unknown how these changes impact affinity and if they have an affect on ADCC. Furthermore, it is not known if CD16a affinity relates to ADCC. Understanding these ideas are important for all antibody therapies, and it may be especially useful for NK cell immunotherapies to consider the impact of CD16a glycosylation.

References

1. Herberman, R. B., Holden, H. T., Ting, C. C., Lavrin, D. L., and Kirchner, H. (1976) Cell-mediated immunity to leukemia virus- and tumor-associated antigens in mice. *Cancer Res* **36**, 615-621
2. Kiessling, R., Klein, E., and Wigzell, H. (1975) "Natural" killer cells in the mouse. I. Cytotoxic cells with specificity for mouse Moloney leukemia cells. Specificity and distribution according to genotype. *Eur J Immunol* **5**, 112-117
3. DiSanto, J. P., Muller, W., Guy-Grand, D., Fischer, A., and Rajewsky, K. (1995) Lymphoid development in mice with a targeted deletion of the interleukin 2 receptor gamma chain. *Proc Natl Acad Sci U S A* **92**, 377-381
4. Kee, B. L., Morman, R. E., and Sun, M. (2020) Transcriptional regulation of natural killer cell development and maturation. *Adv Immunol* **146**, 1-28
5. Chiossone, L., Dumas, P. Y., Vienne, M., and Vivier, E. (2018) Natural killer cells and other innate lymphoid cells in cancer. *Nat Rev Immunol* **18**, 671-688
6. Kim, S., Iizuka, K., Kang, H. S., Dokun, A., French, A. R., Greco, S., and Yokoyama, W. M. (2002) In vivo developmental stages in murine natural killer cell maturation. *Nat Immunol* **3**, 523-528
7. Cooper, M. A., Fehniger, T. A., and Caligiuri, M. A. (2001) The biology of human natural killer-cell subsets. *Trends Immunol* **22**, 633-640
8. Jacobs, R., Hintzen, G., Kemper, A., Beul, K., Kempf, S., Behrens, G., Sykora, K. W., and Schmidt, R. E. (2001) CD56bright cells differ in their KIR repertoire and cytotoxic features from CD56dim NK cells. *Eur J Immunol* **31**, 3121-3127

9. Fehniger, T. A., Shah, M. H., Turner, M. J., VanDeusen, J. B., Whitman, S. P., Cooper, M. A., Suzuki, K., Wechser, M., Goodsaid, F., and Caligiuri, M. A. (1999) Differential cytokine and chemokine gene expression by human NK cells following activation with IL-18 or IL-15 in combination with IL-12: implications for the innate immune response. *J Immunol* **162**, 4511- 4520

10. Campbell, J. J., Qin, S., Unutmaz, D., Soler, D., Murphy, K. E., Hodge, M. R., Wu, L., and Butcher, E. C. (2001) Unique subpopulations of CD56+ NK and NK-T peripheral blood lymphocytes identified by chemokine receptor expression repertoire. *J Immunol* **166**, 6477-6482

11. Fehniger, T. A., Cooper, M. A., Nuovo, G. J., Cella, M., Facchetti, F., Colonna, M., and Caligiuri, M. A. (2003) CD56bright natural killer cells are present in human lymph nodes and are activated by T cell-derived IL-2: a potential new link between adaptive and innate immunity. *Blood* **101**, 3052-3057

12. Ferlazzo, G., Thomas, D., Lin, S. L., Goodman, K., Morandi, B., Muller, W. A., Moretta, A., and Munz, C. (2004) The abundant NK cells in human secondary lymphoid tissues require activation to express killer cell Ig-like receptors and become cytolytic. *J Immunol* **172**, 1455-1462

13. Saito, S., Nakashima, A., Myojo-Higuma, S., and Shiozaki, A. (2008) The balance between cytotoxic NK cells and regulatory NK cells in human pregnancy. *J Reprod Immunol* **77**, 14-22

14. Zhang, J., Basher, F., and Wu, J. D. (2015) NKG2D Ligands in Tumor Immunity: Two Sides of a Coin. *Front Immunol* **6**, 97

15. Baragano Raneros, A., Suarez-Alvarez, B., and Lopez-Larrea, C. (2014) Secretory pathways generating immunosuppressive NKG2D ligands: New targets for

therapeutic intervention. *Oncoimmunology* **3**, e28497

16. Wu, J., Song, Y., Bakker, A. B., Bauer, S., Spies, T., Lanier, L. L., and Phillips, J. H. (1999) An activating immunoreceptor complex formed by NKG2D and DAP10. *Science* **285**, 730-732

17. Vilches, C., and Parham, P. (2002) KIR: diverse, rapidly evolving receptors of innate and adaptive immunity. *Annu Rev Immunol* **20**, 217-251

18. Rajalingam, R. (2018) Diversity of Killer Cell Immunoglobulin-Like Receptors and Disease. *Clin Lab Med* **38**, 637-653

19. Subedi, G. P., and Barb, A. W. (2018) CD16a with oligomannose-type N-glycans is the only "low- affinity" Fc gamma receptor that binds the IgG crystallizable fragment with high affinity in vitro. *J Biol Chem* **293**, 16842-16850

20. Yeap, W. H., Wong, K. L., Shimasaki, N., Teo, E. C., Quek, J. K., Yong, H. X., Diong, C. P., Bertoletti, A., Linn, Y. C., and Wong, S. C. (2016) CD16 is indispensable for antibody-dependent cellular cytotoxicity by human monocytes. *Sci Rep* **6**, 34310

21. Mandelboim, O., Malik, P., Davis, D. M., Jo, C. H., Boyson, J. E., and Strominger, J. L. (1999) Human CD16 as a lysis receptor mediating direct natural killer cell cytotoxicity. *Proc Natl Acad Sci U S A* **96**, 5640-5644

22. Germain, R. N. (1994) MHC-dependent antigen processing and peptide presentation: providing ligands for T lymphocyte activation. *Cell* **76**, 287-299

23. Lanier, L. L., Yu, G., and Phillips, J. H. (1989) Co-association of CD3 zeta with a receptor (CD16) for IgG Fc on human natural killer cells. *Nature* **342**, 803-805

24. Kurosaki, T., and Ravetch, J. V. (1989) A single amino acid in the glycosyl phosphatidylinositol attachment domain determines the membrane topology of Fc gamma RIII. *Nature* **342**, 805-807

25. Ashwell, J. D., and Klusner, R. D. (1990) Genetic and mutational analysis of the T-cell antigen receptor. *Annu Rev Immunol* **8**, 139-167

26. Blazquez-Moreno, A., Park, S., Im, W., Call, M. J., Call, M. E., and Reyburn, H. T. (2017) Transmembrane features governing Fc receptor CD16A assembly with CD16A signaling adaptor molecules. *Proc Natl Acad Sci U S A* **114**, E5645-E5654

27. Ruiz-Navarro, J., Calvo, V., and Izquierdo, M. (2023) Extracellular vesicles and microvilli in the immune synapse. *Front Immunol* **14**, 1324557

28. Courtney, A. H., Lo, W. L., and Weiss, A. (2018) TCR Signaling: Mechanisms of Initiation and Propagation. *Trends Biochem Sci* **43**, 108-123

29. Shah, S. V., Manickam, C., Ram, D. R., Kroll, K., Itell, H., Permar, S. R., Barouch, D. H., Klatt, N. R., and Reeves, R. K. (2018) CMV Primes Functional Alternative Signaling in Adaptive Deltag NK Cells but Is Subverted by Lentivirus Infection in Rhesus Macaques. *Cell Rep* **25**, 2766-2774 e2763

30. Bryceson, Y. T., Ljunggren, H. G., and Long, E. O. (2009) Minimal requirement for induction of natural cytotoxicity and intersection of activation signals by inhibitory receptors. *Blood* **114**, 2657-2666

31. Sancho, D., Vicente-Manzanares, M., Mittelbrunn, M., Montoya, M. C., Gordon-Alonso, M., Serrador, J. M., and Sanchez-Madrid, F. (2002) Regulation of microtubule-organizing center orientation and actomyosin cytoskeleton rearrangement during immune interactions. *Immunol Rev* **189**, 84-97

32. James, A. M., Hsu, H. T., Dongre, P., Uzel, G., Mace, E. M., Banerjee, P. P., and Orange, J. S. (2013) Rapid activation receptor- or IL-2-induced lytic granule convergence in human natural killer cells requires Src, but not downstream signaling.

Blood **121**, 2627-2637

33. Mentlik, A. N., Sanborn, K. B., Holzbaur, E. L., and Orange, J. S. (2010) Rapid lytic granule convergence to the MTOC in natural killer cells is dependent on dynein but not cytolytic commitment. *Mol Biol Cell* **21**, 2241-2256

34. de Saint Basile, G., Menasche, G., and Fischer, A. (2010) Molecular mechanisms of biogenesis and exocytosis of cytotoxic granules. *Nat Rev Immunol* **10**, 568-579

35. Liu, D., Bryceson, Y. T., Meckel, T., Vasiliver-Shamis, G., Dustin, M. L., and Long, E. O. (2009) Integrin-dependent organization and bidirectional vesicular traffic at cytotoxic immune synapses. *Immunity* **31**, 99-109

36. Simone, C. B., and Henkart, P. (1980) Permeability changes induced in erthrocyte ghost targets by antibody-dependent cytotoxic effector cells: evidence for membrane pores. *J Immunol* **124**, 954-963

37. Law, R. H., Lukoyanova, N., Voskoboinik, I., Caradoc-Davies, T. T., Baran, K., Dunstone, M. A., D'Angelo, M. E., Orlova, E. V., Coulibaly, F., Verschoor, S., Browne, K. A., Ciccone, A., Kuiper, M. J., Bird, P. I., Trapani, J. A., Saibil, H. R., and Whisstock, J. C. (2010) The structural basis for membrane binding and pore formation by lymphocyte perforin. *Nature* **468**, 447-451

38. Leung, C., Hodel, A. W., Brennan, A. J., Lukoyanova, N., Tran, S., House, C. M., Kondos, S. C., Whisstock, J. C., Dunstone, M. A., Trapani, J. A., Voskoboinik, I., Saibil, H. R., and Hoogenboom,

B. W. (2017) Real-time visualization of perforin nanopore assembly. *Nat Nanotechnol* **12**, 467- 473

39. Fischer, U., Janicke, R. U., and Schulze-Osthoff, K. (2003) Many cuts to ruin: a comprehensive update of caspase substrates. *Cell Death Differ* **10**, 76-100

40. Bots, M., and Medema, J. P. (2006) Granzymes at a glance. *J Cell Sci* **119**, 5011-5014
41. Sutton, V. R., Davis, J. E., Cancilla, M., Johnstone, R. W., Ruefli, A. A., Sedelies, K., Browne, K. A., and Trapani, J. A. (2000) Initiation of apoptosis by granzyme B requires direct cleavage of bid, but not direct granzyme B-mediated caspase activation. *J Exp Med* **192**, 1403-1414
42. Al-Wasaby, S., de Miguel, D., Aporta, A., Naval, J., Conde, B., Martinez-Lostao, L., and Anel, A. (2015) In vivo potential of recombinant granulysin against human tumors. *Oncoimmunology* **4**, e1036213
43. Lu, C. C., Wu, T. S., Hsu, Y. J., Chang, C. J., Lin, C. S., Chia, J. H., Wu, T. L., Huang, T. T., Martel, J., Ojcius, D. M., Young, J. D., and Lai, H. C. (2014) NK cells kill mycobacteria directly by releasing perforin and granulysin. *J Leukoc Biol* **96**, 1119-1129
44. Romero, V., Fellows, E., Jenne, D. E., and Andrade, F. (2009) Cleavage of La protein by granzyme H induces cytoplasmic translocation and interferes with La-mediated HCV-IRES translational activity. *Cell Death Differ* **16**, 340-348
45. Bird, C. H., Sutton, V. R., Sun, J., Hirst, C. E., Novak, A., Kumar, S., Trapani, J. A., and Bird, P. I. (1998) Selective regulation of apoptosis: the cytotoxic lymphocyte serpin proteinase inhibitor 9 protects against granzyme B-mediated apoptosis without perturbing the Fas cell death pathway. *Mol Cell Biol* **18**, 6387-6398
46. Cohnen, A., Chiang, S. C., Stojanovic, A., Schmidt, H., Claus, M., Saftig, P., Janssen, O., Cerwenka, A., Bryceson, Y. T., and Watzl, C. (2013) Surface CD107a/LAMP-1 protects natural killer cells from degranulation-associated damage. *Blood* **122**, 1411-1418
47. Balaji, K. N., Schaschke, N., Machleidt, W., Catalfamo, M., and Henkart, P. A. (2002) Surface cathepsin B protects cytotoxic lymphocytes from self-destruction after degranulation. *J Exp Med* **196**, 493-503

48. Jing, Y., Ni, Z., Wu, J., Higgins, L., Markowski, T. W., Kaufman, D. S., and Walcheck, B. (2015) Identification of an ADAM17 cleavage region in human CD16 (FcgammaRIII) and the engineering of a non-cleavable version of the receptor in NK cells. *PLoS One* **10**, e0121788

49. Pomeroy, E. J., Hunzeker, J. T., Kluesner, M. G., Lahr, W. S., Smeester, B. A., Crosby, M. R., Lonetree, C. L., Yamamoto, K., Bendzick, L., Miller, J. S., Geller, M. A., Walcheck, B., Felices, M., Webber, B. R., Starr, T. K., and Moriarity, B. S. (2020) A Genetically Engineered Primary Human Natural Killer Cell Platform for Cancer Immunotherapy. *Mol Ther* **28**, 52-63

50. Lajoie, L., Congy-Jolivet, N., Bolzec, A., Gouilleux-Gruart, V., Sicard, E., Sung, H. C., Peiretti, F., Moreau, T., Vie, H., Clemenceau, B., and Thibault, G. (2014) ADAM17-mediated shedding of FcgammaRIIIA on human NK cells: identification of the cleavage site and relationship with activation. *J Immunol* **192**, 741-751

51. Romee, R., Foley, B., Lenvik, T., Wang, Y., Zhang, B., Ankarlo, D., Luo, X., Cooley, S., Verneris, M., Walcheck, B., and Miller, J. (2013) NK cell CD16 surface expression and function is regulated by a disintegrin and metalloprotease-17 (ADAM17). *Blood* **121**, 3599-3608

52. Walcheck, B., Kahn, J., Fisher, J. M., Wang, B. B., Fisk, R. S., Payan, D. G., Feehan, C., Betageri, R., Darlak, K., Spatola, A. F., and Kishimoto, T. K. (1996) Neutrophil rolling altered by inhibition of L- selectin shedding in vitro. *Nature* **380**, 720-723

53. Srpan, K., Ambrose, A., Karampatzakis, A., Saeed, M., Cartwright, A. N. R., Guldevall, K., De Matos, G., Onfelt, B., and Davis, D. M. (2018) Shedding of CD16 disassembles the NK cell immune synapse and boosts serial engagement of target cells. *J Cell Biol* **217**, 3267-3283

54. Iliopoulou, E. G., Kountourakis, P., Karamouzis, M. V., Doufexis, D., Ardavanis, A., Baxevanis, C. N., Rigatos, G., Papamichail, M., and Perez, S. A. (2010) A phase I trial of adoptive transfer of allogeneic natural killer cells in patients with advanced non-small cell lung cancer. *Cancer Immunol Immunother* **59**, 1781-1789

55. Ren, J., Liu, X., Fang, C., Jiang, S., June, C. H., and Zhao, Y. (2017) Multiplex Genome Editing to Generate Universal CAR T Cells Resistant to PD1 Inhibition. *Clin Cancer Res* **23**, 2255-2266

56. Liu, E., Tong, Y., Dotti, G., Shaim, H., Savoldo, B., Mukherjee, M., Orange, J., Wan, X., Lu, X., Reynolds, A., Gagea, M., Banerjee, P., Cai, R., Bdaiwi, M. H., Basar, R., Muftuoglu, M., Li, L., Marin, D., Wierda, W., Keating, M., Champlin, R., Shpall, E., and Rezvani, K. (2018) Cord blood NK cells engineered to express IL-15 and a CD19-targeted CAR show long-term persistence and potent antitumor activity. *Leukemia* **32**, 520-531

57. Han, J., Chu, J., Keung Chan, W., Zhang, J., Wang, Y., Cohen, J. B., Victor, A., Meisen, W. H., Kim, S. H., Grandi, P., Wang, Q. E., He, X., Nakano, I., Chiocca, E. A., Glorioso Iii, J. C., Kaur, B., Caligiuri, M. A., and Yu, J. (2015) CAR-Engineered NK Cells Targeting Wild-Type EGFR and EGFRvIII Enhance Killing of Glioblastoma and Patient-Derived Glioblastoma Stem Cells. *Sci Rep* **5**, 11483

58. Topfer, K., Cartellieri, M., Michen, S., Wiedemuth, R., Muller, N., Lindemann, D., Bachmann, M., Fussel, M., Schackert, G., and Temme, A. (2015) DAP12-based activating chimeric antigen receptor for NK cell tumor immunotherapy. *J Immunol* **194**, 3201-3212

59. Majzner, R. G., and Mackall, C. L. (2018) Tumor Antigen Escape from CAR T-cell Therapy. *Cancer Discov* **8**, 1219-1226

60. Carlsten, M., Levy, E., Karambelkar, A., Li, L., Reger, R., Berg, M., Peshwa, M. V., and Childs, R. W. (2016) Efficient mRNA-Based Genetic Engineering of Human NK Cells with High-Affinity CD16 and CCR7 Augments Rituximab-Induced ADCC against Lymphoma and Targets NK Cell Migration toward the Lymph Node-Associated Chemokine CCL19. *Front Immunol* **7**, 105

61. Lee, J., Kang, T. H., Yoo, W., Choi, H., Jo, S., Kong, K., Lee, S. R., Kim, S. U., Kim, J. S., Cho, D., Kim,J., Kim, J. Y., Kwon, E. S., and Kim, S. (2019) An Antibody Designed to Improve Adoptive NK-Cell Therapy Inhibits Pancreatic Cancer Progression in a Murine Model. *Cancer Immunol Res* **7**, 219- 229

62. Patel, K. R., Roberts, J. T., and Barb, A. W. (2019) Multiple Variables at the Leukocyte Cell Surface Impact Fc gamma Receptor-Dependent Mechanisms. *Front Immunol* **10**, 223

63. Mahaweni, N. M., Olieslagers, T. I., Rivas, I. O., Molenbroeck, S. J. J., Groeneweg, M., Bos, G. M. J., Tilanus, M. G. J., Voorter, C. E. M., and Wieten, L. (2018) A comprehensive overview of FCGR3A gene variability by full-length gene sequencing including the identification of V158F polymorphism. *Sci Rep* **8**, 15983

64. Apweiler, R., Hermjakob, H., and Sharon, N. (1999) On the frequency of protein glycosylation, as deduced from analysis of the SWISS-PROT database. *Biochim Biophys Acta* **1473**, 4-8

65. Moremen, K. W., Tiemeyer, M., and Nairn, A. V. (2012) Vertebrate protein glycosylation: diversity, synthesis and function. *Nat Rev Mol Cell Biol* **13**, 448-462

66. Moremen, K. W., and Molinari, M. (2006) N-linked glycan recognition and

processing: the molecular basis of endoplasmic reticulum quality control. *Curr Opin Struct Biol* **16**, 592-599

67. Shrimal, S., and Gilmore, R. (2013) Glycosylation of closely spaced acceptor sites in human glycoproteins. *J Cell Sci* **126**, 5513-5523

68. Shrimal, S., Trueman, S. F., and Gilmore, R. (2013) Extreme C-terminal sites are posttranslocationally glycosylated by the STT3B isoform of the OST. *J Cell Biol* **201**, 81-95

69. Patel, K. R., Rodriguez Benavente, M. C., Lorenz, W. W., Mace, E. M., and Barb, A. W. (2021) Fc gamma receptor IIIa/CD16a processing correlates with the expression of glycan-related genes in human natural killer cells. *J Biol Chem* **296**, 100183

70. Patel, K. R., Nott, J. D., and Barb, A. W. (2019) Primary Human Natural Killer Cells Retain Proinflammatory IgG1 at the Cell Surface and Express CD16a Glycoforms with Donor-dependent Variability. *Mol Cell Proteomics* **18**, 2178-2190

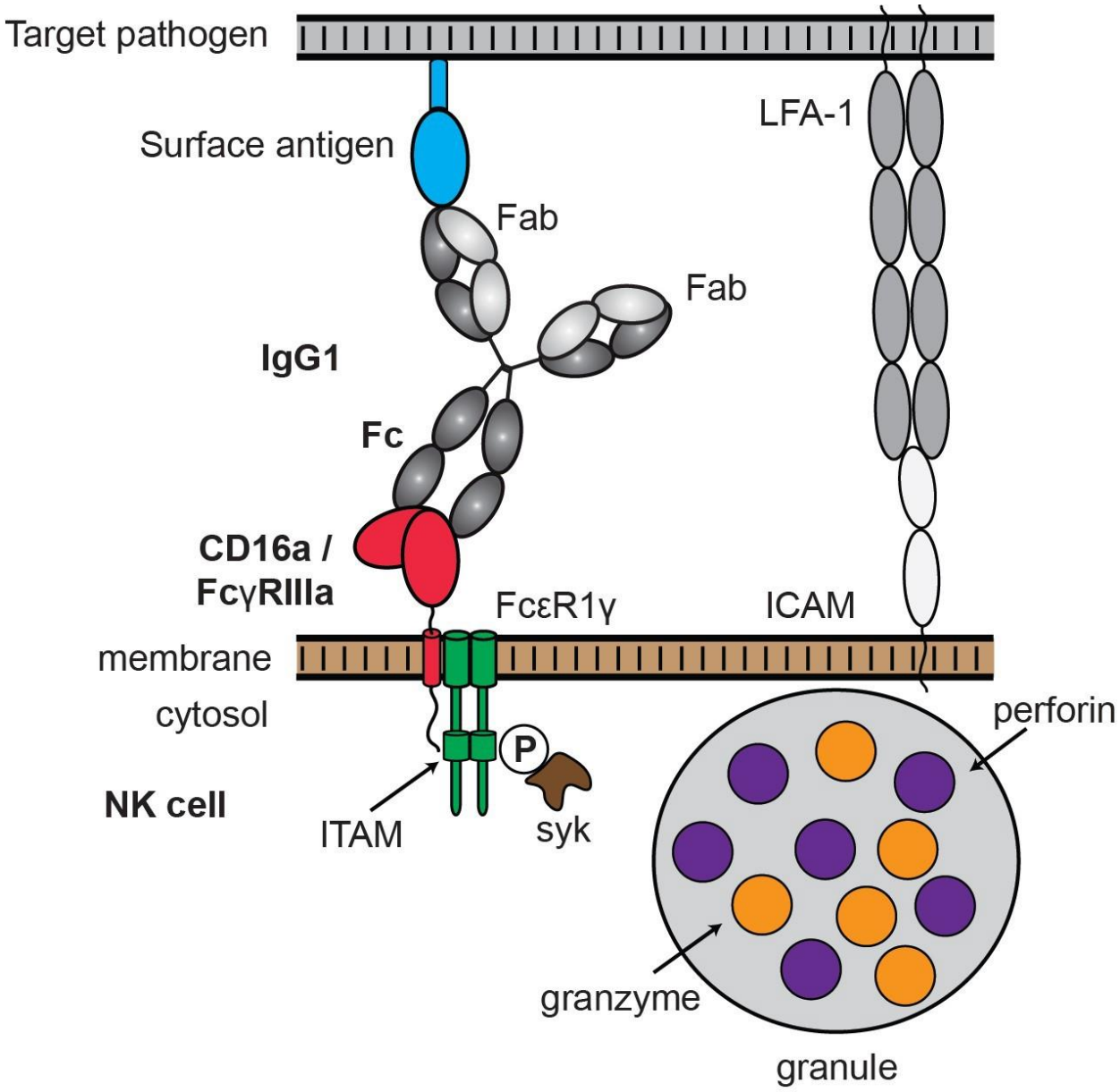

Figure 1.1 The nature of natural killer cell CD16a engagement.

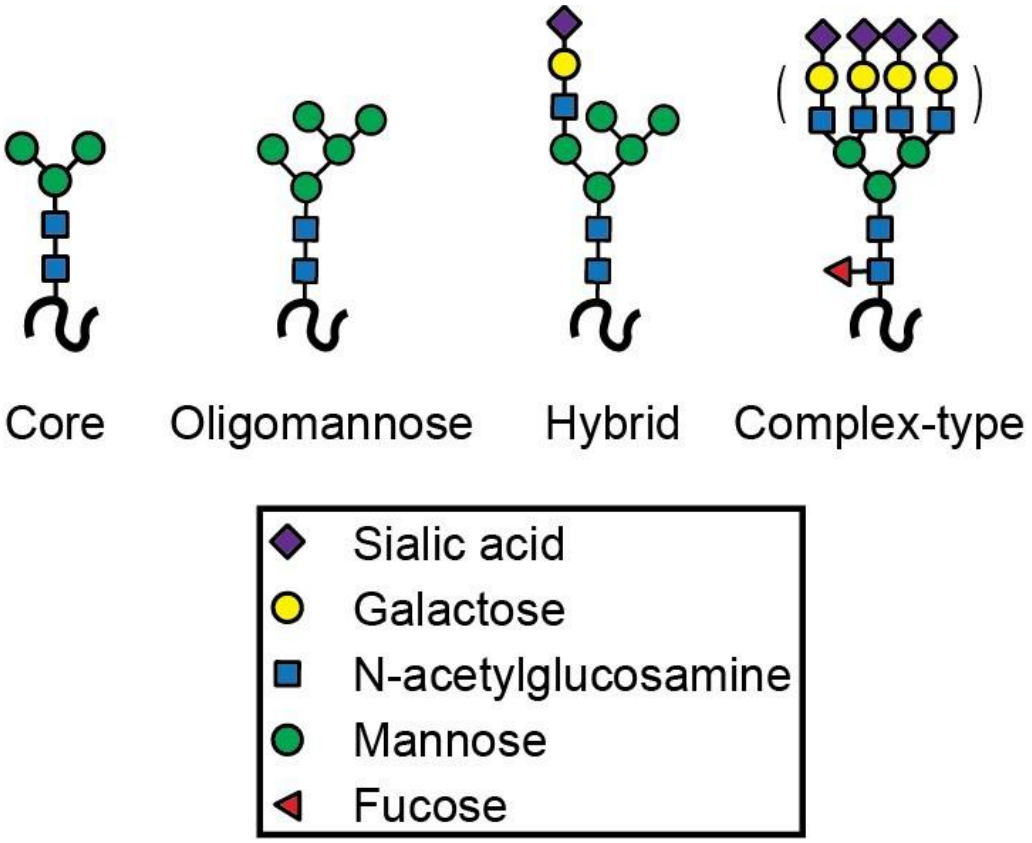

Figure 1.2 The different types of N-glycosylation.

CHAPTER 2

THE WEAKER-BINDING FC γ RECEPTOR IIIA F158 ALLOTYPE RETAINS SENSITIVITY TO N-GLYCAN COMPOSITION AND EXHIBITS A DESTABILIZED ANTIBODY-BINDING INTERFACE[1]

[1]Kremer, Paul G, and Adam W Barb. 2022. *The Journal of biological chemistry* vol. 298,9.

Abstract

Antibodies engage Fc γ Receptors (FcγRs) to elicit healing cellular immune responses, following binding to a target antigen. FcγRIIIa / CD16a triggers natural killer cells to destroy target tissues with cytotoxic proteins and enhances phagocytosis mediated by macrophages. Multiple variables affect CD16a antibody binding strength and the resulting immune response, including a genetic polymorphism. The predominant CD16a F158 allotype binds antibody with less affinity than the less common V158 allotype. This polymorphism likewise affects cellular immune responses and clinical efficacy of antibodies relying on CD16a engagement, though it remains unclear how V/F158 affects CD16a structure. Another relevant variable shown to affect affinity is composition of the CD16a asparagine linked (N)-glycans. It is currently not known how N-glycan composition affects CD16a F158 affinity. We determined N-glycan composition affects the V158 and F158 allotypes similarly, and N-glycan composition does not explain differences in V158 and F158 binding affinity. Analysis of binding kinetics indicated the N162 glycan slows the binding event, and shortening the N-glycans or removing the N162 glycan increased the speed of binding. F158 displayed a slower binding rate than V158. Surprisingly, N-glycan composition had a smaller effect on the dissociation rate. We also identified conformational heterogeneity of CD16a F158 backbone amide and N162 glycan resonances using NMR spectroscopy. Residues exhibiting chemical shift perturbations between V158 and F158 mapped to the antibody-binding surface. These data support a model for CD16a F158 with increased conformational heterogeneity in the antibody-binding interface resulting in decreased affinity.

Introduction

Fc γ Receptor (FcγR) IIIa / CD16a binds to the crystallizable fragment (Fc) of immunoglobulin G (IgG) antibodies (Figure 2.1). CD16a triggers cell activation upon encountering antibodies clustered on a surface, which may include a damaged tissue, foreign pathogen or particle. Possible cell-mediated immune responses are phagocytic and cytotoxic, leading to destruction of the antibody-coated target (1,2). The strength of the cellular response depends on the antibody-binding affinity of CD16a.

Two major CD16a forms in humans result from a genetic polymorphism affecting the amino acid residue at position 158 on the extracellular antibody-binding domain (3). The allele frequency varies by population but several studies collectively suggest the V158-encoding allele is present at 30-39% frequency, with the remainder encoding F158 (3-5). In binding affinity assays, the CD16a F158 allotype binds IgG1 4-5 fold weaker than V158 (6,7).

Natural Killer (NK) cells function in the innate immune system but respond to antibody-coated targets through CD16a as the primary FcγR. NK cells expressing F158 showed less cytotoxic activity following antibody treatment when compared to V158 (8). Similarly, Binyamin et al showed increased ADCC for V158 with NK92 cells (9). Data from primary human NK cells also supports V158 having higher ADCC over F158 (7). Clinical studies link the F158 allotype to increased susceptibility to a wide assortment of diseases (10-14). Furthermore, V158 patients experienced superior responses to clinical antibody treatments (15-17). Though these correlations are known, it is not known why a single amino acid substitution in this receptor affects the ligand binding affinity.

In addition to the CD16a residue at 158, glycosylation was recently shown to affect antibody binding affinity. CD16a is a transmembrane receptor modified with five asparagine(N)-linked carbohydrates (glycans). N-glycans on secreted proteins exhibit a high degree of compositional heterogeneity due to the template-independent glycan processing in the ER and Golgi (18). CD16a exhibits a high degree of heterogeneity. Among the five N-glycosylation sites, N162 appears the most heterogeneous on CD16a isolated from primary human cells (19,20). Furthermore, CD16a N162 glycan heterogeneity impacts Fc binding affinity. Minimally-processed oligomannose glycans, present on CD16a isolated from human donors, provide greater affinity than highly-processed complex-type glycans on CD16a (21,22). Hayes and coworkers also found binding differences related to CD16a glycosylation and the 158 allotype (23). It is not currently known how the N162 N-glycan composition affects the antibody-binding affinity of the CD16a F158 allotype.

We investigated the structural and functional consequences of a phenylalanine residue at CD16a position 158 relative to a valine. We first characterized the impact of N-glycans on antibody-binding affinity by CD16a F158. Next, we identified backbone and N-glycan atoms that were differentially affected by V158 and F158 using NMR spectroscopy. These data provide insight into the unique structural and functional characteristics of the predominant CD16a F158 allotype with atomic-level resolution.

Results

Structural similarity of V158 and F158 – Multiple examples of the CD16a V158 structure from X-ray crystallography are reported and are highly similar (24-26). As of this writing, no models

of the F158 variant derived from X-ray crystallography or cryoEM are reported despite the single amino acid difference and greater prevalence in the human population. AlphaFold, however, provided a computational model for comparison (27). As expected, the structures of the extracellular antibody-binding domains are highly similar (Figure 2.1). Subtle differences in the packing around position 158 are notable, stemming from steric contacts that prevent the F158 sidechain from occupying the same position as V158. This comparison does not provide a clear indication why F158 binds weaker than V158. However, relatively small changes in binding affinity, like those noted for F158 and V158, may not result from large structural rearrangements and may be due instead to differences in conformational sampling or glycosylation that are not always identifiable in models from X-ray crystallography or AlphaFold.

The effect of N-glycan composition on CD16a F158 affinity – We examined whether glycosylation explained the reported differences in affinity. Our laboratory previously determined that the composition of the N162 glycan affects CD16a V158 antibody-binding affinity (22). Thus, it is possible that F158 affects N-glycan processing, thus weakening affinity. Wild-type HEK293F cells expressed both CD16a V158 and F158, and are capable of performing extensive N-glycan remodeling reactions and generating complex-type N-glycoforms. SDS-PAGE showed substantial processing as both proteins migrated much higher than expected based on the predicted molecular weight of the unmodified polypeptide (50.5 kDa; S2.1).

The CD16a F158 allotype bound IgG1 Fc with a 6-fold reduction in affinity compared to V158 (Figure 2.2), consistent with previous reports (6,21,28). We next expressed both CD16a allotypes in a Gnt1- cell line that expresses glycoproteins with predominantly oligomannose

(Man5GlcNAc2) N-glycans (29). The mobility of these proteins in SDS-PAGE increased from the presence of smaller N-glycans (S2.1). Both proteins bound IgG1 Fc with increased affinity compared to the same protein expressed in the wild-type cell line, however, the F158 allotype bound with a 13-fold weaker affinity compared to V158 (S2.2). While both allotypes gain increased affinity with oligomannose glycans, the gain in affinity by V158 is more substantial than F158 (3.1x vs. 1.6x; Table S2.1). This result indicates that the factor causing weaker F158 binding is also present in the oligomannose N-glycoform.

The F158-encoding polymorphism introduces an aromatic residue at a position not found in V158. Aromatic residues form strong interactions through CH-π dispersive forces with carbohydrate residues (30). Thus, it is possible that F158 introduces an inhibitory intramolecular contact. We enzymatically truncated the N-glycans to a single GlcNAc residue, and again found that F158 bound with 6-fold weaker affinity when compared to V158. Lastly, we prevented N162 glycosylation through the S164A mutation to disrupt the NVS glycosylation sequon. Again, the F158 allotype bound IgG1 Fc with 6-fold weaker affinity compared to V158. When comparing to the native form of the receptor, both allotypes possess nearly identical relative affinity of the single GlcNAc and S164A forms (Table S2.1). These data demonstrate that the weaker F158 binding affinity is independent of N-glycan composition and the presence of the N162 glycan.

CD16a F158 exhibits slower binding kinetics – A detailed analysis of the binding curves revealed differences in binding rates. We fitted a two-state binding model to the sensorgrams that revealed major (k_a1, k_d1) and minor (k_a2, k_d2) events, with the major event dominating the

observed data (Figure 2.4, Table 2.2). The fitting errors were less than 2% in all instances. Dissociation constants resulting from the kinetic fits were smaller than those found with fitting the equilibrium responses, however, the relative differences between forms were preserved. Fitting a 1:1 binding model revealed rates highly comparable to the major event in the two-state model, however with slightly increased residuals due to an inability of this model to accommodate slight non-linearity at the later timepoints of the association curves. This non-linearity may be due to reversible non-specific interactions with the chip surface or a slow conformational rearrangement once bound.

We observed differences between CD16a V158 binding and binding of the V158 S164A variant, both with complex-type N-glycans but the latter lacking the N162 glycan. The V158 S164A variant bound with an 8-fold increased on rate, and a 7-fold increased off rate. These data indicate that the N162 glycan slows complex formation, and the resulting complex is less stable. Shortening the V158 N-glycan with the Man5 glycoforms increased the binding rate by 4.2-fold and also increased the dissociation rate by 2.8-fold. The F158 association proved too weak and too fast for reproducible analysis of the binding kinetics.

The CD16a V158 variant with the truncated (1)GlcNAc N-glycans revealed a 15-fold faster association rate compared to the complex-type glycoform, however, the dissociation rates were similar (1.6-fold difference). These results support the evidence from the S164A example above that the extended N-glycan slowed the association rate. In contrast to S164A, however, the truncated (1)GlcNAc proved sufficient to stabilize the complex.

The increased binding affinity for the CD16a F158 allotype with truncated (1)GlcNAc N-glycans provided the opportunity to measure binding kinetics and compare V158 and F158

directly. The CD16a F158 (1)GlcNAc protein exhibited an on rate that was 2.3-fold slower than the CD16a V158 (1)GlcNAc glycoform, and a dissociation rate 2-fold faster. Thus, the presence of F158 slowed the binding and increased the rate of complex dissociation. These differences are consistent with a greater conformational heterogeneity of the F158 allotype.

NMR shows CD16a structural differences – We evaluated CD16a V158 and F158 using solution NMR spectroscopy to identify possible structural differences. Glycosylated proteins represent a substantial challenge for solution NMR spectroscopy, largely because the common expression host for NMR, *Escherichia coli*, does not N-glycosylate. We expressed CD16a in the same human cell line used for the binding affinity measurements (HEK293F). These cells glycosylate appropriately, but do not allow uniform amino acid labeling from metabolic precursors. Instead, we first supplemented the expression medium with [^{15}N]-phenylalanine, an essential amino acid that does not scramble under the conditions used for expression.

An HSQC-TROSY spectrum of [^{15}N-phenylalanine]-CD16a V158 showed seven clear peaks corresponding to seven phenylalanine residues (Figure 2.5A). A similar spectrum of [^{15}N-F]-CD16a F158 showed nine peaks, seven of these similar to V158 peaks. The two remaining peaks are likely due to F158. It is curious to note that the F158 N-H correlation revealed two peaks, indicating the presence of two different conformations exchanging slowly on the NMR timescale. It is not known if the V158 N-H correlation likewise samples two conformations; the nitrogen atom from [^{15}N]-valine is metabolically scrambled to other amino acids during expression and a V158 peak was not identified (data not shown). It is also notable that the F133

and F153 peaks do not perfectly overlay in spectra of the [^{15}N- phenylalanine]-CD16a allotypes, instead showing chemical shift perturbations.

We next probed chemical shift perturbations in other amino acid residues by adding [^{15}N]-lysine, [^{15}N]-phenylalanine and [^{15}N]-tyrosine to the expression medium. Lysine and tyrosine likewise did not scramble. We were able to match each peak to a residue using the assignment of a related receptor by Kato and coworkers (31). In total, these spectra showed ten residues with chemical shift perturbations, notably at F133, K147, F153, and K161 (Figure 2.5B).

The N162 glycan is also in the general vicinity of these perturbed residues. N-glycans can be labeled by supplementing the expression medium with [^{13}C]-glucose, which is then incorporated into each N-glycan sugar and alanine methyls (32,33). One unique N-glycan proton-carbon correlation provides unique insight into each individual N-glycan at the point of attachment; the $^{1}H_{1}$-$^{13}C_{1}$ correlation on the (1)GlcNAc residue that is covalently bonded to the N-glycosylated asparagine residue (34). NMR observation of this correlation provides a fingerprint of the glycoprotein N-glycans with one peak expected for each N-glycan. We previously assigned the peaks for the CD16a V158 allotype, including a distinct single peak for the N162 glycan (35).

Comparing the CD16a V158 and F158 N-glycan peaks in NMR spectra showed a high degree of similarity for the N38, N45, N74 and N169 peaks (Figure 2.5C). Surprisingly, CD16a F158 showed two peaks for the N162 glycan, indicating the presence of conformational exchange. One of these peaks overlayed with the single CD16a V158 N162 peak, indicating that CD16a F158 populates conformations either not visible or minimally populated with V158.

Individual atoms that demonstrated a chemical shift perturbation between V158 and F158 clustered on a structural model of the CD16a V158 extracellular domain (Figure 2.5D). This hotspot is directly adjacent to the antibody-binding interface. It is notable that the NMR experiments revealed differences with unliganded CD16a. We were unable to identify CD16a residues in a complex with Fc, presumably due to the relatively short lifetime of the bound state (data not shown). Data from the unliganded receptors reflects the unbound state and the slower association of the F158 allotype is consistent with greater conformational heterogeneity observed by NMR.

Discussion

These experiments identified structural, kinetic and functional differences in the two predominant CD16a allotypes that differ by a single amino acid residue. Multiple aspects of this study are notable. The F158 and V158 allotypes bind ligand with different affinities and at different rates, despite the high degree of sequence similarity. F158 appeared to bind slower and form a less stable complex compared to V158. The lower stability, and thus lower affinity, may be explained by structural modeling that indicated the F158 residue displaces local amino acid residues due to a greater size of the F sidechain (Figure 2.1). These slight structural differences are potentially sufficient to destabilize regions outside of the residues that directly contact F158. Indeed, NMR revealed structure differences in the F158 and V158 allotypes that extended far from residue 158. NMR spectra revealed the presence of at least two conformations sampled by the F158 N162 glycan at the point of attachment. Only one conformation was observed for V158. Furthermore, the F158 backbone amide likewise sampled two conformations. The

structural changes were not isolated to F158 and residues directly contacting F158, but rather spread throughout the antibody-binding interface.

Previous observations of CD16a isolated from primary human NK cells and monocytes identified the presence of oligomannose N162-glycans (19,20). These underprocessed forms increased affinity for the V158 allotype (22), though it remained unknown how N-glycan composition affected F158. We determined that the composition of the N162 glycan did not affect F158 and V158 differently and V158 bounds with higher affinity with each glycoform. It should be noted that V158 saw a greater affinity increase with Man5 N-glycans (Table 2.1). Small N-glycans increased the affinity for both allotypes ((1)GlcNAc > Man5 > complex type), thus the mechanism underlying the affinity increases appears to be shared by both proteins.

Removing or shortening the N162 glycan increased binding rates. This observation is consistent with previous computational modeling of the CD16a/IgG1 complex predicting that N162 glycan conformational heterogeneity negatively affects binding affinity (26,36). Our data indicate the distal portions of the N-glycan slow binding, with shorter N-glycans binding with increased rates as was evident for the (1)GlcNAc glycoform that bound more quickly than the S164A variant lacking an N162 glycan. However, the distal portions of the N-glycan largely appear dispensable for high affinity binding, though the complex-type N-glycans do promote receptor/antibody stability to a greater extent than (1)GlcNAc (1.6-fold), Man5 (2.9-fold), and S164A (7.1-fold). These data indicate an N162 glycoform for optimal binding may be found at a size between (1)GlcNAc and Man5.

The prevalence of the F158 allotype in the human population suggests increased fitness is associated with at least one copy of the weaker binding allele. Unfortunately, patients expressing

F158 show decreased responses to many antibody-based therapeutics, though advances in antibody engineering may surmount this barrier (37). It is notable that a common anti-CD16 antibody, 3G8, likewise binds F158 with reduced affinity. Increasing the antibody-binding affinity of the F158 allotype may be achieved by developing reagents to specifically truncate the F158 N162 glycan, or antibody Fc designs that accommodate the unique structural features including multiple conformations of the antibody binding interface.

Experimental Methods

Materials – All materials were purchased from Millipore-Sigma unless otherwise noted.

Protein expression for binding affinity measurements – The V and F CD16a allotypes were cloned into the pGen2 plasmid downstream of and in frame with DNA encoding the 8x-histidine tag, green florescent protein (GFP) and tobacco etch virus (TEV) protease digestion site as described (38). Human IgG1 Fc (residues 216-447) was expressed from a plasmid previously described (39). All proteins were expressed through transient transfection of either HEK293F (Life Technologies) or HEK293S (Gnt1-) cells (29). Unless otherwise specified, cells were grown in FreeStyle293™ medium (Life Technologies) supplemented with ExCell (Sigma Aldrich) media, 10% of total volume, on a shaker (ATR Biotech) at 125 RPM with 8% CO2 and 80% humidity at 37°C. Cell densities were 3.0 x 10^6 live cells/ mL at the time of transfection. We added 2.5 μg/mL DNA and 10 μg/mL PEI (40 KDa). Following a 24 h incubation, cultures were diluted 1:1 with the same media containing 4.4 mM valproic acid. Culture supernatant was harvested after 5 d by centrifugation at 1000 *g* for 5 min. CD16a was purified using a Ni-NTA

column (Qiagen) while Fc was purified using a Protein A-Sepharose® column. All proteins were stored in a buffer containing 25 mM 3-(N-morpholino) propanesulfonic acid (MOPS), 0.1 M sodium chloride, pH 7.2.

Endoglycosidase F1 digestion – EndoF1 was expressed with *Escherichia coli* and coupling at a density of (15 mg protein per mL of resin) to AminoLink Coupling Resin (Thermo Scientific) following manufacturers protocol as previously described (26) in a buffer containing 0.1M sodium phosphate, 0.15M NaCl, pH 7.2. CD16a was digested at a ratio of 1 mg per 50 µL of prepared resin overnight at room temperature. Digestion was analyzed using SDS-PAGE.

Surface plasmon resonance – All affinity measurements were performed with a Biacore T200 (GE Life Sciences) using amine coupling to a CM5 chip. Fc was coupled at 1 µg/mL for saturation experiments. Several different CD16a concentrations, ranging between 0.01 µM and 20.48 µM, was flowed over the chip surface at a rate of 10 µL/min. CD16a was diluted in running buffer containing 20 mM MOPS, 100 mM sodium chloride, 1 µM bovine serum albumin and 0.05% P20 surfactant (GE Life Sciences), pH 7.4. Contact and dissociation times of at least 300 seconds were used for all proteins. The chip was regenerated after each step with 100 mM glycine, pH 3.0 for 30 s.

Kinetic Measurements – All kinetic measurements were performed in the same manner as SPR unless specified. The chip was coupled in lanes 2 and 4 at 0.33 µg/mL. Protein concentrations ranged from 0.04 µM and 5.12 µM were flowed over the chip at 60 µL/min with a contact time

of 30 s and a dissociation time of 250 s. Bovine serum albumin was not included in the running buffer.

Protein expression for NMR – Freestyle293 medium without amino acids or glucose or osmolarity adjustment was purchased (Life Technologies). This base medium was supplemented with all amino acids at 100 mg/L, with the exception of glutamine, phenylalanine, lysine and tyrosine. Glutamine (1 g/L) and glucose (3 g/L) were added. Next, 100 mg/L [^{15}N]-lysine, [^{15}N]-phenylalanine and [^{15}N]-tyrosine were added. For NMR experiments utilizing ^{13}C, the medium was supplemented with 3 g/L [$^{13}C_U$]-glucose. pH was adjusted to 7.20 before adjusting osmolarity with 5 M NaCl to 260-280 mOsm/kg, followed by a final adjustment of pH to 7.20. The labeled media was passed through a sterile 0.2 µm aPES membrane (Fischer Scientific) and stored at 4 ºC.

Isotope-labeled CD16a for NMR was expressed and diluted with the labeling culture medium using the transfection, dilution and purification methods stated above. TEV was expressed from a plasmid provided by Dr. Kelley Moremen (UGA) in *E. coli* and purified with a Ni-NTA resin. GFP-CD16a was buffer exchanged with 50 mM Tris-HCl, 0.5 mM EDTA, 1 mM dithiothreitol, pH 8.0, then digested with 1:25 (w:w) GFP-CD16a:TEV ratio overnight at room temperature with end-over-end mixing. The following day, the mixture was passed over a Superdex 75 column (GE Health Sciences). Fractions containing CD16a were identified with SDS-PAGE and were subsequently pooled. The protein was buffer exchanged into a buffer containing 20 mM sodium phosphate, 100 mM potassium chloride, 5% D_2O, 0.05 mM

trimethylsilylpropanesulfonate and concentrated to approximately 150 µL using Amicon Ultra 0.5 mL 10 kDa cellulose cartridge.

NMR Spectroscopy – NMR spectra were collected at a 30 ºC sample temperature on a 21.1 T spectrometer equipped with a Bruker NEO console and 5 mm TXO cryoprobe. Direct ^{13}C observe experiments were collected with the hxinepph pulse sequence, with 16384 and 128 complex points in the direct and indirect dimensions, respectively. The Bruker hsqcetfpf3gpsi2 pulse sequence was used to collect ^{1}H-^{15}N correlations with 1024 and 256 complex points in the direct and indirect dimensions, respectively. Spectra were processed with a sine-squared and 40 Hz exponential multiplier line broadening function applied in the direct dimension and a sine function with a 10 Hz exponential multiplier in the indirect dimension. Spectra were processed in NMRPipe (40) and analyzed in NMRViewJ (41).

Acknowledgement

We thank Eric Roush (Cytiva) for help with optimizing SPR experiment parameters.

Funding Sources

Funding to A.W.B. by the National Institutes of Health under Awards No. U01 AI148114 (NIAID). The content is solely the responsibility of the authors and does not necessarily represent the official views of the National Institutes of Health.

Works Cited

1. Chiesa, S., Tomasello, E., Vivier, E., and Vely, F. (2005) Coordination of activating and inhibitory signals in natural killer cells. *Mol Immunol* **42**, 477-484
2. Weiskopf, K., and Weissman, I. L. (2015) Macrophages are critical effectors of antibody therapies for cancer. *MAbs* **7**, 303-310
3. Mahaweni, N. M., Olieslagers, T. I., Rivas, I. O., Molenbroeck, S. J. J., Groeneweg, M., Bos, G. M. J., Tilanus, M. G. J., Voorter, C. E. M., and Wieten, L. (2018) A comprehensive overview of FCGR3A gene variability by full-length gene sequencing including the identification of V158F polymorphism. *Sci Rep* **8**, 15983
4. Lehrnbecher, T., Foster, C. B., Zhu, S., Leitman, S. F., Goldin, L. R., Huppi, K., and Chanock, S. J. (1999) Variant genotypes of the low-affinity Fcgamma receptors in two control populations and a review of low-affinity Fcgamma receptor polymorphisms in control and disease populations. *Blood* **94**, 4220-4232
5. Kastbom, A., Coster, L., Arlestig, L., Chatzidionysiou, A., van Vollenhoven, R. F., Padyukov, L., Rantapaa-Dahlqvist, S., and Saevarsdottir, S. (2012) Influence of FCGR3A genotype on the therapeutic response to rituximab in rheumatoid arthritis: an observational cohort study. *BMJ Open* **2**
6. Bruhns, P., Iannascoli, B., England, P., Mancardi, D. A., Fernandez, N., Jorieux, S., and Daeron, M. (2009) Specificity and affinity of human Fcgamma receptors and their polymorphic variants for human IgG subclasses. *Blood* **113**, 3716-3725
7. Dekkers, G., Treffers, L., Plomp, R., Bentlage, A. E. H., de Boer, M., Koeleman, C. A. M., Lissenberg-Thunnissen, S. N., Visser, R., Brouwer, M., Mok, J. Y., Matlung, H., van

den Berg, T. K., van Esch, W. J. E., Kuijpers, T. W., Wouters, D., Rispens, T., Wuhrer, M., and Vidarsson, G. (2017) Decoding the Human Immunoglobulin G-Glycan Repertoire Reveals a Spectrum of Fc-Receptor- and Complement-Mediated-Effector Activities. *Front Immunol* **8**, 877

8. Hatjiharissi, E., Xu, L., Santos, D. D., Hunter, Z. R., Ciccarelli, B. T., Verselis, S., Modica, M., Cao, Y., Manning, R. J., Leleu, X., Dimmock, E. A., Kortsaris, A., Mitsiades, C., Anderson, K. C., Fox, E. A., and Treon, S. P. (2007) Increased natural killer cell expression of CD16, augmented binding and ADCC activity to rituximab among individuals expressing the Fc{gamma}RIIIa-158 V/V and V/F polymorphism. *Blood* **110**, 2561-2564

9. Binyamin, L., Alpaugh, R. K., Hughes, T. L., Lutz, C. T., Campbell, K. S., and Weiner, L. M. (2008) Blocking NK cell inhibitory self-recognition promotes antibody-dependent cellular cytotoxicity in a model of anti-lymphoma therapy. *J Immunol* **180**, 6392-6401

10. Wu, J., Edberg, J. C., Redecha, P. B., Bansal, V., Guyre, P. M., Coleman, K., Salmon, J. E., and Kimberly, R. P. (1997) A novel polymorphism of FcgammaRIIIa (CD16) alters receptor function and predisposes to autoimmune disease. *J Clin Invest* **100**, 1059-1070

11. Karassa, F. B., Trikalinos, T. A., Ioannidis, J. P., and Fc gamma, R.-S. L. E. m.-a. i. (2003) The Fc gamma RIIIA-F158 allele is a risk factor for the development of lupus nephritis: a meta-analysis. *Kidney Int* **63**, 1475-1482

12. Zhu, X. W., Wang, Y., Wei, Y. H., Zhao, P. P., Wang, X. B., Rong, J. J., Zhong, W. Y., Zhang, X. W., Wang, L., and Zheng, H. F. (2016) Comprehensive Assessment of the

Association between FCGRs polymorphisms and the risk of systemic lupus erythematosus: Evidence from a Meta-Analysis. *Sci Rep* **6**, 31617

13. Hayat, S., Babu, G., Das, A., Howlader, Z. H., Mahmud, I., and Islam, Z. (2020) Fc-gamma IIIa-V158F receptor polymorphism contributes to the severity of Guillain-Barre syndrome. *Ann Clin Transl Neurol* **7**, 1040-1049
14. Saremi, L., Esmaeilzadeh, E., Ghorashi, T., Sohrabi, M., Ekhlasmand Kermani, M., and Kadkhodazadeh, M. (2019) Association of Fc gamma-receptor genes polymorphisms with chronic periodontitis and Peri-Implantitis. *J Cell Biochem*
15. Morales-Lara, M. J., Conesa-Zamora, P., Garcia-Simon, M. S., Pedrero, F., Santaclara, V., Perez-Guillermo, M., and Soriano-Navarro, E. (2010) Association between the FCGR3A V158F polymorphism and the clinical response to infliximab in rheumatoid arthritis and spondyloarthritis patients. *Scand J Rheumatol* **39**, 518-520
16. Shimizu, C., Mogushi, K., Morioka, M. S., Yamamoto, H., Tamura, K., Fujiwara, Y., and Tanaka, H. (2016) Fc-Gamma receptor polymorphism and gene expression of peripheral blood mononuclear cells in patients with HER2-positive metastatic breast cancer receiving single-agent trastuzumab. *Breast Cancer* **23**, 624-632
17. Weng, W. K., and Levy, R. (2003) Two immunoglobulin G fragment C receptor polymorphisms independently predict response to rituximab in patients with follicular lymphoma. *J Clin Oncol* **21**, 3940-3947
18. Moremen, K. W., Tiemeyer, M., and Nairn, A. V. (2012) Vertebrate protein glycosylation: diversity, synthesis and function. *Nat Rev Mol Cell Biol* **13**, 448-462

19. Patel, K. R., Nott, J. D., and Barb, A. W. (2019) Primary Human Natural Killer Cells Retain Proinflammatory IgG1 at the Cell Surface and Express CD16a Glycoforms with Donor-dependent Variability. *Mol Cell Proteomics* **18**, 2178-2190

20. Roberts, J. T., Patel, K. R., and Barb, A. W. (2020) Site-specific N-glycan Analysis of Antibody-binding Fc gamma Receptors from Primary Human Monocytes. *Mol Cell Proteomics* **19**, 362-374

21. Patel, K. R., Roberts, J. T., Subedi, G. P., and Barb, A. W. (2018) Restricted processing of CD16a/Fc gamma receptor IIIa N-glycans from primary human NK cells impacts structure and function. *J Biol Chem* **293**, 3477-3489

22. Subedi, G. P., and Barb, A. W. (2018) CD16a with oligomannose-type N-glycans is the only "low-affinity" Fc gamma receptor that binds the IgG crystallizable fragment with high affinity in vitro. *J Biol Chem* **293**, 16842-16850

23. Hayes, J. M., Frostell, A., Karlsson, R., Muller, S., Martin, S. M., Pauers, M., Reuss, F., Cosgrave, E. F., Anneren, C., Davey, G. P., and Rudd, P. M. (2017) Identification of Fc Gamma Receptor Glycoforms That Produce Differential Binding Kinetics for Rituximab. *Mol Cell Proteomics* **16**, 1770-1788

24. Ferrara, C., Grau, S., Jager, C., Sondermann, P., Brunker, P., Waldhauer, I., Hennig, M., Ruf, A., Rufer, A. C., Stihle, M., Umana, P., and Benz, J. (2011) Unique carbohydrate-carbohydrate interactions are required for high affinity binding between FcgammaRIII and antibodies lacking core fucose. *Proc Natl Acad Sci U S A* **108**, 12669-12674

25. Mizushima, T., Yagi, H., Takemoto, E., Shibata-Koyama, M., Isoda, Y., Iida, S., Masuda, K., Satoh, M., and Kato, K. (2011) Structural basis for improved efficacy of therapeutic antibodies on defucosylation of their Fc glycans. *Genes Cells* **16**, 1071-1080

26. Falconer, D. J., Subedi, G. P., Marcella, A. M., and Barb, A. W. (2018) Antibody Fucosylation Lowers the FcgammaRIIIa/CD16a Affinity by Limiting the Conformations Sampled by the N162-Glycan. *ACS Chem Biol* **13**, 2179-2189

27. Varadi, M., Anyango, S., Deshpande, M., Nair, S., Natassia, C., Yordanova, G., Yuan, D., Stroe, O., Wood, G., Laydon, A., Zidek, A., Green, T., Tunyasuvunakool, K., Petersen, S., Jumper, J., Clancy, E., Green, R., Vora, A., Lutfi, M., Figurnov, M., Cowie, A., Hobbs, N., Kohli, P., Kleywegt, G., Birney, E., Hassabis, D., and Velankar, S. (2022) AlphaFold Protein Structure Database: massively expanding the structural coverage of protein-sequence space with high-accuracy models. *Nucleic Acids Res* **50**, D439-D444

28. Cambay, F., Forest-Nault, C., Dumoulin, L., Seguin, A., Henry, O., Durocher, Y., and De Crescenzo, G. (2020) Glycosylation of Fcgamma receptors influences their interaction with various IgG1 glycoforms. *Mol Immunol* **121**, 144-158

29. Reeves, P. J., Callewaert, N., Contreras, R., and Khorana, H. G. (2002) Structure and function in rhodopsin: high-level expression of rhodopsin with restricted and homogeneous N-glycosylation by a tetracycline-inducible N-acetylglucosaminyltransferase I-negative HEK293S stable mammalian cell line. *Proc Natl Acad Sci U S A* **99**, 13419-13424

30. Chen, W., Enck, S., Price, J. L., Powers, D. L., Powers, E. T., Wong, C. H., Dyson, H. J., and Kelly, J. W. (2013) Structural and energetic basis of carbohydrate-aromatic packing interactions in proteins. *J Am Chem Soc* **135**, 9877-9884

31. Yogo, R., Yanaka, S., and Kato, K. (2018) Backbone (1)H, (13)C, and (15)N assignments of the extracellular region of human Fcgamma receptor IIIb. *Biomol NMR Assign* **12**, 201-204

32. Yamaguchi, Y., Kato, K., Shindo, M., Aoki, S., Furusho, K., Koga, K., Takahashi, N., Arata, Y., and Shimada, I. (1998) Dynamics of the carbohydrate chains attached to the Fc portion of immunoglobulin G as studied by NMR spectroscopy assisted by selective 13C labeling of the glycans. *J Biomol NMR* **12**, 385-394

33. Rogals, M. J., Yang, J. Y., Williams, R. V., Moremen, K. W., Amster, I. J., and Prestegard, J. H. (2021) Sparse isotope labeling for nuclear magnetic resonance (NMR) of glycoproteins using 13C-glucose. *Glycobiology* **31**, 425-435

34. Barb, A. W., Falconer, D. J., and Subedi, G. P. (2019) The Preparation and Solution NMR Spectroscopy of Human Glycoproteins Is Accessible and Rewarding. *Methods Enzymol* **614**, 239-261

35. Subedi, G. P., Falconer, D. J., and Barb, A. W. (2017) Carbohydrate-Polypeptide Contacts in the Antibody Receptor CD16A Identified through Solution NMR Spectroscopy. *Biochemistry* **56**, 3174-3177

36. Sakae, Y., Satoh, T., Yagi, H., Yanaka, S., Yamaguchi, T., Isoda, Y., Iida, S., Okamoto, Y., and Kato, K. (2017) Conformational effects of N-glycan core fucosylation of

immunoglobulin G Fc region on its interaction with Fcgamma receptor IIIa. *Sci Rep* **7**, 13780

37. Stewart, R., Thom, G., Levens, M., Guler-Gane, G., Holgate, R., Rudd, P. M., Webster, C., Jermutus, L., and Lund, J. (2011) A variant human IgG1-Fc mediates improved ADCC. *Protein Eng Des Sel* **24**, 671-678

38. Subedi, G. P., Johnson, R. W., Moniz, H. A., Moremen, K. W., and Barb, A. (2015) High Yield Expression of Recombinant Human Proteins with the Transient Transfection of HEK293 Cells in Suspension. *J Vis Exp*, e53568

39. Subedi, G. P., Hanson, Q. M., and Barb, A. W. (2014) Restricted motion of the conserved immunoglobulin G1 N-glycan is essential for efficient FcgammaRIIIa binding. *Structure* **22**, 1478-1488

40. Delaglio, F., Grzesiek, S., Vuister, G. W., Zhu, G., Pfeifer, J., and Bax, A. (1995) NMRPipe: a multidimensional spectral processing system based on UNIX pipes. *J Biomol NMR* **6**, 277-293

41. Johnson, B. A. (2004) Using NMRView to visualize and analyze the NMR spectra of macromolecules. *Methods Mol Biol* **278**, 313-352

Table 2.1 CD16a Binding affinities averaged from at least five individual measurements.

Allotype	N-Glycoform	K_D (nM)	error (nM)
V158	Complex	270	40
V158	Man5	86	13
V158	(1)GlcNAc	22	3
V158	S164A	230	40
F158	Complex	1660	150
F158	Man5	1070	120
F158	(1)GlcNAc	126	16
F158	S164A	1470	100

Table 2.2. Kinetic parameters from a two-state binding model.

							error			
Protein	N-glycoform	k_a1 (1/Ms)	k_a2 (1/s)	k_d1 (1/s)	k_d2 (1/s)	K_D (nM)	k_a1 (1/Ms)	k_a2 (1/s)	k_d1 (1/s)	k_d2 (1/s)
V158	Complex-type	1.7E+05	6.1E-03	2.5E-02	6.6E-03	76	0.65%	0.67%	0.84%	0.25%
V158	Man5	7.1E+05	4.9E-03	7.1E-02	6.0E-03	55	0.72%	0.33%	0.78%	0.17%
V158 S164A	Complex-type	1.4E+06	1.4E-03	1.8E-01	7.8E-03	109	0.82%	0.64%	0.85%	0.51%
V158	(1)GlcNAc	2.5E+06	3.2E-03	4.0E-02	4.7E-03	9.2	0.81%	0.90%	1.01%	0.52%
F158	(1)GlcNAc	1.1E+06	1.8E-03	7.9E-02	5.0E-03	52	1.81%	0.91%	1.94%	0.72%

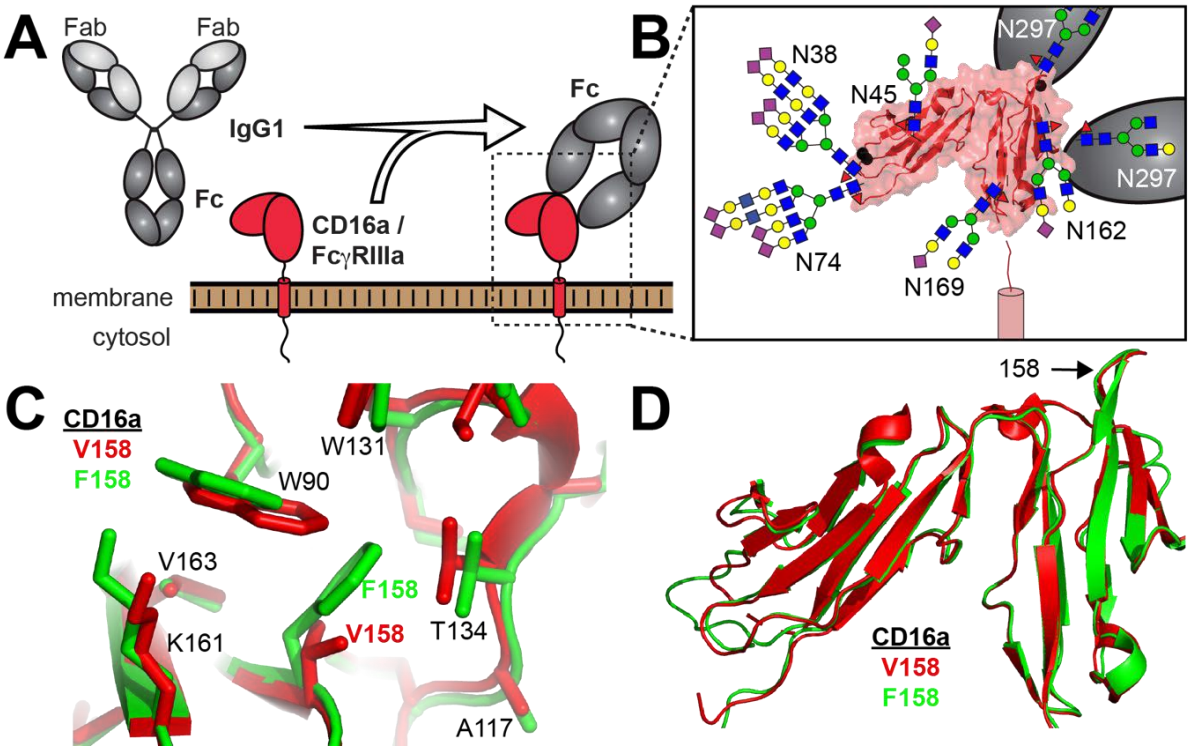

Figure 2.1. Two common receptor allotypes in the human genome differ by a single amino acid substitution at position 158 in the extracellular antibody-binding domain. **A**. CD16a / Fc γ receptor (FcγR) IIIa binds the crystallizable fragment (Fc) of immunoglobulin G1 (IgG1) **B**. CD16a is heavily N-glycosylated with five N-glycans. The predominant glycoforms identified on primary human natural killer cells are shown as cartoons and scaled to the appropriate size. Fc is likewise glycosylated at N297. An overlay of the CD16a V158 structure (*red*, pdb 5vu0) with an AlphaFold model of CD16a F158 (*green*) shows residues surrounding the 158 position (**C**.) and the global structural similarity (**D**.).

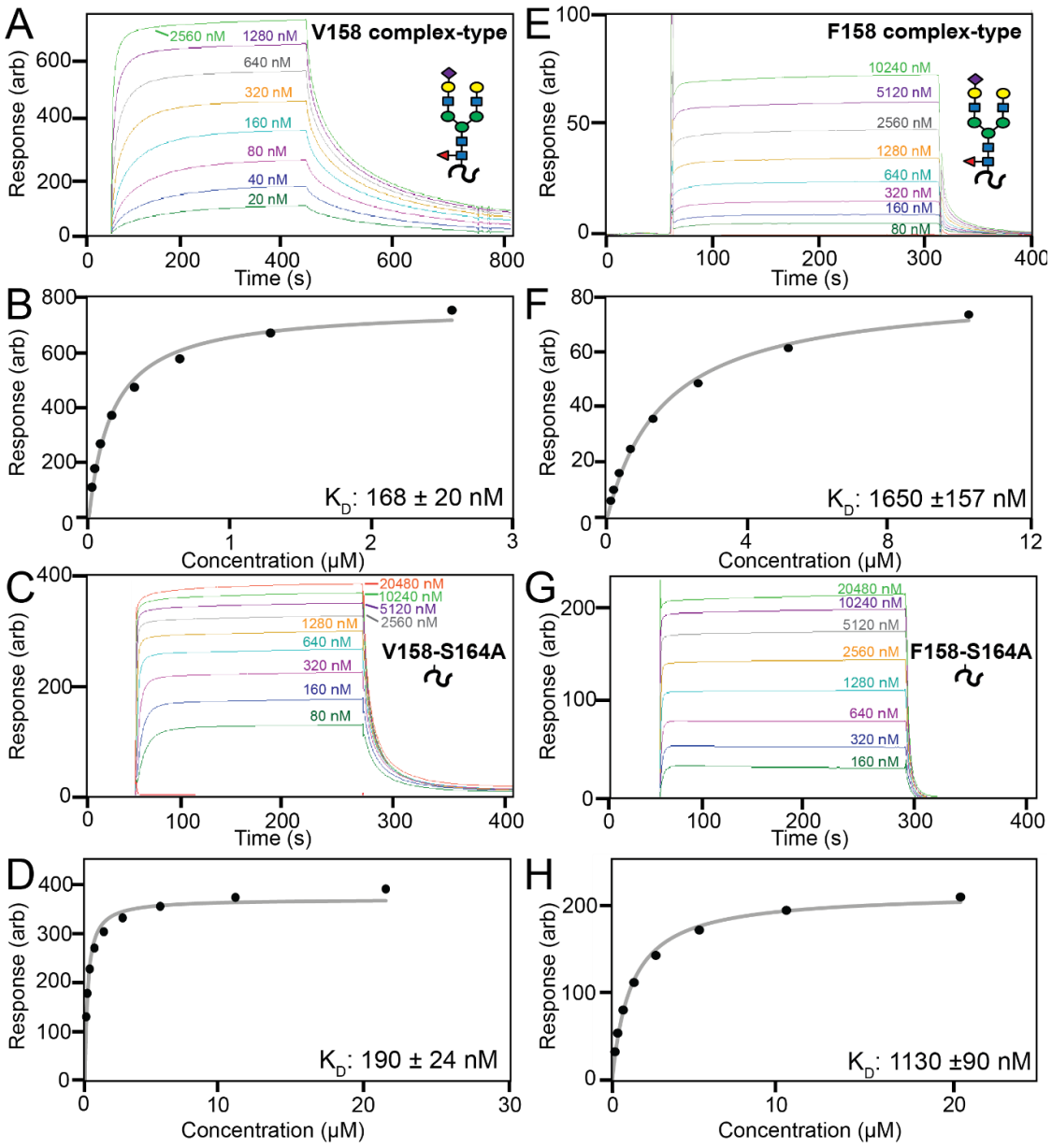

Figure 2.2. Representative surface plasmon resonance (SPR) sensorgrams of CD16a allotypes with either complex-type glycans (A,E) or missing the N162 glycan (C,G). Fits of the dissociation constants and associated errors from equilibrium binding measurements are also shown (B,D,F,H). Cartoons show the expected N-glycan at the N162 site. The S164A mutation disrupts the N162 N-glycan sequon and thus lacks an N-glycan at that site.

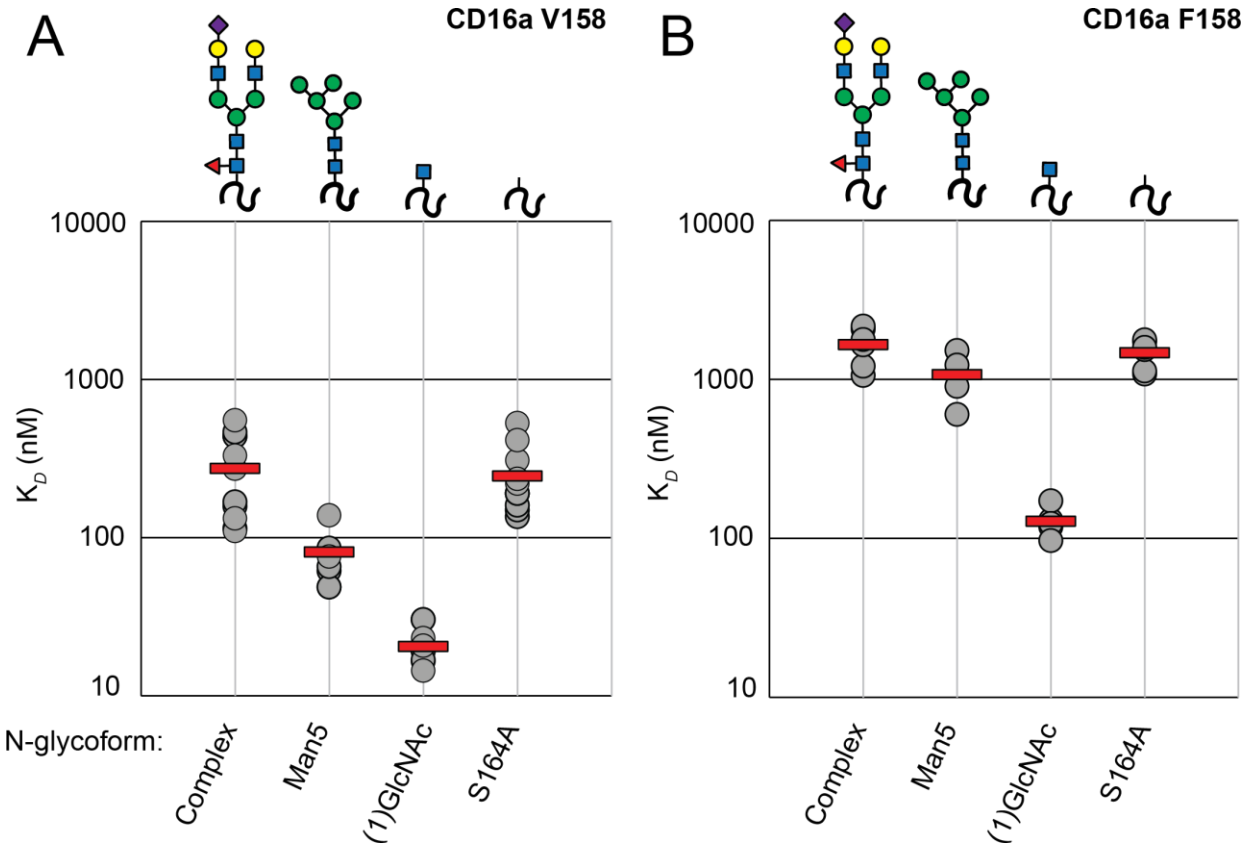

Figure 2.3. Affinity of each CD16a allotype glycoform. Each mean (horizontal *red* bar) represents a minimum of five individual measurements (*grey* circles). Glycan representations reflect the modification at the N162 site.

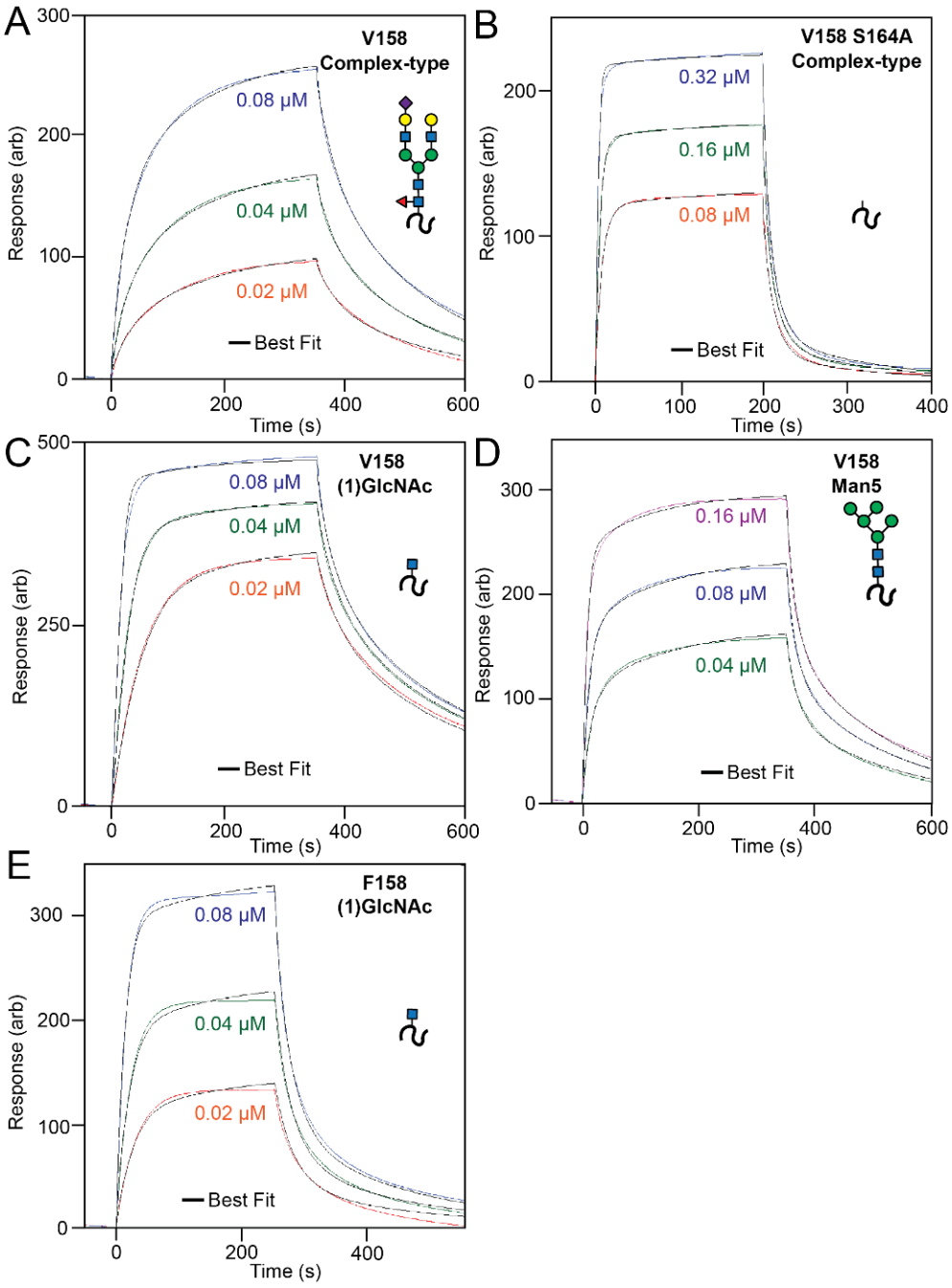

Figure 2.4. Binding kinetics show different rates for the glycoform and allotype variants. IgG1 Fc binding (**A**) CD16a V158 with complex-type N-glycans, (**B**) CD16a V158 S164A with complex-type N-glycans, (**C**) CD16a V158 with truncated (1)GlcNAc N-glycans, or (**D**) with

Man5 glycans. (**E**) CD16a F158 with (1)GlcNAc N-glycans. Sensorgrams were fitted with a two-state kinetic model (*black* line). Cartoons show the expected N-glycan at the N162 site

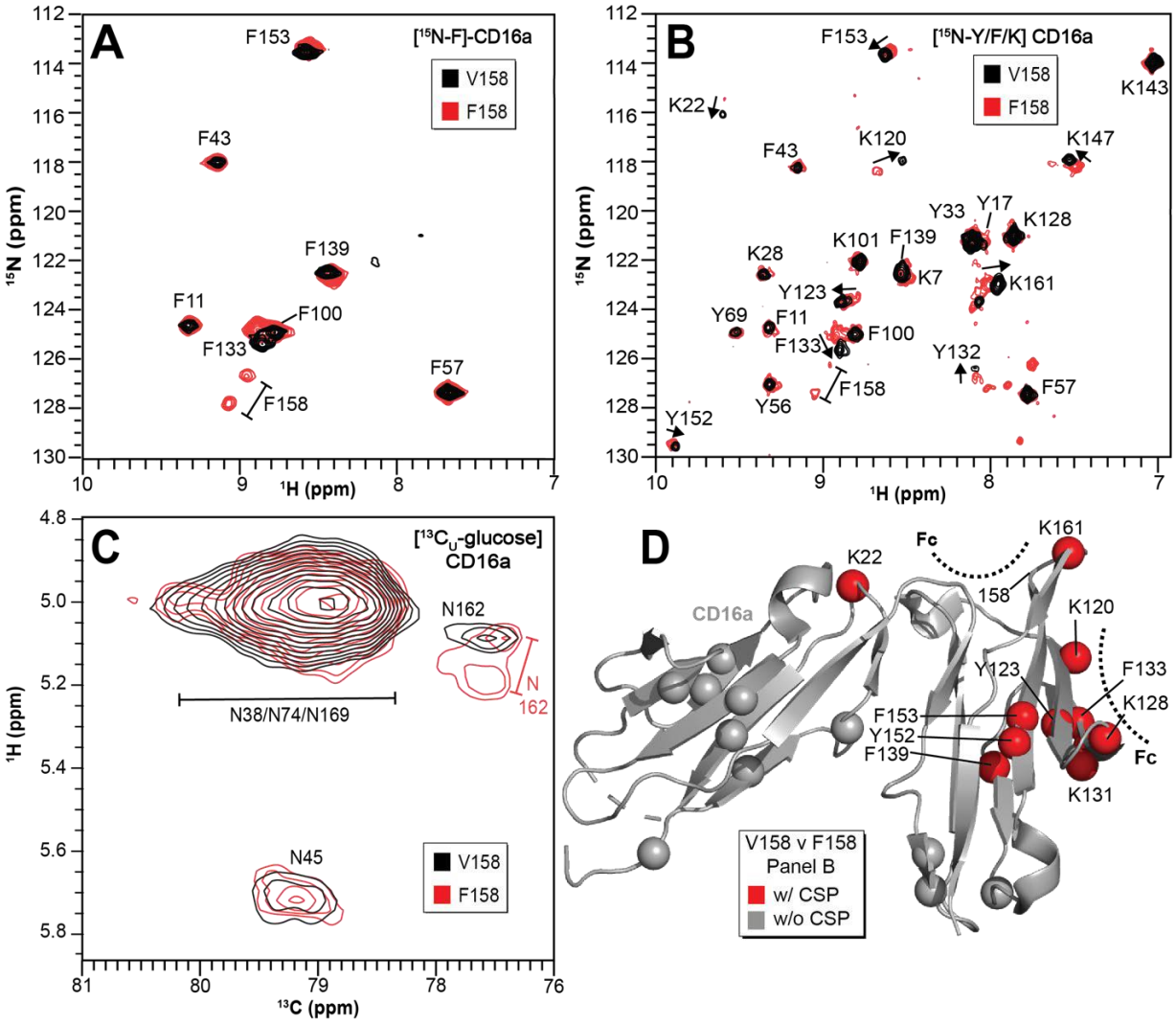

Figure 2.5. NMR spectroscopy of the CD16a allotypes. (A) Overlay of HSQC-TROSY spectra for [^{15}N-phenylalanine]-labeled CD16a collected at 30 ºC and 21.1T. (B) Overlay of HSQC-TROSY spectra for [^{15}N-phenylalanine/lysine/tyrosine]-labeled CD16a. (C) Overlay of ^{1}H-(^{13}C direct observe) spectra of [^{13}C-glucose]-labeled CD16a showing the region corresponding to the (1)GlcNAc $^{1}H_1$-$^{13}C_1$ correlation. (D) Mapping residues with different positions (*red* spheres) and similar positions (*grey* spheres) from panel (B) onto a structure of CD16a. The IgG1 Fc binding interface is shown with *dashed* lines.

Supplemental Table 2.1. CD16a affinities relative to the complex-type glycoform

	Complex-type	Man5	(1)GlcNAc	S164A
V158	1.0	3.4	13	1.1
F158	1.0	1.6	13	1.1

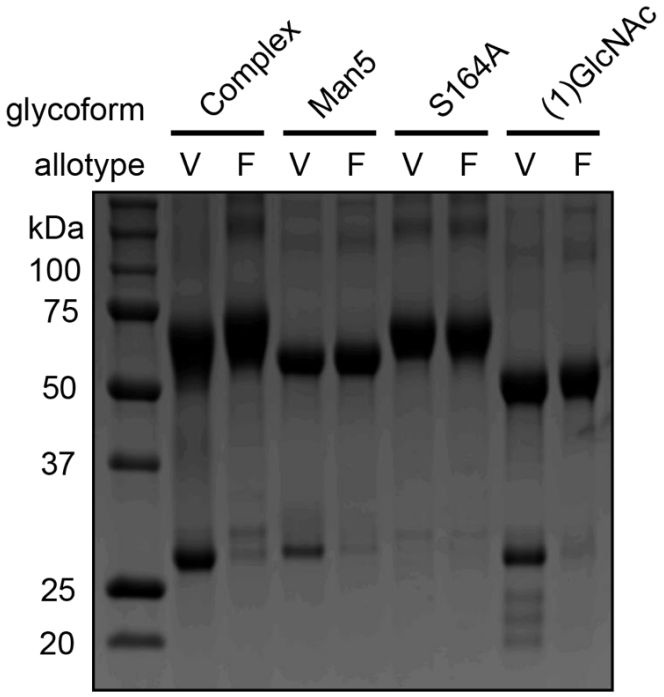

Supplemental Figure 2.1. SDS-PAGE of GFP-srCD16a fusions. The two different allotypes are expressed with four different glycosylation patterns. Distinct shifts in migration are observed between each type of glycosylated protein.

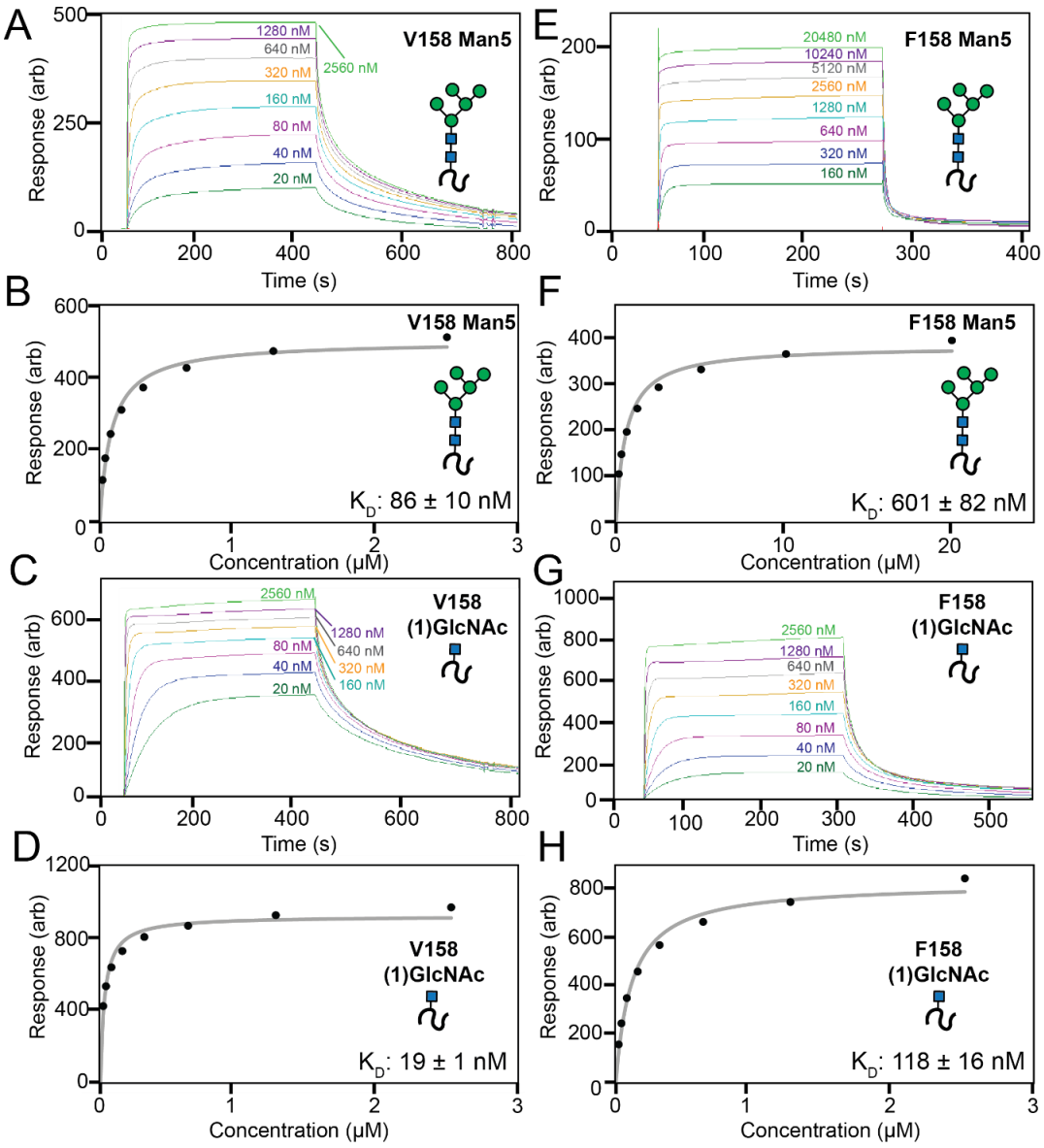

Supplemental Figure 2.2. Representative surface plasmon resonance (SPR) sensorgrams of CD16a allotypes with either Man5 oligomannose N-glycans (A,E) or (1)GlcNAc N-glycans (C,G). Fits of the dissociation constants and associated errors from equilibrium binding measurements are also shown (B,D,F,H). Cartoons show the expected N-glycan at the N162 site.

CHAPTER 3

ONE N-GLYCAN REGULATES NATURAL KILLER CELL ANTIBODY-DEPENDENT CELL-MEDIATED CYTOTOXICITY AND MODULATES FC γ RECEPTOR IIIA / CD16A STRUCTURE[1]

[1]Kremer, Paul G., Lampros, Elizabeth A., Blocker, Allison M., & Barb, Adam W. 2024. Submitted to *Elife*, June 15th, 2024

Abstract

Both endogenous antibodies and a subset of antibody therapeutics engage Fc gamma receptor (FcγR)IIIa / CD16a to stimulate a protective immune response. Increasing the FcγRIIIa/IgG1 interaction improves the immune response and thus represents a strategy to improve therapeutic efficacy. FcγRIIIa is a heavily glycosylated receptor and glycan composition affects antibody-binding affinity. Though our laboratory previously demonstrated that natural killer (NK) cell N-glycan composition affected the potency of one key protective mechanism, antibody-dependent cell-mediated cytotoxicity (ADCC), it was unclear if this effect was due to FcγRIIIa glycosylation. Furthermore, the structural mechanism linking glycan composition to affinity and cellular activation remained undescribed. To define the role of individual amino acid and N-glycan residues we measured affinity using multiple FcγRIIIa glycoforms. We observed stepwise affinity increases with each glycan truncation step with the most severely truncated glycoform displaying the highest affinity. Removing the N162 glycan demonstrated its predominant role in regulating antibody-binding affinity, in contrast to four other FcγRIIIa N-glycans. We next evaluated the impact of the N162 glycan on NK cell ADCC. NK cells expressing the FcγRIIIa V158 allotype exhibited increased ADCC following kifunensine treatment to limit N-glycan processing. Notably, an increase was not observed with cells expressing the FcγRIIIa V158 S164A variant that lacks N162 glycosylation, indicating the N162 glycan is required for increased NK cell ADCC. To gain structural insight into the mechanisms of N162 regulation, we applied a novel protein isotope labeling approach in combination with solution NMR spectroscopy. FG loop residues proximal to the N162 glycosylation site showed large chemical shift perturbations following glycan truncation. These data support a model for the regulation of

FcγRIIIa affinity and NK cell ADCC whereby composition of the N162 glycan stabilizes the FG loop and thus the antibody-binding site.

Introduction

Natural killer (NK) cells rapidly respond to destroy tissue coated with antibodies. This protective mechanism, termed antibody-dependent cell-mediated cytotoxicity (ADCC), is likewise exploited by many therapeutic monoclonal antibodies (mAbs) recognizing specific epitopes that escape detection by endogenous antibodies. However, NK cell ADCC elicited both by endogenous antibodies and mAbs fails to ameliorate disease in many patients. There is sufficient evidence to expect that increased NK cell ADCC will improve patient responses though few strategies exist to achieve this outcome.

NK cells require binding of antibodies to only a single receptor type, Fc gamma receptor IIIa (FcγRIIIa/CD16a), to elicit ADCC. Multiple lines of evidence support the role of increased antibody-binding affinity in improved NK cell responses. NK cells expressing the higher affinity FcγRIIIa V158 allotype demonstrate greater ADCC than those expressing the weaker-binding F158 allotype (hereafter referred to as V158F) [1-4]. Furthermore, improving the FcγRIIIa-binding affinity of antibodies, which bind through the Fc region, likewise increases ADCC and therapeutic potency [5-7]. Antibody engineering efforts have been widely explored to improve ADCC by increasing FcγRIIIa engagement, however, substantially less is known about structural mechanisms that affect FcγRIIIa function.

Our laboratory identified an unexpected strategy to increase FcγRIIIa affinity. We determined that FcγRIIIa glycosylation affected antibody-binding affinity, with oligomannose-type N-glycans providing higher affinity interactions [8,9]. Oligomannose N-glycans are minimally-remodeled forms that are not expected at high percentages on secreted proteins in contrast to highly remodeled complex-type glycans found on most serum glycoproteins [10].

Among the five FcγRIIIa N-glycosylation sites, the composition of the glycan at N162 is responsible for increased antibody-binding affinity and is located near the interface formed with the antibody Fc [9,11]. Furthermore, we identified a high degree of glycan compositional heterogeneity at the N162 site on FcγRIIIa purified from NK cells of healthy human donors including both complex-type and oligomannose glycoforms [12-14]. The N162 glycan heterogeneity on NK cells is reflected in the presence of both high-affinity and low-affinity FcγRIIIa forms in the periphery of healthy donors, with high affinity forms more abundant in adult donors compared to children [15].

We likewise demonstrated that NK cell N-glycan processing reduced ADCC potency. NK cells with limited N-glycan remodeling capability, following either treatment with kifunensine or knockdown of the bottleneck glycan processing enzyme MGAT1, demonstrated increased ADCC [15,16]. These studies, however, did not determine that FcγRIIIa N-glycan processing, nor the composition of the N162 glycan, mediated the increased ADCC. It is equally possible that this role is mediated by other NK cell glycans, of which hundreds are expected. Demonstration of the role of the N162 glycan in ADCC is expected to promote improved ADCC responses through efforts to tune glycan composition of endogenous NK cells or infused NK cells. Furthermore, such a demonstration is expected to promote FcγRIIIa engineering to increase ADCC beyond levels available from endogenous NK cells and naturally-occurring FcγRIIIa variants.

Here we investigate the N162 glycan's role in FcγRIIIa structure, antibody-binding affinity and NK cell ADCC. We performed a mutational screen to identify FcγRIIIa residues that mediate antibody binding affinity and sensitivity to the N-glycan composition. Introducing a

subset of these FcγRIIIa variants, displaying a range of affinities, into cytotoxic NK cells provided insight into the relationship between antibody-binding affinity and ADCC. We then defined the impact of N162 glycan composition on NK cell ADCC and FcγRIIIa structure. As a result, we define a link between the N162 glycan composition and NK cell ADCC.

Results

FcγRIIIa affinity impacts ADCC

The FcγRIIIa V158 allotype (hereafter referred to as the wildtype) binds ~4-fold tighter than the more common V158F allotype and NK cells expressing the wildtype likewise exhibit greater ADCC [1,17], however, beyond these two points the relationship between FcγRIIIa affinity and ADCC remains undefined [18]. A positive correlation between affinity and ADCC would indicate improved NK-cell mediated therapies may result from increasing the FcγRIIIa antibody-binding affinity beyond that of the wild type. To evaluate this relationship, we generated a library of FcγRIIIa proteins with mutations at the antibody-binding interface to increase the range of affinities. The resulting FcγRIIIa proteins revealed a wide range of affinities between slightly higher than wild type (S164A) to a handful with no apparent binding to 2.5 μM fucosylated IgG1 Fc (Y132S, W90A, W113A; **Figure 3.1A, Table S3.1**). Mapping the impact of these mutations onto a FcγRIIIa structural model identified two key regions consistent with empirically-derived structural models of the antibody:receptor complex [11], though our data provide greater detail showing how each residue affects affinity. These two regions center around Y132 and a pair of tryptophan residues (W90 and W113) which overlaps with the contact interface identified by X-ray crystallography (**Figure 3.1B**). Surprisingly, although the K161A mutation reduces affinity by 10-fold, mutating adjacent residues including S160 showed little

direct impact on affinity. It was likewise surprising that the solvent-exposed, large hydrophobic side chains of F153 and I88 minimally impacted affinity (<2 fold). A majority of the mutations only impacted affinity by 3-fold or less.

We next evaluated the impact of FcγRIIIa mutations on ADCC potency. We transduced cytotoxic YTS NK cells to express a subset of FcγRIIIa variants from our affinity screen, encompassing a broad affinity range, using lentivirus to establish stable cytotoxic NK cell lines. Each YTS cell line displayed comparable FcγRIIIa expression, however at levels somewhat reduced from the original YTS-FcγRIIIa cell line provided by Dr. Mace (Columbia U., **Figure S3.1**). A comparison of the original YTS-FcγRIIIa (V158) cells and our transduced YTS cell line expressing the same wildtype receptor showed greater expression and greater ADCC from the original YTS-FcγRIIIa cell line likely resulting from our cell isolation strategy that selected only for GFP+ cells rather than FcγRIIIa expression. Within our library, YTS cells expressing the FcγRIIIa S164A variant displayed the highest average ADCC and the tryptophan mutants showed no detectable ADCC, indicating higher affinity leads to higher ADCC (**Figure 3.1C**). A plot of the affinity for each variant versus the ADCC potency demonstrated a trend linking high affinity and greater ADCC. These results indicate that greater FcγRIIIa antibody-binding affinity on NK cells increases ADCC and FcγRIIIa engineering represents an unexplored avenue to improve NK cell-mediated immunotherapies.

<u>The FcγRIIIa N162-glycan is required for high affinity interactions with afucosylated IgG</u>

Because affinity is a key determinant of ADCC potency, we further explored FcγRIIIa changes that affect affinity and to identify variants with altered sensitivity to IgG1 Fc glycan

composition. Shields et al. previously showed that antibody fucosylation reduces affinity for FcγRIIIa [19] and it is known that the N162 glycan mediates the response to fucose, though the underlying mechanism remains disputed [20-23]. We identified FcγRIIIa residues within the contact distance of the N162 glycan to explore the impact of proximal residues to antibody fucosylation. We next evaluated mutations at each contact site using both the wild type and S164A variant that prevents N162 glycosylation. These variants largely exhibited decreased affinity compared with the wild type FcγRIIIa when evaluated against fucosylated IgG1 Fc (**Figure 3.2A**). Surprisingly, each variant displayed reduced sensitivity to fucose when the N162 glycan was absent. The impact of fucose reduced from a 2.2-fold average effect when the N162 glycan was present to a 1.3-fold change when the N162 glycan was absent (**Figure 3.2B**). Most variants bound afucosylated IgG1 Fc with weaker affinity. The F153S and R155S variants lacking the N162 glycan are notable outliers in that both bind antibody glycoforms with higher affinity than the wild type. These data also are consistent with the hypothesis that intermolecular glycan-glycan contacts provide minimal stability to the antibody/receptor complex because higher affinity was achieved by removing the N162 glycan. In summary, this result demonstrates that the sensitivity to antibody fucosylation may be eliminated through FcγRIIIa engineering while preserving antibody-binding affinity.

N-glycan truncations reveal how each residue contributes to affinity.

In addition to glycan composition of the IgG1 Fc ligand affecting affinity, composition of the FcγRIIIa glycans likewise impacts antibody-binding affinity [8,9]. It is tempting to conclude from the preceding study that higher affinity interactions can be achieved through removing the

N162 glycan entirely, however, our previous work showed that truncating the glycan to a single (1)GlcNAc residue provides superior affinity though it was unclear if these changes mapped to the N162 site [18]. It is also possible that glycoforms slightly longer than the (1)GlcNAc truncated form provide even greater affinity though this possibility remained untested. To identify which N-glycan residues affected affinity, we treated recombinant FcγRIIIa with a series of glycosidases to sequentially remove terminal sugars from the non-reducing end. We observed a step-wise increase in affinity following the removal of each type of terminal sugar (**Figure 3.2C**, left panel). Removing the core α-linked mannose or sialic acid residues showed the greatest change for a single removal step, increasing affinity by 5-fold or 2-fold respectively. Overall, glycan truncation was observed to decrease K_D by 12-fold. To evaluate the individual impact of the N162 glycan, we next truncated glycans of the S164A variant that lacks N162 glycosylation but retains four other N-glycans (**Figure 3.2B**, right panel). While the S164A affinities followed the same trend as the wild type, the changes were substantially smaller in magnitude with only a 4-fold overall change. The removal of the core α-linked mannose residues increased affinity by less than 1.5-fold, in contrast to the 5-fold increase observed for the wild type. These results demonstrate the primary contribution of the N162 glycan composition to antibody-binding affinity, with smaller contributions from N-glycans at the remaining four sites. Furthermore, these data demonstrate the negative impact of adding additional residues throughout the processing pathway, further indicating that N-glycan processing inhibits antibody-binding affinity.

The FcγRIIIa N162 glycan is required for increased ADCC potency following kifunensine treatment.

The data above demonstrate the impact of FcγRIIIa N162 glycan composition on antibody-binding affinity. Furthermore, our lab previously showed that inhibiting NK cell glycan processing, and thus FcγRIIIa processing, increased ADCC potency [15,16]. However, these studies did not determine that composition of the FcγRIIIa N162 glycan affected ADCC potency. We expect that the FcγRIIIa N162 glycan composition that was shown to mediate high affinity interactions with IgG1 Fc likewise is required for the potent ADCC observed following blockage of NK cell N-glycan processing [9,16]. To evaluate the role of N162 glycosylation in NK cell ADCC, we treated our FcγRIIIa-expressing YTS NK cell lines from **Figure 3.1C** with kifunesine, an inhibitor of N-glycan processing that specifically reduced YTS cell N-glycan processing [15]. As expected based on our lab's previous work, the YTS cells expressing the FcγRIIIa wild type demonstrated increased ADCC following kifunesine treatment (**Figure 3.3**). Cells expressing the V158F variant likewise demonstrated a 2-fold ADCC increase following kifunensine treatment. We observed a similar result for YTS cells expressing the T167Y variant. However, YTS FcγRIIIa cells lacking only the N162 glycan through the S164A mutation demonstrated no increase following kifunensine treatment. Notably, the wild type, V158F and T167Y variants all contain the N162 glycan but only S164A does not, thus, the N162 glycan is required for increased ADCC potency following kifunensine treatment.

We next evaluated afucosylated antibodies in combination with kifunensine in our cell lines, having previously demonstrated afucosylated antibodies acted synergistically with kifunensine treatment to increase NK cell ADCC [16]. The YTS cells expressing wild type

FcγRIIIa evaluated with afucosylated antibody showed a significant increase following kifunensine treatment compared to those evaluated with the fucosylated antibody (**Figure 3.3**). Notably, we observed no further benefit for the S164A variant with afucosylated antibodies. This result indicates that the N162 glycan is a critical mediator of increased ADCC responses following inhibiting both NK cell glycan remodeling and antibody fucosylation.

FcγRIIIa backbone resonance assignment

Having demonstrated the role for the FcγRIIIa N162 glycan in antibody binding affinity and NK cell ADCC, we next evaluated how glycan composition affects FcγRIIIa structure to identify regions of the protein that modulate affinity. We probed the effect of N-glycan composition using solution NMR spectroscopy, a technique that evaluates FcγRIIIa structure in dilute solutions and can identify the impact of highly mobile elements including disordered loops, N and C termini, and glycans. First, individual peaks in the NMR spectra must be assigned to unique atoms in the protein to evaluate structural changes with atomic resolution. N-glycoproteins, including FcγRIIIa, represent a significant challenge for NMR spectroscopy due to exceptional line broadening and thus signal loss resulting from the presence of extended N-glycans that slow molecular tumbling. As a result of these physical limitations, N-glycoproteins are seldom investigated by NMR despite their prevalence in the human proteome (22% of the human proteome enters the secretory pathway and contains an N-glycosylation site). Broad spectral lines dramatically limit the quality of multi-dimensional spectra required for the standard resonance assignment strategies, preventing the collection of CB frequencies that provide a high degree of amino acid discrimination.

To surmount these limitations, we first increased tumbling and thus spectral quality by mutating three of the five N-glycosylation sites, retaining N-glycans at N45 and N162 that stabilize antibody binding and solubility [9]. The spectrum of the FcγRIIIa N38Q/N74Q/N169Q variant with two N-glycans improved and peak positions proved highly comparable to those from FcγRIIIa with five N-glycans. Next, we simplified the assignment problem by defining the amino acid type for many peaks in the spectrum through specific amino acid labeling. Our strategy supplements the HEK293F growth medium with individual [^{15}N]-labeled amino acids [24], and provided residue information for 13 types (C,F,G,H,I,K,N,R,S,T,V,W,Y; an example spectrum is shown in **Figure S3.2**). These residue-type assignments guided the definition of residue connections, and thus the backbone assignment, in three-dimensional HNCA and HN(CO)CA spectra. Carbonyl carbon resonances were then assigned using an HNCO experiment. As a result, we assigned a high percentage of the backbone resonances (87% N, 90% HN, 86% CO, 86% CA) and almost all the peaks in the 2d HSQC-TROSY spectrum (**Figure 3.4AB**). This resonance assignment is suitable for interpreting structural changes associated with changing the N-glycan composition and represents a significant triumph due to the challenges associated with glycoprotein NMR. To our knowledge, this is the only NMR resonance assignment of a glycoprotein with two N-glycans attached. A small handful of assignments exist for proteins with one N-glycan, notably CD2 and the Fc region of IgG1 (a thermostable dimer) [25,26].

A comparison of the peak positions between the FcγRIIIa assignment and a previous assignment of the similar FcγRIIIb protein reveals a high degree of overlap but a few notable differences (**Figure 3.4C**). These two proteins differ by eight amino acids, though FcγRIIIb was

expressed in *E. coli* and thus is not glycosylated [27]. Two notable differences occur at C71 and C110 that are distinguished in the HNCA and HN(CO)CA spectra support this assignment (**Figure S3.3**). Surprisingly, the N-glycosylation of the N45 and N162 residues revealed minimal impact on the backbone peak positions for these asparagine residues. A few other differences emerged in regions near amino acid differences, notably position 18 and the contact region of ~80-99, as well as 38, 129 140 and 169. We previously defined local structural differences resulting from substitution at position 129 using X-ray crystallography that are consistent with this NMR-based analysis [28].

FcγRIIIa N-glycan composition affects the structure of the antibody-binding site

We applied our protein labeling approach and backbone resonance assignment to define individual FcγRIIIa atoms that experience different environments based on N-glycan composition. We expressed three FcγRIIIa glycoforms with six [^{15}N]-labeled amino acids to introduce probes throughout the polypeptide (**Figure 3.5A, Figure S3.4**). The spectra showed dispersed peaks that revealed differences between different glycoforms (**Figure 3.5C**). A few residues showed evidence for the sampling of multiple conformations, notably V158 and K161. These residues are located on the FG loop that contains the N162 glycan. The peaks simplify as the glycan becomes shorter, up to the point of a single peak observed for V158 with the (1)GlcNAc glycoform that may indicate either sampling of a single conformation or more rapid exchange between two or more conformations.

Mapping the chemical shift perturbations to the primary sequence revealed residues proximal to the five N-glycosylation sites when comparing the receptor with complex-type

glycans to that with Man5 N-glycans (**Figure 3.5DE**). Truncation to the (1)GlcNAc glycoform caused greater changes to the regions around the N45 and N162 glycans (**Figure 3.5DF**). These data likely indicate a change in the FcγRIIIa conformation sampled by residues near the FG loop, and potentially changes in the orientation between the two extracellular domains as chemical shift differences likewise map to regions near the connection between these two domains. Features associated with the (1)GlcNAc spectra represent conformations that promote higher affinity interactions, as this glycoform binds antibody with the greatest affinity of those evaluated. We anticipate that these conformations are sampled by these residues on the surface of natural killer cells, and the conformational sampling on the cell surface is dictated by the N162 glycan composition.

Evidence supporting distinct conformations of the FcγRIIIa FG loop

Solution NMR evidence identified differential FcγRIIIa conformational sampling, particularly residues in the FG loop, and is supported by the appearance of distinct conformations identified by X-ray crystallography. A recent structure isolated one conformation of the FG loop that differed from those previously observed, mostly through structures bound to IgG1 Fc [11,23,29]. In this recent structure of glycosylated FcγRIIIa, the FG loop is free from contacts with the Fc ligand or with the crystal lattice, revealing a conformation that is sterically prohibited in the complex with antibody (**Figure 3.6A**). To bind, the N162 glycan and the FG loop must reorient to avoid steric clashes with IgG1 Fc. The backbone conformation of the supporting beta strands shows minimal displacement, though larger backbone deviations are observed for the L157, K161 and S164 residues (**Figure S3.5**). The presence of these distinct conformations is

supported by the NMR spectra showing two peaks, including V158 and K161 (**Figure 3.5C**). We investigated conformational sampling further with 1 μs all-atom MD simulations and found the presence of both conformations identified by X-ray crystallography in trajectories of FcγRIIIa with complex-type or Man5 N-glycans (**Figure 3.6B**). These simulations were initialized with a starting structure representing the bound state-conformation but sampled both conformations throughout the experiment. One notable detail from these simulations was the formation of non-covalent interactions between the aliphatic portion of the R155 sidechain with the hydrophobic surface of the (1)GlcNAc residue in the ligand-bound conformation that were absent in the unliganded conformation. To evaluate the importance of this interaction, we measured the binding affinity of the truncated FcγRIIIa (1)GlcNAc glycoform lacking the R155 sidechain. The FcγRIIIa R155S (1)GlcNAc glycoform bound IgG1 Fc with a 5-fold weaker affinity compared to the wild type in the same glycoform (**Figure 3.6C, Table S3.1**). The R155S binding is comparable to the S164A mutant lacking the N162-glycan, and mutation of a nearby residue retaining the N-glycan F153S retains the benefit of the (1)GlcNAc/R155 interaction. These data demonstrate a role for the R155 sidechain to stabilize the binding-competent conformation.

Discussion

The N162 glycan regulates NK cell ADCC

Removing the N162 glycan eliminated the ADCC gains following inhibiting NK cell N-glycan processing with kifunensine, demonstrating a unique role for this protein modification in the immune system. These data demonstrate why NK cell ADCC is sensitive to changes of the N-glycan composition, an effect that was previously shown to require antibody binding to FcγRIIIa

[16]. This result is likewise consistent with prior binding affinity measurements defining a role for N162 glycan composition as a factor in antibody-binding affinity [8,9]. The binding affinity differences due to glycan composition are supported through studies of both human FcγRIIIa and macaque FcγRIII [2,30,31]. The simple observation that the N162 glycan alone accounts for the sensitivity of differences in NK cell ADCC due to N-glycan processing is belied by the potentially enormous number of alternative hypotheses that ADCC is influenced by any other N-glycan on the NK cell surface. However, a distinction can be made between these explanations because of the simple difference of a single S164A mutation that eliminated the N162 glycosylation site. The specificity of this result defines a role for N162 glycan composition in NK cell ADCC.

We propose that the N162 glycan regulates NK cell ADCC, representing a previously undescribed regulatory element. The appearance of endogenous heterogeneity of the N162-glycan supports the assertion. The N162 glycan composition isolated from peripheral NK cells is notably heterogeneous, in contrast to the four remaining FcγRIIIa N-glycans that show remarkable similarity between different donors and cell types [12-14]. Thus, the FcγRIIIa N162 glycan composition is variable on endogenous NK cells, likely providing a range of ADCC potency. It remains unclear how cells produce variability restricted to the N162 N-glycan, with a high degree of similarity at the remaining four sites on the same protein despite the physical linkage that exposes these glycans to comparable conditions during secretion. Identifying this mechanism that affects N162 glycan processing has the potential to impact cellular immunotherapies if endogenous processing can be tuned in vivo. Furthermore, the advent of infused NK cell-based therapies provides a mechanism to deploy FcγRIIIa engineered with

greater affinity or altered sensitivity to glycan composition of the expressing cell of the antibody ligand [32]. Removing the N162 glycan with the S164A mutation removes variability related to NK cell glycan processing, a potential confounding but unexplored factor in NK cell culture. Removing this glycan likewise reduces the impact of afucosylated antibodies on ADCC, which may be preferable if pathogenic afucosylated antibodies are present or enhanced ADCC is not desirable. Afucosylated antibodies have been reported at high titers during various autoimmune or viral diseases [33-35].

Relationship between FcγRIIIa affinity and ADCC

Multiple lines of evidence indicate ADCC responses improve with antibodies engineered to engage FcγRIIIa with improved affinity, however, much less information is available for how improved the FcγRIIIa antibody-binding affinity affects ADCC. This information is important to predict how future affinity improvements will impact ADCC. It is not obvious that increased antibody-binding affinity would promote greater ADCC considering the highly multivalent nature of the NK cell interaction with an opsonized target cell. Here we quantified ADCC using NK cells expressing a range of FcγRIIIa affinities outside the range defined by the natural V158 and V158F allotypes. Affinities lower than 300 nM showed little, if any, ADCC. Though donor NK cells displaying the V158F allotype exhibit measurable ADCC [36], our reduced ADCC is likely due to the lowered FcγRIIIa expression, as noted in **Figure S3.1**. Affinities greater than 300 nM showed substantial cytotoxicity with a sharp increase at greater affinities indicating that greater FcγRIIIa antibody-binding affinity is expected to further increase ADCC. Thus, these data define a positive relationship between FcγRIIIa affinity and ADCC.

A structural mechanism linking N162 composition to increased affinity

Analysis of unliganded and Fc-bound FcγRIIIa reveals structural differences proximal to N162 that are supported by the appearance of multiple conformations in NMR spectra and MD simulations. Both the FG loop and its attached N162 glycan move from a position in the unliganded state that allows maximum flexibility to a restricted state to accommodate Fc binding (**Figure 3.6A**). Furthermore, the sequential truncation of glycan residues provides increasingly greater affinity that is due largely to the N162 glycan (**Figure 3.2C**). We believe this result is best explained by a conformational entropy penalty introduced upon complex formation by shifting the N162 glycan to a restricted space between surfaces formed by the Fc and FcγRIIIa polypeptide. An alternative hypothesis, analogous to IgG1 Fc with intramolecular interactions stabilizing the N-glycan to increase affinity, appears to be less suitable for the FcγRIIIa data presented here largely because FcγRIIIa affinity increases following glycan truncation unlike IgG1 Fc N-glycan truncation that decrease affinity [37,38]. Indeed, previous MD simulations likewise demonstrated a loss of N162 glycan conformational heterogeneity upon binding [23].

A loss of N162 glycan conformational entropy alone is sufficient to explain the observed 1.7 - 2.2 kcal mol^{-1} difference in binding affinities [9]. A simple calculation, assuming three equally populated conformations in the unliganded state per rotatable bond, provides an estimate of the difference between the change of conformational entropy upon binding for the complex-type and Man5 N-glycans of 4.8 kcal mol^{-1} [39]. This value likely overestimates the penalty, being based on sampling only one N-glycan conformation in the Fc-bound state and notably excludes solvent entropy. Prior ITC analyses of these interactions revealed enthalpy/entropy

compensation that precluded a clear definition of the contribution from conformational entropy from those data alone [23]. The entropic penalty is likely also alleviated by stabilizing interactions between the (1)GlcNAc residue and the R155 sidechain, explaining why the truncated glycoform displays a greater affinity than the S164A variant that lacks the N162 glycan.

FcγRIIIa hotspots at the antibody-binding interface

Though high resolution structural models for the antibody binding interface are available, the impact of individual residues on binding affinities are not always trivial to predict and thus it is often unclear which residue to target in protein engineering efforts to tune affinity. Our FcγRIIIa mutant screen mapped important residues involved in antibody binding as shown in **Figure 3.1** to complement one prior study of G129 [28]. Here we identify two hotspots, one formed by W90 and W113 on the FcγRIIIa hinge and another centered on Y132. W90 and W113 are conserved among human low affinity FcγRs and sandwich the IgG1 Fc P329 residue which is likewise conserved in IgG and IgE [11,40]. Previous studies suggest that this proline sandwich interaction is the primary binding interaction in FcγRs, which is consistent with results that mutation abolished binding. The important of W90 and W113 is also supported by our functional data showing YTS cells expressing the FcγRIIIa W90A or W113A mutants do not exhibit measurable ADCC. Within this same region, I88A bound with 2-fold lower than V158. Although I88 was not detected in our amino acid selective NMR experiments, nearby V86 and L91 show large perturbations indicating conformational sampling of the interdomain interface, potentially reflecting domain flexibility. In the other hotspot, Y132 is one of many FcγRIIIa residues along

the D and E beta strands that interacts with Fc [11]. We further probed this region testing Y132, H119, H134, K120, K131 and T122. The Y132S mutation eliminated binding, likely due to removing numerous stabilizing interactions. The IgG1 Fc D265 residue is critical and thought to stabilize the N297 glycan, in which mutation abolishes FcγRIIIa binding [41]. FcγRIIIa K120 is within distance to interact with D265, possibly playing an important role in Fc binding. We found the K120A mutation reduced binding 5-fold. Other mutations in this region revealed a comparatively minor impact compared to Y132, suggesting Y132 is the critical residue for binding one Fc domain. In addition, the FG loop plays a critical role in Fc binding. While mutation of residues L157 and S160 did not change affinity, K161A lowered affinity by 10-fold. The impact of the K161 mutation is interesting because K161 is not predicted to make direct contacts with Fc, although it may contribute to loop stabilization or may transiently contact the IgG1 Fc [11].

Conclusion

These results indicate FcγRIIIa engineering through substitutions aimed at stabilizing the Fc-bound conformation in the absence of ligand is expected to promote affinity and ADCC. Affinity gains are possible beyond that provided by the tighter-binding V158 allotype, and we demonstrate that relatively small affinity improvements have a substantial impact on ADCC. Finally, we revealed new structural insights into FcγRIIIa that may lead to NK cells engineered to bind antibody through FcγRIIIa with high affinity as a novel strategy to improve immunotherapies.

Materials and Methods

Materials. All materials were purchased from Millipore-Sigma unless otherwise noted.

SPR. Affinity measurements were performed using the amine coupling strategy with a Biacore T200 (GE Life Sciences) as previously noted [18].

Protein expression. Plasmid construction, protein expression and purification were performed as previously described [18]. Briefly, all FcγRIIIa variants were cloned in the pGen2 vector with an 8x-histidine tag, green florescent protein (GFP) and tobacco etch virus (TEV) protease site. These constructs were transiently transfected into HEK293F (Life Technologies) or HEK293S (Gnt1-) cells [42] and harvested after 5 days. The collected media was spun down and passed over a Ni-NTA column (Qiagen) before being stored in 5 mM 3-(N-morpholino) propanesulfonic acid (MOPS), 0.1 M sodium chloride, pH 7.2 buffer.

Glycosidase Digestion. were purchased from NEB inc. 500 ug of FcγRIIIa-GFP was digested in 5 mM CaCl2, 50 mM sodium acetate pH 5.5 buffer at a 100 uL volume. Digestions of α2-3,6,8 Neuraminidase, β1-4 Galactosidase S, and β-N-Acetylglucosaminidase S (NEB), or all three enzymes were performed overnight at 37 °C using 1 unit each of enzyme. Digestion was analyzed using SDS-PAGE and mass spectrometry.

EndoF1 was expressed with *Escherichia coli* and exchanged into 20 mM sodium phohsphate monobasic, 0.1 M KCl and 0.05 mM 4,4-dimethyl-4-silapentane-1-sulfonic acid in deuterium oxide. 2 uL of 7.5 mg/mL EndoF1 was added to 500 ug of FcγRIIIa in 40 uL and digested in the NMR tube for 2.5 hours at 4 ºC.

Selective FcγRIIIa isotope labeling for NMR. FcγRIIIa-GFP was expressed in one of two labeling strategies, either 100 mg/L [^{15}N]-lysine, [^{15}N]-glycine and [^{15}N]-serine or 100 mg/L [^{15}N]-valine, [^{15}N]-isoleucine and [^{15}N]-leucine. These labels were supplemented in amino acid-free carbohydrate free FreeStyle293™ medium (Life Technologies) along with 1g/L glutamine,100 mg/L of the other amino acids and 3 g/L glucose. pH then osmolarity were adjusted to 7.2 and 260-280 mOsm/kg respectively. The final media solutions were confirmed to be at pH 7.2 again before filtration through a sterile 0.2 μm aPES membrane (Fischer Scientific) and storage at 4 ºC. Following expression in these media, the labeled FcγRIIIa-GFP was TEV protease digested and purified as described [18].

NMR Spectroscopy of FcγRIIIa N38Q/N74Q/N169Q. The expression plasmid encoding FcγRIIIa N38Q/N74Q/N169Q was generated from the plasmid encoding GFP-FcγRIIIa, using site directed mutagenesis [37]. HEK293F cells were transfected, and protein prepared for NMR as previously described [37,43]. Expression media for individual isotope [^{15}N] labeling was prepared as previously described [24]. [^{13}C, ^{15}N]-FcγRIIIa N38Q/N74Q/N169Q was expressed in custom Freestyle amino acid and carbohydrate dropout medium (Invitrogen) containing 3 g/L [^{13}C]-glucose and 100 mg/L of each [^{15}N]-labeled amino acid, including: alanine, cysteine, aspartate, glutamate, phenylalanine, glycine, histidine, isoleucine, lysine, leucine, methionine, asparagine, arginine, serine, threonine, valine, tryptophan, and tyrosine. Unlabeled proline and glutamine were added a 100 mg/L and 2 g/L, respectively. FcγRIIIa was exchanged into NMR buffer containing 20 mM MOPS, 100 mM potassium chloride, 0.5 mM

trimethylsilylpropanesulfonic acid (DSS) and 5% deuterium oxide at a final concentration of 100-300 μM.

NMR spectra were collected at a 30°C sample temperature using 700 and 800 MHz AVANCEIII spectrometers (Bruker) equipped with triple resonance cryoprobes. TROSY-based HSQC, HNCA, HNCOCA and HNCO experiments were selected form the Bruker pulse sequence library. NMR data were processing in NMRPipe and analyzed using NMRViewJ [44,45].

Lentivirus generation. Plasmids pMD2.G and psPAX2 were gifts from Didier Trono (Addgene plasmid # 12259; # 12260). Full length FcγRIIIa variant sequences were cloned under the CMV promoter in pCDH-CMV-MCS-EF1α-copGFP (System Biosciences). These three plasmids were cotransfected into HEK293T cells using Fugene 6 (Promega). Media was exchanged after three days and ultimately collected after five days total then passed through a 0.45μm syringe filter before being stored at -80C.

Transduction. 1.5 x 10^6 YTS NK cells were cultured in 3 mL of media containing 1.8 mL of previously obtained viral media and 8μg/mL polybrene (Sigma). The culture plates were spun for 2 hours at 400 x g and then placed in an incubator overnight at 37 °C, 5% CO_2 and 80% humidity. The following day each well was transferred to 20 mL of fresh media and allowed to expand for another day. GFP signal was used to sort the cells on an S3 bulk sorter (Biorad), with transduction efficiencies as high as 30%.

Cell Culture. YTS cells (a gift from Dr.Mace, Columbia) and Raji cells (ATCC) were grown in RPMI 1640 medium supplemented with 10% FBS, l-glutamine (2 mM), HEPES (10 mM), sodium pyruvate (1 mM), non-essential amino acids (1 mM), and penicillin/streptomycin (50 U/mL) in suspension at 37°C, 5% CO_2. The ADCC assay was performed by flow cytometry performed as described previously [16].

Western blotting. 1.28 x 10^7 YTS NK cells were collected and lysed in 100 µl of 1% SDS. Lysates were placed on ice for 1 minute and then sonicated for 10 seconds, repeated three times. Western blotting was performed as previously described [46]. Blots were stained with either for FcγRIIIa (AF1597; R&D) or GAPDH (NC1955142; R&D Systems). Both primary stainings were followed by anti-Goat secondary staining (A32860; Thermo-Fisher) before imaging on a LI-COR Odyssey CLx.

Molecular dynamics simulations were performed as previously described using Amber and the Glycam forcefield [23]. Data were analyzed using VMD.

Statistical analyses. All statistical analyses were performed with Excel (Microsoft) and Prism 6.09 (GraphPad software).

Acknowledgements

We thank Dr. Ganesh Subedi (Iowa State University) for preparing the [^{13}C,^{15}N]-labeled receptor and collecting the triple-resonance-based NMR experiments and Dr. Ryan Weiss (UGA) for guidance with the lentiviral transduction procedure.

Author Contributions

P.G.K and A.M.B. carried out experiments. P.G.K and A.W.B performed statistical analysis. A.W.B., is responsible for funding acquisition. A.W.B. and P.G.K designed the study and wrote the manuscript. All authors read and approved the final manuscript.

Data Availability Statement

Backbone resonance assignments were deposited in the BioMagResBank as accession 52304. All other data generated or analyzed during this study are included in this published article (and its Supplementary Information files). Additional information is available to the corresponding author on reasonable request.

Funding

Funding to A.W.B. by the National Institutes of Health under Award No. U01 AI148114 (NIAID) and from the Biochemistry and Molecular Biology Department at the University of Georgia, Athens. The content is solely the responsibility of the authors and does not necessarily represent the official views of the National Institutes of Health.

Competing Interests

The authors declare no conflict of interest.

Works Cited

1. Bruhns, P., B. Iannascoli, P. England, D.A. Mancardi, N. Fernandez, S. Jorieux, and M. Daeron, *Specificity and affinity of human Fcgamma receptors and their polymorphic variants for human IgG subclasses.* Blood, 2009. **113**(16): p. 3716-25.
2. Hayes, J.M., et al., *Identification of Fc Gamma Receptor Glycoforms That Produce Differential Binding Kinetics for Rituximab.* Mol Cell Proteomics, 2017. **16**(10): p. 1770-1788.
3. Cartron, G., L. Dacheux, G. Salles, P. Solal-Celigny, P. Bardos, P. Colombat, and H. Watier, *Therapeutic activity of humanized anti-CD20 monoclonal antibody and polymorphism in IgG Fc receptor FcgammaRIIIa gene.* Blood, 2002. **99**(3): p. 754-8.
4. Weng, W.K. and R. Levy, *Two immunoglobulin G fragment C receptor polymorphisms independently predict response to rituximab in patients with follicular lymphoma.* J Clin Oncol, 2003. **21**(21): p. 3940-7.
5. Presta, L.G., R.L. Shields, A.K. Namenuk, K. Hong, and Y.G. Meng, *Engineering therapeutic antibodies for improved function.* Biochem Soc Trans, 2002. **30**(4): p. 487-90.
6. Mossner, E., et al., *Increasing the efficacy of CD20 antibody therapy through the engineering of a new type II anti-CD20 antibody with enhanced direct and immune effector cell-mediated B-cell cytotoxicity.* Blood, 2010. **115**(22): p. 4393-402.

7. Townsend, W., et al., *Obinutuzumab Versus Rituximab Immunochemotherapy in Previously Untreated iNHL: Final Results From the GALLIUM Study.* Hemasphere, 2023. **7**(7): p. e919.

8. Patel, K.R., J.T. Roberts, G.P. Subedi, and A.W. Barb, *Restricted processing of CD16a/Fc gamma receptor IIIa N-glycans from primary human NK cells impacts structure and function.* J Biol Chem, 2018. **293**(10): p. 3477-3489.

9. Subedi, G.P. and A.W. Barb, *CD16a with oligomannose-type N-glycans is the only "low-affinity" Fc gamma receptor that binds the IgG crystallizable fragment with high affinity in vitro.* J Biol Chem, 2018. **293**(43): p. 16842-16850.

10. Moremen, K.W., M. Tiemeyer, and A.V. Nairn, *Vertebrate protein glycosylation: diversity, synthesis and function.* Nat Rev Mol Cell Biol, 2012. **13**(7): p. 448-62.

11. Sondermann, P., R. Huber, V. Oosthuizen, and U. Jacob, *The 3.2-A crystal structure of the human IgG1 Fc fragment-Fc gammaRIII complex.* Nature, 2000. **406**(6793): p. 267-73.

12. Patel, K.R., J.D. Nott, and A.W. Barb, *Primary Human Natural Killer Cells Retain Proinflammatory IgG1 at the Cell Surface and Express CD16a Glycoforms with Donor-dependent Variability.* Mol Cell Proteomics, 2019. **18**(11): p. 2178-2190.

13. Roberts, J.T., K.R. Patel, and A.W. Barb, *Site-specific N-glycan Analysis of Antibody-binding Fc gamma Receptors from Primary Human Monocytes.* Mol Cell Proteomics, 2020. **19**(2): p. 362-374.

14. Patel, K.R., J.T. Roberts, and A.W. Barb, *Allotype-specific processing of the CD16a N45-glycan from primary human natural killer cells and monocytes.* Glycobiology, 2020. **30**(7): p. 427-432.

15. Benavente, M.C.R., Z.A. Hakeem, A.R. Davis, N.B. Murray, P. Azadi, E.M. Mace, and A.W. Barb, *Distinct CD16a features on human NK cells observed by flow cytometry correlate with increased ADCC.* Sci Rep, 2024. **14**(1): p. 7938.

16. Rodriguez Benavente, M.C., H.B. Hughes, P.G. Kremer, G.P. Subedi, and A.W. Barb, *Inhibiting N-glycan processing increases the antibody binding affinity and effector function of human natural killer cells.* Immunology, 2023. **170**(2): p. 202-213.

17. Vidarsson, G., G. Dekkers, and T. Rispens, *IgG subclasses and allotypes: from structure to effector functions.* Front Immunol, 2014. **5**: p. 520.

18. Kremer, P.G. and A.W. Barb, *The weaker-binding Fc gamma receptor IIIa F158 allotype retains sensitivity to N-glycan composition and exhibits a destabilized antibody-binding interface.* J Biol Chem, 2022. **298**(9): p. 102329.

19. Shields, R.L., J. Lai, R. Keck, L.Y. O'Connell, K. Hong, Y.G. Meng, S.H. Weikert, and L.G. Presta, *Lack of fucose on human IgG1 N-linked oligosaccharide improves binding to human Fcgamma RIII and antibody-dependent cellular toxicity.* J Biol Chem, 2002. **277**(30): p. 26733-40.

20. Ferrara, C., et al., *Unique carbohydrate-carbohydrate interactions are required for high affinity binding between FcgammaRIII and antibodies lacking core fucose.* Proc Natl Acad Sci U S A, 2011. **108**(31): p. 12669-74.

21. Mizushima, T., H. Yagi, E. Takemoto, M. Shibata-Koyama, Y. Isoda, S. Iida, K. Masuda, M. Satoh, and K. Kato, *Structural basis for improved efficacy of therapeutic antibodies on defucosylation of their Fc glycans.* Genes Cells, 2011. **16**(11): p. 1071-80.

22. Sakae, Y., T. Satoh, H. Yagi, S. Yanaka, T. Yamaguchi, Y. Isoda, S. Iida, Y. Okamoto, and K. Kato, *Conformational effects of N-glycan core fucosylation of immunoglobulin G Fc region on its interaction with Fcgamma receptor IIIa.* Sci Rep, 2017. **7**(1): p. 13780.

23. Falconer, D.J., G.P. Subedi, A.M. Marcella, and A.W. Barb, *Antibody Fucosylation Lowers the FcgammaRIIIa/CD16a Affinity by Limiting the Conformations Sampled by the N162-Glycan.* ACS Chem Biol, 2018. **13**(8): p. 2179-2189.

24. Subedi, G.P., E.T. Roberts, A.R. Davis, P.G. Kremer, I.J. Amster, and A.W. Barb, *A comprehensive assessment of selective amino acid (15)N-labeling in human embryonic kidney 293 cells for NMR spectroscopy.* J Biomol NMR, 2024.

25. Wyss, D.F., J.S. Choi, and G. Wagner, *Composition and sequence specific resonance assignments of the heterogeneous N-linked glycan in the 13.6 kDa adhesion domain of human CD2 as determined by NMR on the intact glycoprotein.* Biochemistry, 1995. **34**(5): p. 1622-34.

26. Yagi, H., Y. Zhang, M. Yagi-Utsumi, T. Yamaguchi, S. Iida, Y. Yamaguchi, and K. Kato, *Backbone (1)H, (13)C, and (15)N resonance assignments of the Fc fragment of human immunoglobulin G glycoprotein.* Biomol NMR Assign, 2015. **9**(2): p. 257-60.

27. Yogo, R., S. Yanaka, and K. Kato, *Backbone (1)H, (13)C, and (15)N assignments of the extracellular region of human Fcgamma receptor IIIb.* Biomol NMR Assign, 2018. **12**(1): p. 201-204.

28. Roberts, J.T. and A.W. Barb, *A single amino acid distorts the Fc gamma receptor IIIb/CD16b structure upon binding immunoglobulin G1 and reduces affinity relative to CD16a.* J Biol Chem, 2018. **293**(51): p. 19899-19908.

29. Kakiuchi-Kiyota, S., et al., *A BCMA/CD16A bispecific innate cell engager for the treatment of multiple myeloma.* Leukemia, 2022. **36**(4): p. 1006-1014.

30. Van Coillie, J., et al., *Role of N-Glycosylation in FcgammaRIIIa interaction with IgG.* Front Immunol, 2022. **13**: p. 987151.

31. Tolbert, W.D., et al., *Decoding human-macaque interspecies differences in Fc-effector functions: The structural basis for CD16-dependent effector function in Rhesus macaques.* Front Immunol, 2022. **13**: p. 960411.

32. Page, A., N. Chuvin, J. Valladeau-Guilemond, and S. Depil, *Development of NK cell-based cancer immunotherapies through receptor engineering.* Cell Mol Immunol, 2024. **21**(4): p. 315-331.

33. Larsen, M.D., et al., *Afucosylated IgG characterizes enveloped viral responses and correlates with COVID-19 severity.* Science, 2021. **371**(6532).

34. Kapur, R., et al., *A prominent lack of IgG1-Fc fucosylation of platelet alloantibodies in pregnancy.* Blood, 2014. **123**(4): p. 471-80.

35. Ackerman, M.E., et al., *Natural variation in Fc glycosylation of HIV-specific antibodies impacts antiviral activity.* J Clin Invest, 2013. **123**(5): p. 2183-92.

36. Hatjiharissi, E., et al., *Increased natural killer cell expression of CD16, augmented binding and ADCC activity to rituximab among individuals expressing the FcgammaRIIIa-158 V/V and V/F polymorphism.* Blood, 2007. **110**(7): p. 2561-4.

37. Subedi, G.P., Q.M. Hanson, and A.W. Barb, *Restricted motion of the conserved immunoglobulin G1 N-glycan is essential for efficient FcgammaRIIIa binding.* Structure, 2014. **22**(10): p. 1478-88.

38. Subedi, G.P. and A.W. Barb, *The Structural Role of Antibody N-Glycosylation in Receptor Interactions.* Structure, 2015. **23**(9): p. 1573-1583.

39. Imberty, A., S. Perez, M. Hricovini, R.N. Shah, and J.P. Carver, *Flexibility in a tetrasaccharide fragment from the high mannose type of N-linked oligosaccharides.* Int J Biol Macromol, 1993. **15**(1): p. 17-23.

40. Tamm, A. and R.E. Schmidt, *IgG binding sites on human Fc gamma receptors.* Int Rev Immunol, 1997. **16**(1-2): p. 57-85.

41. Baudino, L., et al., *Crucial role of aspartic acid at position 265 in the CH2 domain for murine IgG2a and IgG2b Fc-associated effector functions.* J Immunol, 2008. **181**(9): p. 6664-9.

42. Reeves, P.J., N. Callewaert, R. Contreras, and H.G. Khorana, *Structure and function in rhodopsin: high-level expression of rhodopsin with restricted and homogeneous N-glycosylation by a tetracycline-inducible N-acetylglucosaminyltransferase I-negative HEK293S stable mammalian cell line.* Proc Natl Acad Sci U S A, 2002. **99**(21): p. 13419-24.

43. Subedi, G.P., D.J. Falconer, and A.W. Barb, *Carbohydrate-Polypeptide Contacts in the Antibody Receptor CD16A Identified through Solution NMR Spectroscopy.* Biochemistry, 2017. **56**(25): p. 3174-3177.

44. Delaglio, F., S. Grzesiek, G.W. Vuister, G. Zhu, J. Pfeifer, and A. Bax, *NMRPipe: a multidimensional spectral processing system based on UNIX pipes.* J Biomol NMR, 1995. **6**(3): p. 277-93.

45. Johnson, B.A., *Using NMRView to visualize and analyze the NMR spectra of macromolecules.* Methods Mol Biol, 2004. **278**: p. 313-52.

46. Shenoy, A., S. Yalamanchili, A.R. Davis, and A.W. Barb, *Expression and Display of Glycoengineered Antibodies and Antibody Fragments with an Engineered Yeast Strain.* Antibodies (Basel), 2021. **10**(4).

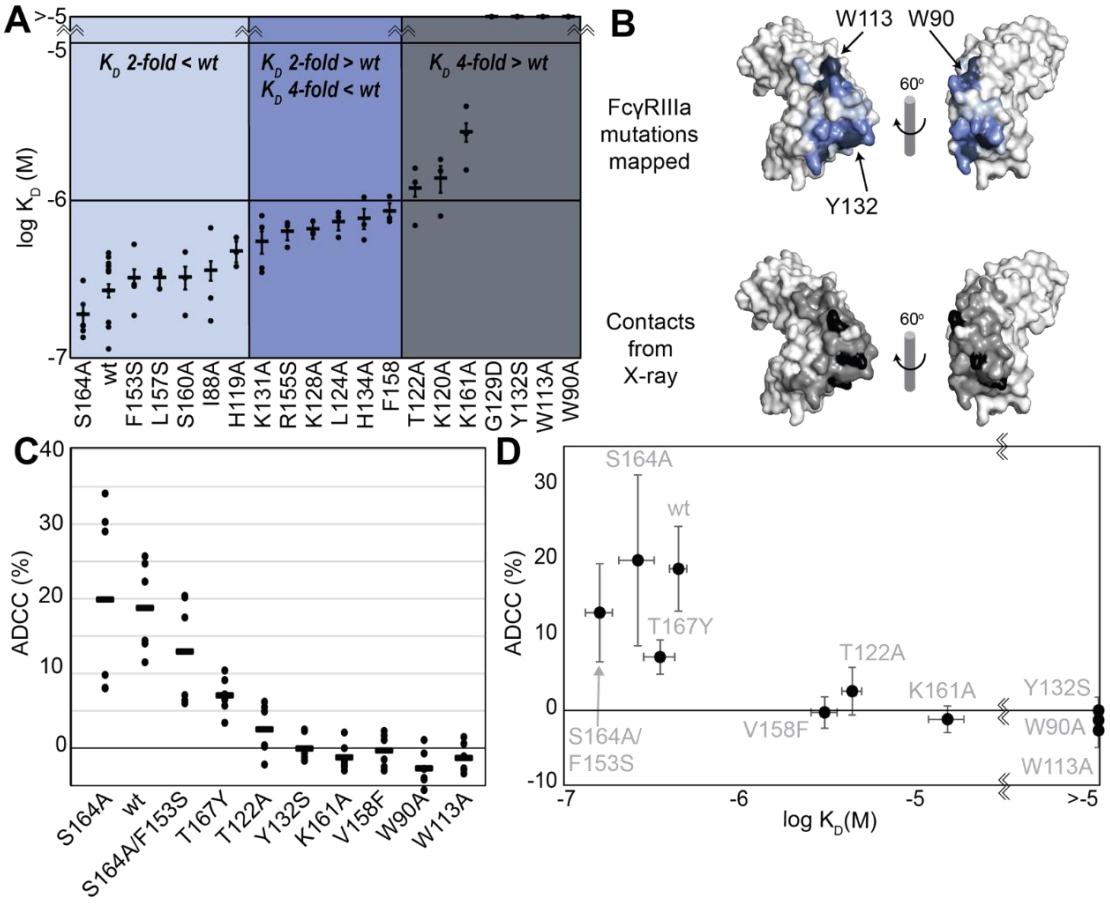

Figure 3.1. **FcγRIIIa antibody-binding affinities correlate with ADCC potency. A**. Affinities of FcγRIIIa amino acid variants determined by SPR are binned into impact: 2-fold lower (*light blue*), between 2 and 4-fold (*blue*), or greater than 4-fold lower than V158 (*dark blue*). **B**. Plotting these values onto a surface representation of FcγRIIIa, using the same coloring scheme as in A., reveals two critical areas for binding centered around W113 and Y132 (top panel). These values provide more detail in contrast to the interface defined by X-ray crystallography with contacts shown <3 Å (*black* surface) and <5 Å (*grey* surface). **C**. ADCC of YTS cells transduced to express a panel of FcγRIIIa variants. Horizontal black bars represent average

ADCC values, with individual point representing individual assays. Experiments were completed in triplicate and the figure includes data from multiple experiments collected on multiple days. **D**. A comparison of ADCC values from panel C and binding affinity from panel A shows a correlation.

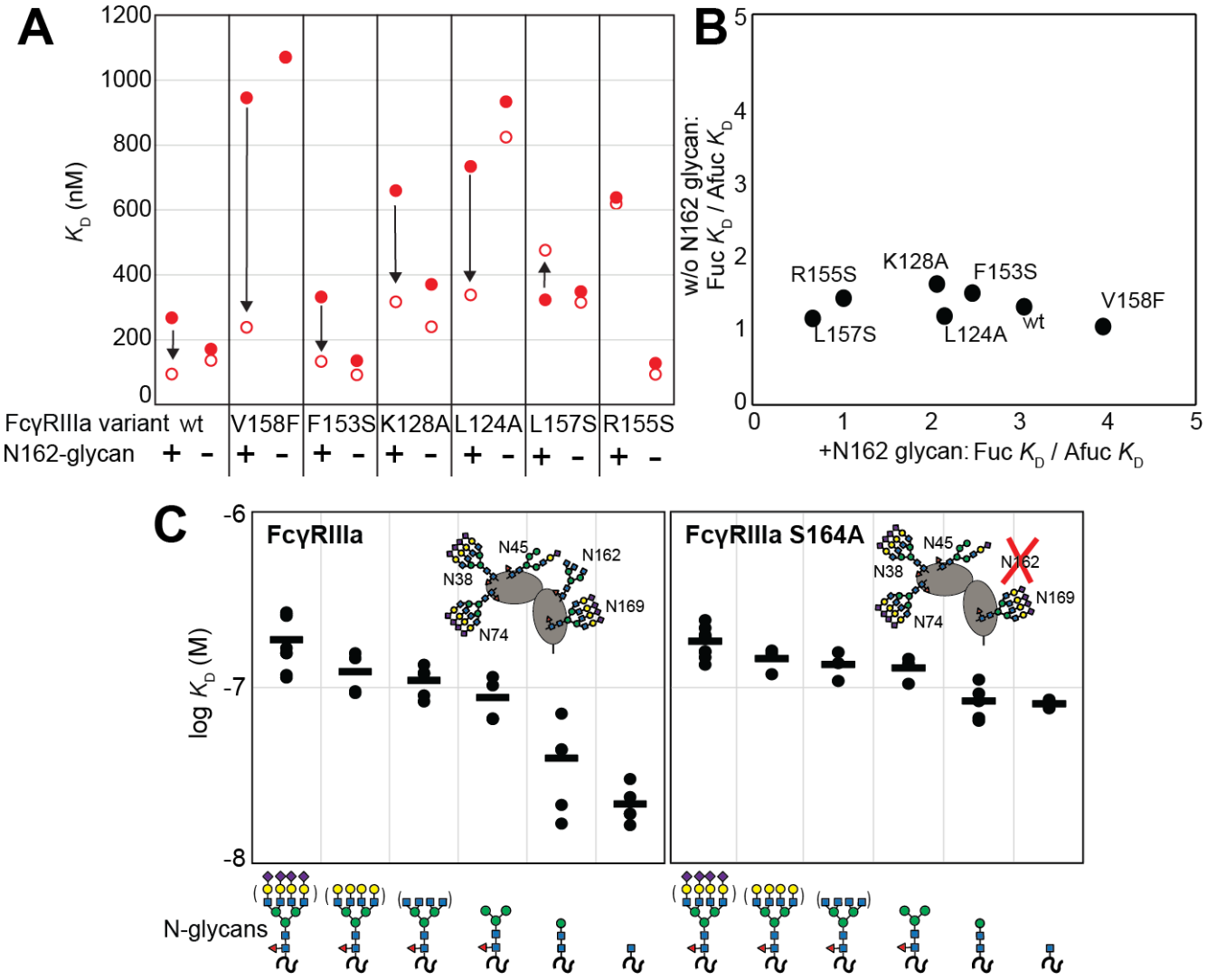

Figure 3.2. The FcγRIIIa N162 glycan regulates affinity towards fucosylated and afucosylated IgG1 Fc. A. FcγRIIIa variants demonstrate higher affinity towards without IgG1 Fc core-fucosylation (*open* circles) than with this modification (*red* circles). The affinity increase is demarcated with a vertical arrow. When the N162 glycan was removed through the S164A mutation, the fucose sensitivity greatly diminished. **B**. Comparison of the fold affinity increase in

panel A. due to removing IgG1 Fc fucose. Averages for the fold increase with the N162 glycan present and absent are noted on the x and y axes, respectively. **C**. The affinities of six different FcγRIIIa glycoforms were measured with and without the N162 glycan (wt and S164A, respectively). Horizontal black bars represent the means and individual measurements are shown with closed *black* circles. Cartoon models utilize the SNFG nomenclature and represent the possible N-glycan compositions for each species.

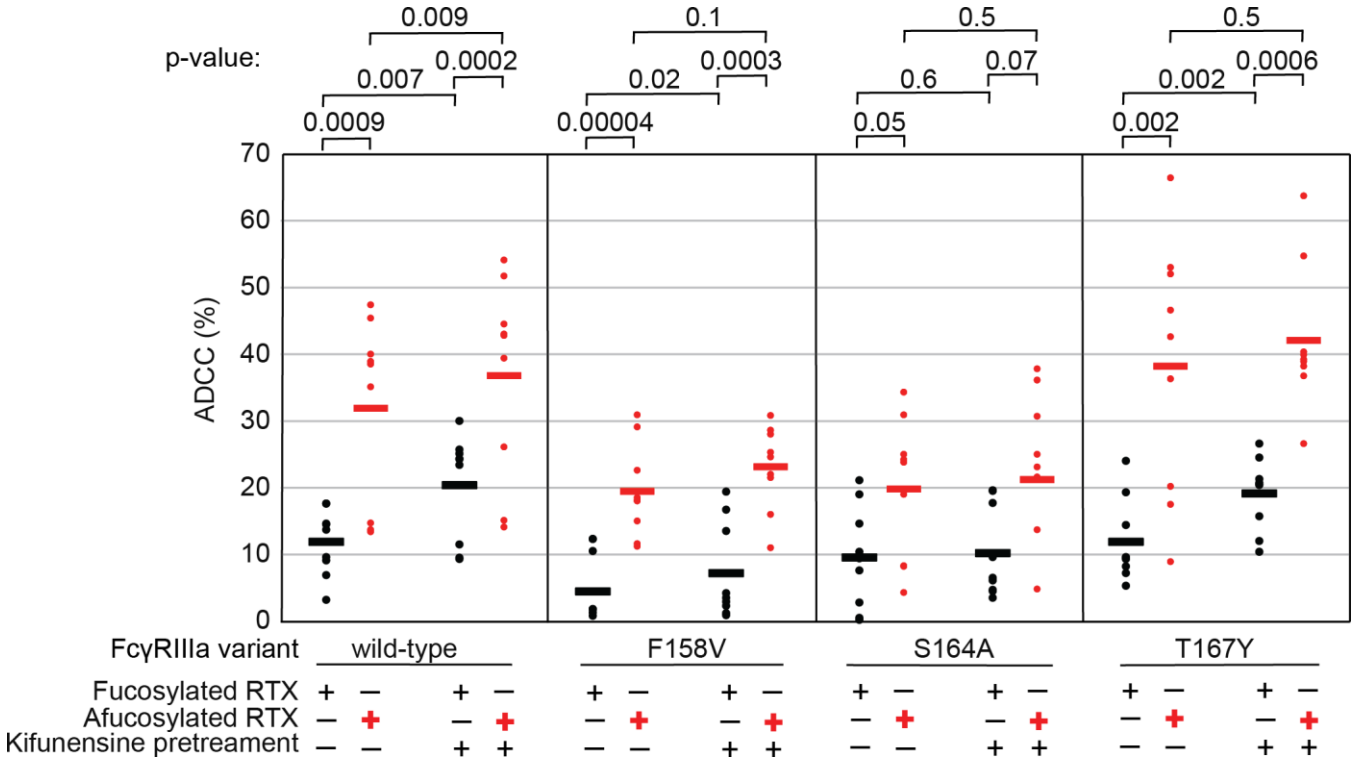

Figure 3.3. The FcγRIIIa N162 glycan regulates NK cell ADCC. The ADCC of NK cells increases significantly following 20 μM kifunensine for YTS cells expressing FcγRIIIa that retains the N162 glycan (wild type, V158F, T167Y). Removing the N162 glycan with the S164A mutation eliminates this increase. In addition to kifunensine, these cells demonstrate significant ADCC increases from afucosylated rituximab (RTX) compared to fucosylated RTX. The YTS cells FcγRIIIa S164A cells likewise demonstrate no increased ADCC following kifunensine treatment when using afucosylated RTX, unlike YTS cells expressing the wild-type FcγRIIIa. Observations made using an afucosylated antibody are shown in *red*. Data shown include three independent experiments collected on three different days, each with three replicates. P-values from two-tailed t-tests are shown at the top.

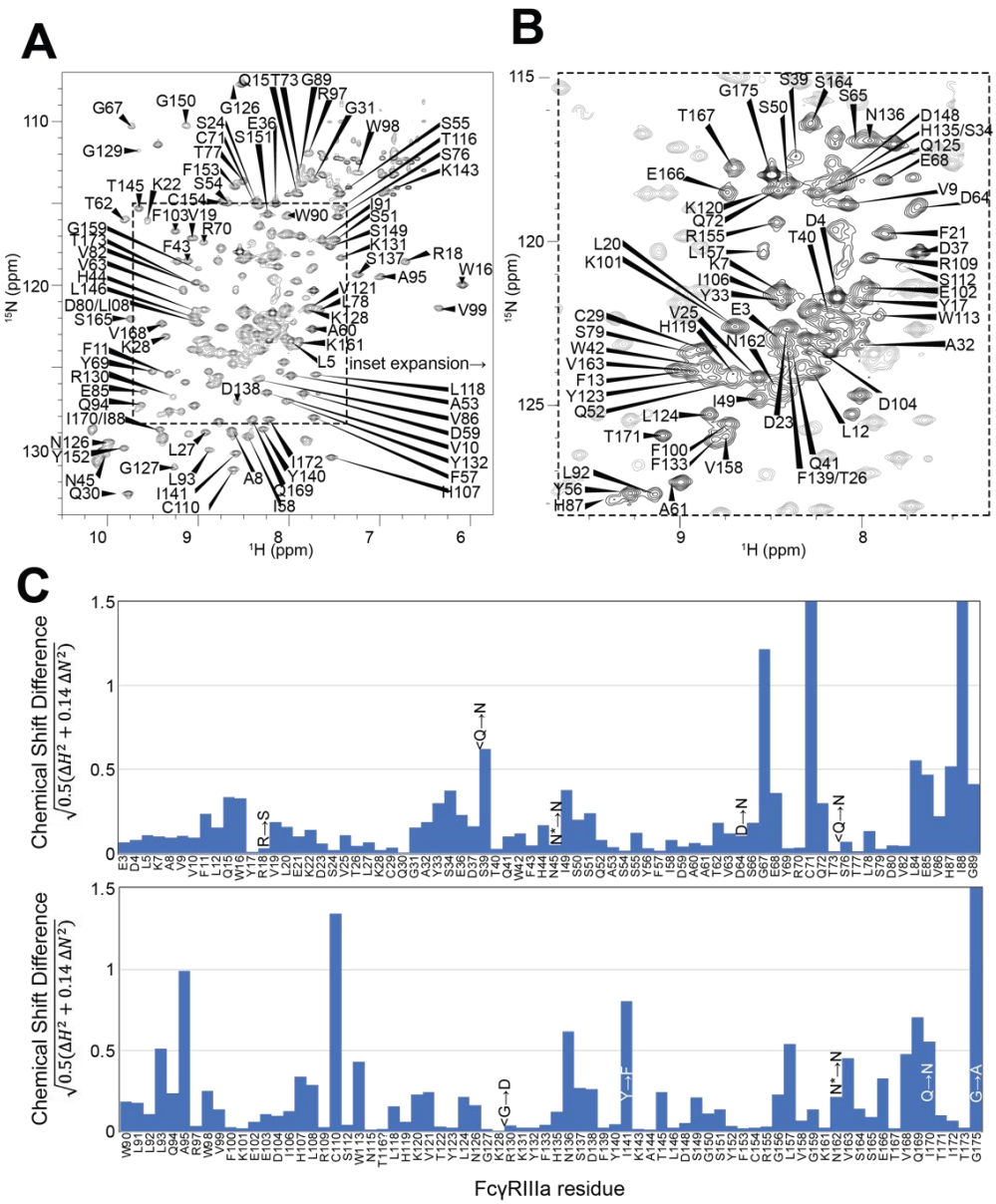

Figure 3.4. Backbone resonance assignment of FcγRIIIa with N-glycans at N45 and N162. Amino acid position within the sequence of 175 residues and the residue type are shown. **A**. the entire ^{1}H-^{15}N HSQC-TROSY spectrum. **B**. expansion and additional assignments within the inset. **C**. A comparison of the assigned ^{1}H and ^{15}N resonances from the glycosylated FcγRIIIa to

FcγRIIIb expressed from *E. coli* that contains no N-glycans. Sequence differences are noted in the figure, with the bottom letter denoting the FcγRIIIa residue. N* = a glycosylated asparagine residue.

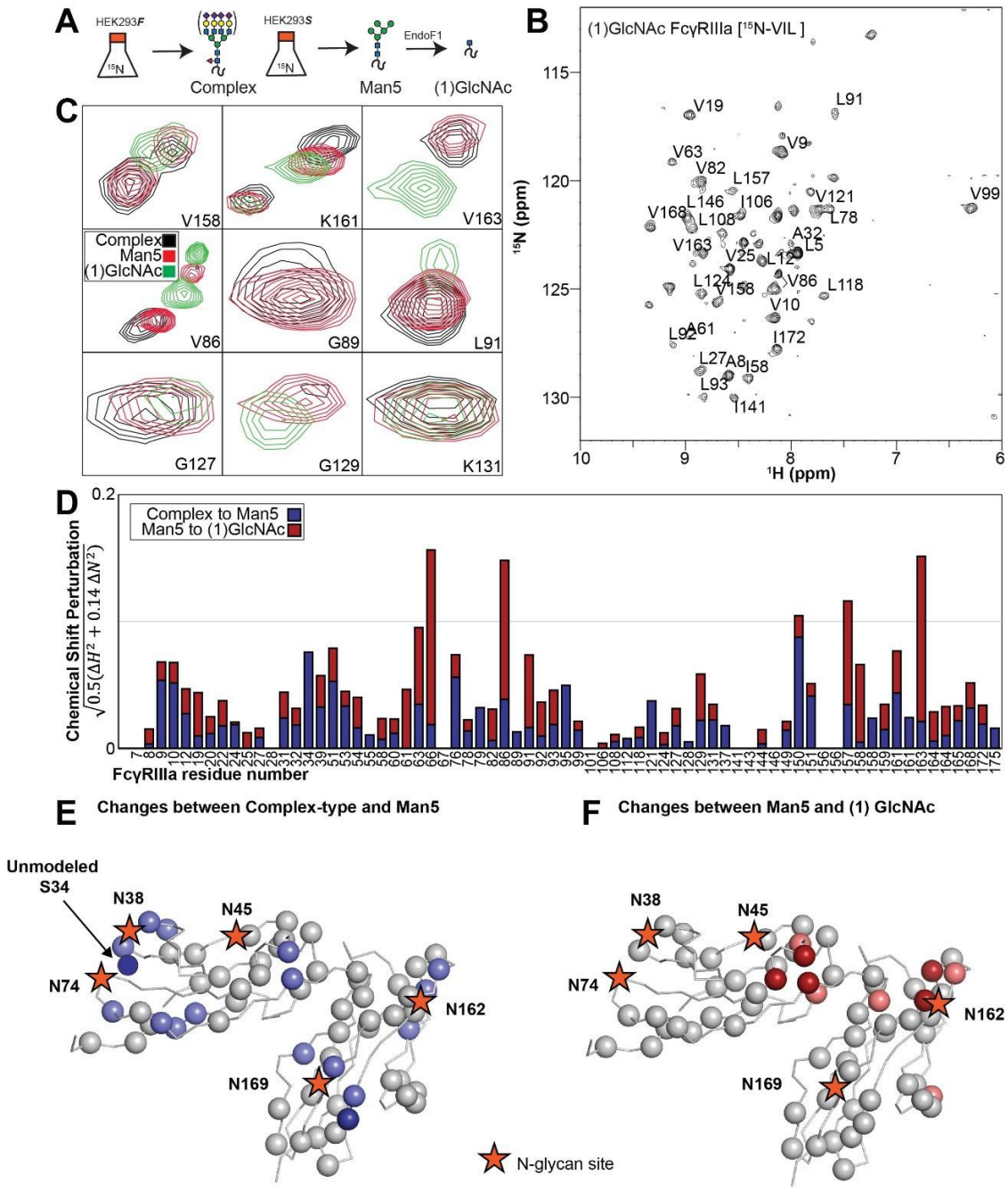
A
HEK293F
15N
Complex
HEK293S
15N
Man5
EndoF1
(1)GlcNAc
B
(1)GlcNAc FcγRIIIa [15N-VIL]
15N (ppm)
1H (ppm)
C
V158
K161
V163
Complex
Man5
(1)GlcNAc
V86
G89
L91
G127
G129
K131
D
Complex to Man5
Man5 to (1)GlcNAc
Chemical Shift Perturbation
FcγRIIIa residue number
E
Changes between Complex-type and Man5
Unmodeled
S34
N38
N45
N74
N162
N169
N-glycan site
F
Changes between Man5 and (1) GlcNAc
N38
N45
N74
N162
N169

Figure 3.5. Glycan composition changes the FcγRIIIa backbone conformation. A. Diagram of the protein expression, labeling and glycan remodeling procedures. **B**. Example HSQC-TROSY spectrum of FcγRIIIa with the truncated (1)GlcNAc N-glycan labeled with ^{15}N-(Val,Leu,Ile) during expression. **C**. Isolated peaks show differences in position between different glycoforms. **D**. The observed Chemical Shift Perturbation (CSP) between complex-type and Man5 N-glycans (*blue*) or Man5 and (1)GlcNAc N-glycans (*red*) is shown by residue number. **D**.**E**. CSP's >0.03 (*light*) and >0.06 (*dark*) mapped to a ribbon model of FcγRIIIa. Truncation to (1)GlcNAc causes CSPs near the Fc-binding interface that is proximal to N162.

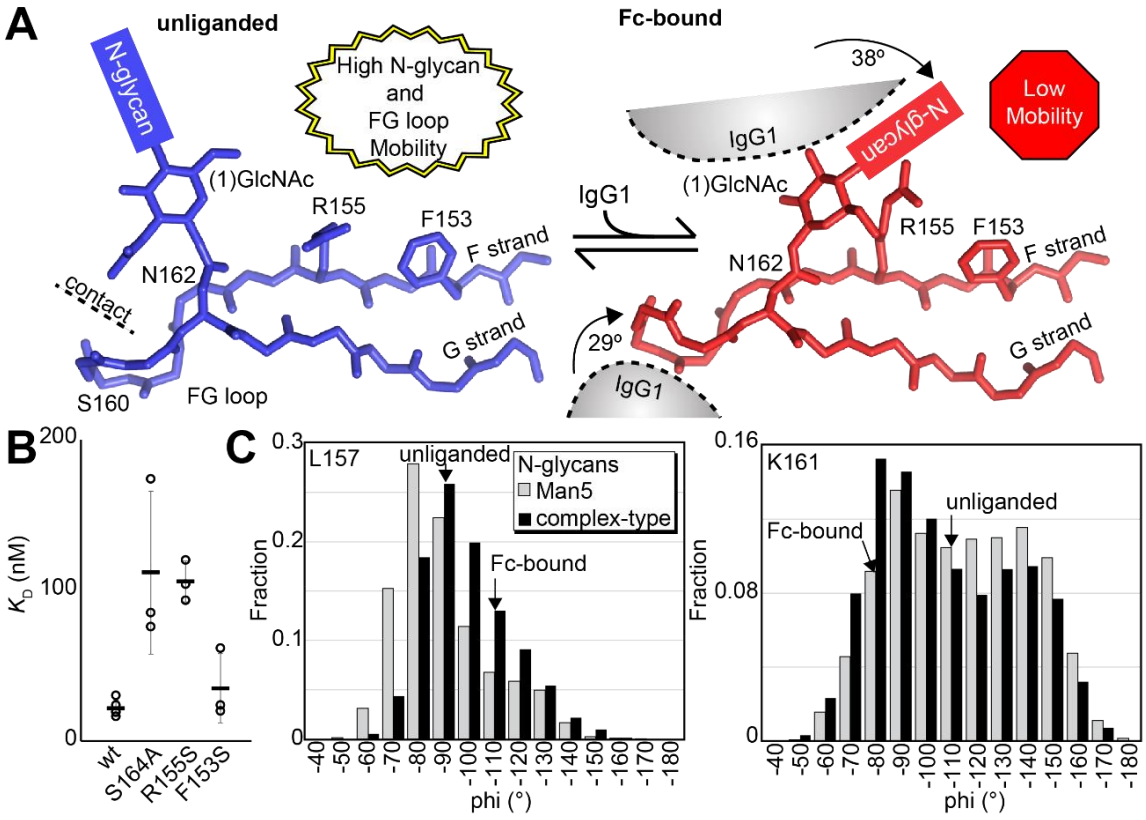

Figure 3.6. Binding antibody induces an FcγRIIIa conformational change. **A**. Two conformations of the FG loop previously captured by X-ray crystallography (pbd 7seg, 5vu0). Both the FG loop and the N-glycan become restricted to accommodate IgG1 Fc. The conformational entropy of a complex-type N-glycan, with more rotatable bonds, is greater as is the loss of entropy upon binding compared to smaller N-glycans. **B**. Binding affinity of FcγRIIIa variants following EndoF1 digestion, displaying a truncated (1)GlcNAc N-glycan. **C**. Evidence for conformational sampling in the unliganded FcγRIIIa revealed by all-atom molecular dynamics simulations. Each data set show the average of two independent 1 μs trajectories, with separate experiments for FcγRIIIa with Man5 N-glycans or complex-type N-glycans.

Supplemental Table 3.1. Binding affinity measurements for each FcγRIIIa variant

	Binding to fucosylated IgG1 Fc		Binding to afucosylated IgG1 Fc	
FcγR3a Variant	K_D (nM)	StdDev (nM)	K_D (nM)	StdDev (nM)
EndoF F153S	35.07	22.98	44.40	38.18
EndoF R155S	105.77	13.44	86.27	3.57
EndoF S164A	111.73	54.12	118.80	41.30
EndoF S164A F153S	243.00	59.40	167.00	55.15
EndoF S164A V158F	381.50	62.93	320.00	72.12
EndoF S164A R155S	116.00	18.38	124.50	16.26
EndoF T167Y	261.00	151.32	225.50	95.46
EndoF V158	21.74	5.41	17.88	6.61
EndoF Y132S	12876.67	7035.73	7530.00	1547.87
F153S	322.75	144.04	133.95	44.51
V158F	944.75	228.50	238.75	58.96
G129D	>10000	n.a.	>10000	n.a.
H119A	477.00	100.80	225.67	78.78
H134A	771.67	251.14	339.67	80.03
I88A	360.33	269.47	227.77	239.49
K120A	1385.00	529.79	597.00	142.28
K128A	659.67	68.97	316.67	175.30
K128A R155S	n.b.	n.a.	n.b.	n.a.
K131A	549.00	223.76	330.60	211.95
K161A	2723.33	1201.68	1153.33	55.08
L124A	734.67	134.94	339.00	198.55
L157S	324.33	44.41	475.67	304.08
N162Q	200.00	103.58	118.30	44.83
R155S	637.67	117.59	619.00	435.44
S160A	326.00	142.04	131.53	59.71
S164A	159.13	76.79	92.19	67.71
S164A F153S	136.33	5.86	93.13	20.82
S164A V158F	1105.00	35.36	710.50	154.86
S164A I158	124.55	64.28	87.70	38.61
S164A K128A	252.50	58.69	189.00	84.85
S164A Man 3	108.53	42.75	15.43	3.88
S164A Man1	95.93	31.82	n.t.	n.a.
S164A N	131.98	34.70	n.t.	n.a.
S164A NG	112.45	50.15	n.t.	n.a.

S164A NGG	106.35	49.22	n.t.	n.a.
S164A R155S	128.30	88.67	94.25	71.77
S164A T171A	147.35	140.93	132.70	110.73
T122A	1197.67	462.08	640.33	221.41
T167Y	229.00	62.22	164.00	58.56
T171A	n.b.	n.a.	555.66	1031.54
V158	305.35	130.44	168.37	295.84
V158 Man 1	95.00	53.53	n.t.	n.a.
V158 Man3	27.50	14.65	15.63	3.42
V158 N	123.15	33.57	20.90	12.54
V158 NG	109.92	22.05	17.57	9.95
V158 NGG	87.78	24.99	13.71	7.19
V158I	210.27	98.28	101.77	67.45
W113A	n.b.	n.a.	>10000	n.a.
W90A	n.b.	n.a.	9040.00	1559.52
Y132S	n.b.	n.a.	>10000	n.a.

n.b.- no binding detected

n.a. - not

applicable

n.t. - not tested

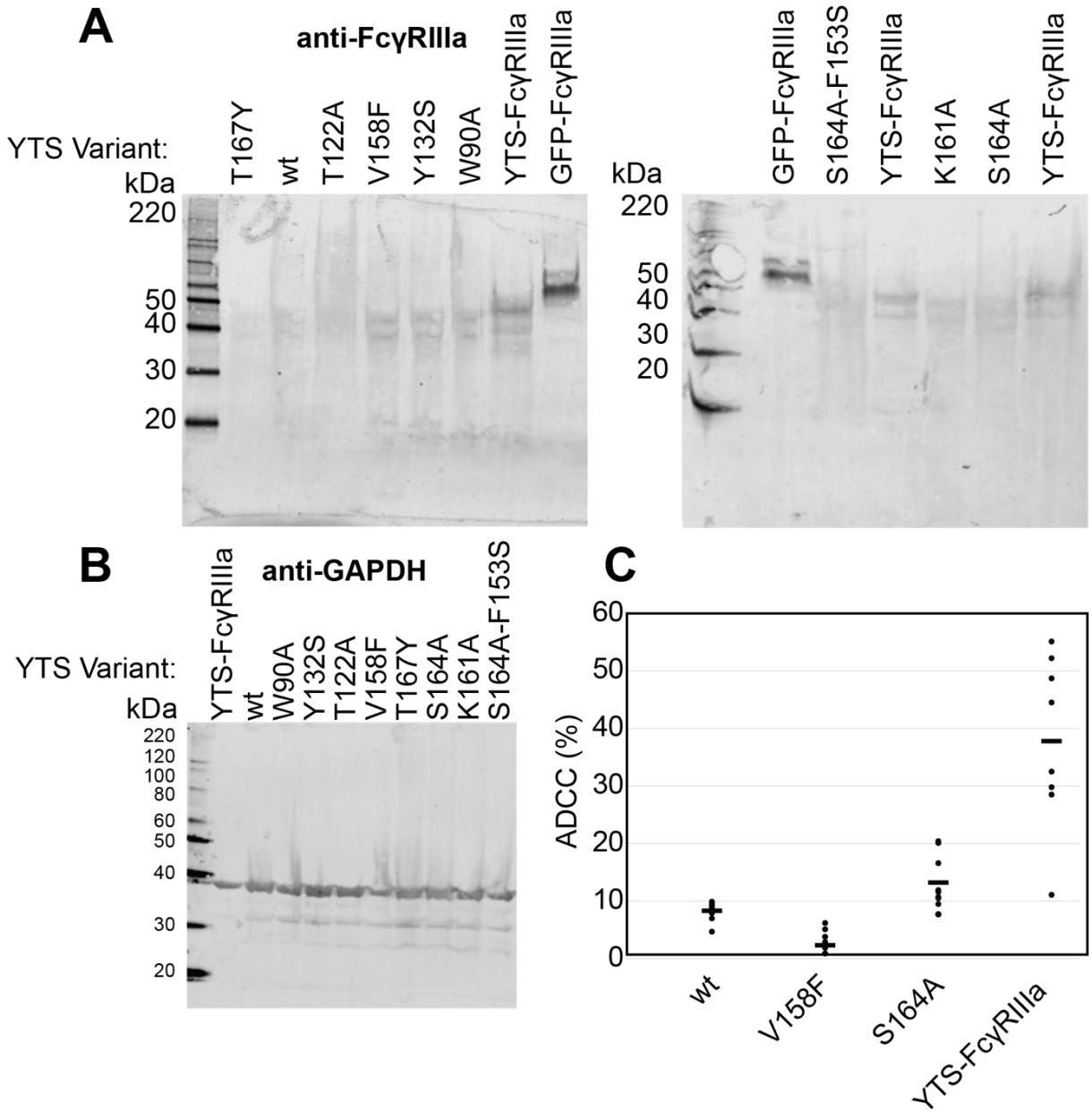

Supplemental Figure 3.1. Comparison of expression and ADCC of the previously-established YTS-FcγRIIIa NK cell line and the lentivirus-transduced cell lines prepared herein. **A.** Western blots showing expression levels compared to 40 ng of recombinant GFP-FcγRIIIa protein. "YTS-FcγRIIIa" refers to the previously established YTS-FcγRIIIa" cell line in

contrast to the lenti-virus transduced YTS cells expressing various FcγRIIIa variants described herein. **B**. GAPDH expression levels of the YTS cells. **C.** The ADCC of the YTS-FcγRIIIa cell line is greater than our YTS cells transduced with FcγRIIIa V158. Data shown include three independent experiments collected on different days, each with three replicates.

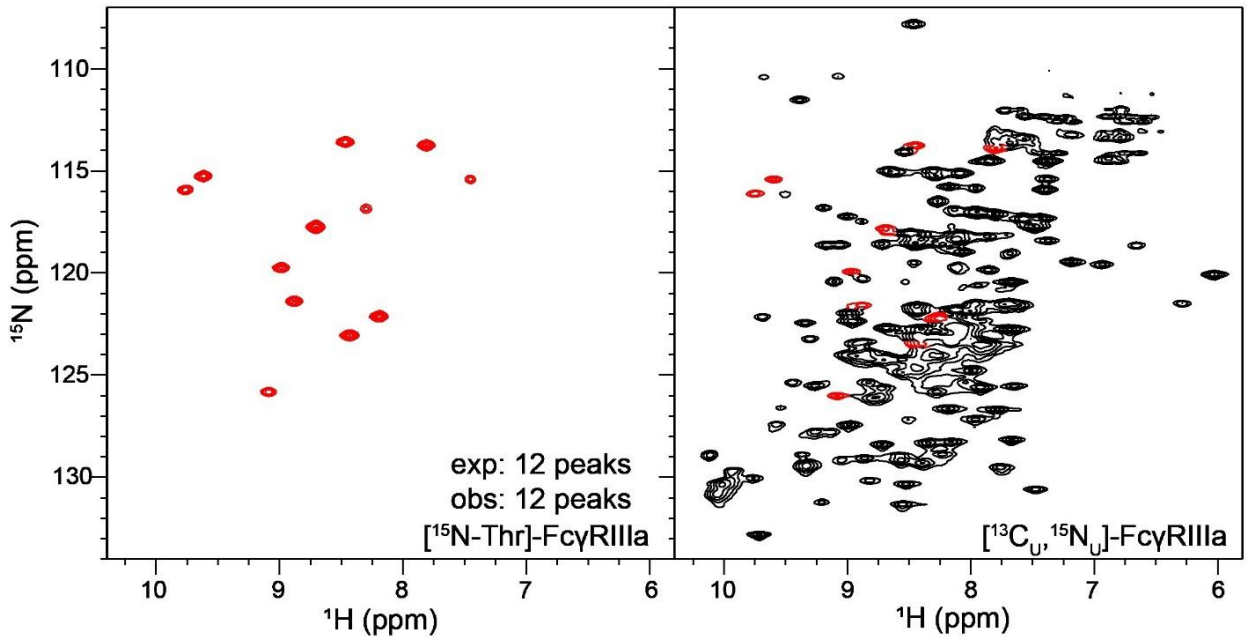

Supplemental Figure 3.2. Residue-specific labeling of the glycosylated FcγRIIIa. A. FcγRIIIa with two N-glycans expressed from HEK293F cells grown in medium supplemented with [^{15}N]-Threonine. **B.** Peaks in the spectrum of [^{13}C,^{15}N]-FcγRIIIa corresponding to threonine residues (*red* contours).

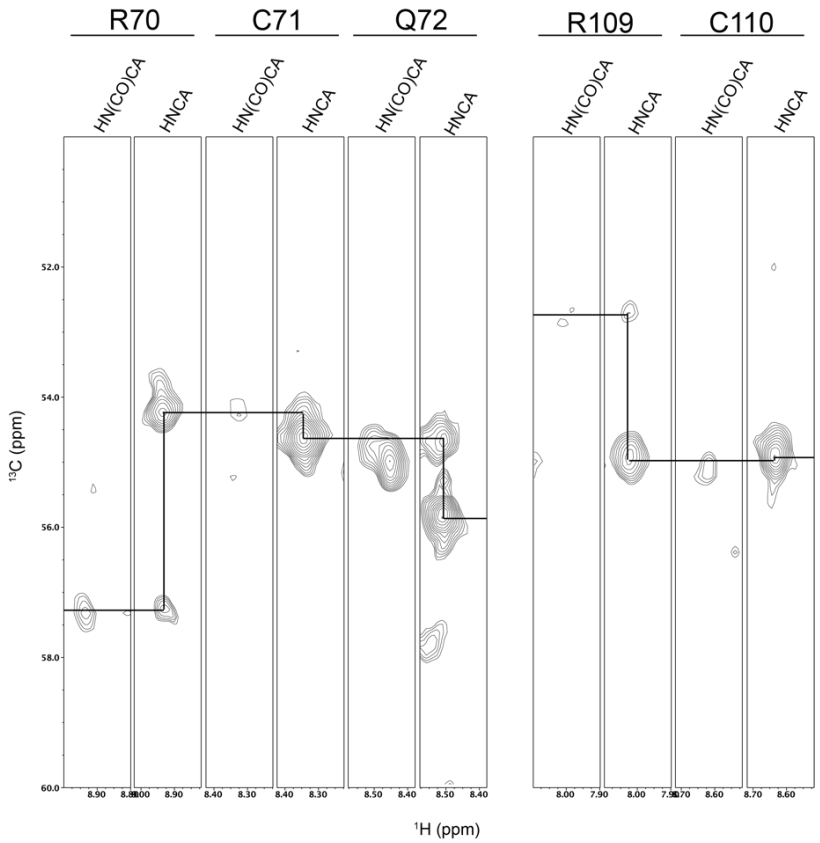

Supplemental Figure 3.3. Strip plots from triple resonance HNCA and HN(CO)CA experiments showing the assignments of the C71 and C110 resonances. The resonances for H111 were not identified. Residue connectivites are shown with a black line.

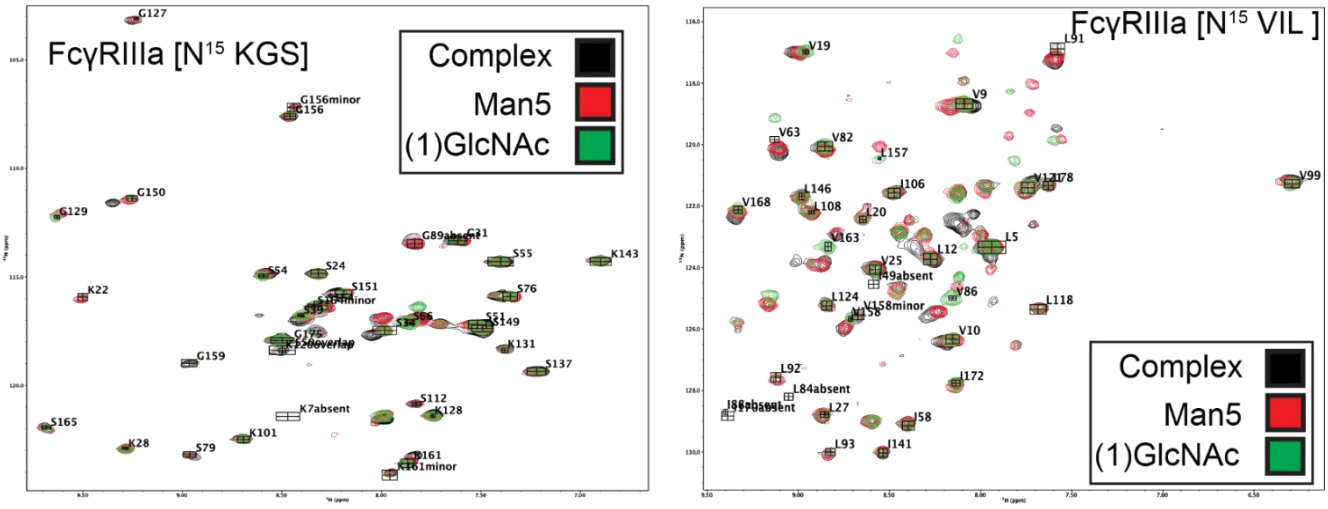

Supplemental Figure 3.4. Overlayed HSQC-TROSY spectra of ^{15}N-labeled FcγRIIIa with complex-type (*black*) 5-mannose (*red*) or (1)GlcNAc (*green*) N-glycans.

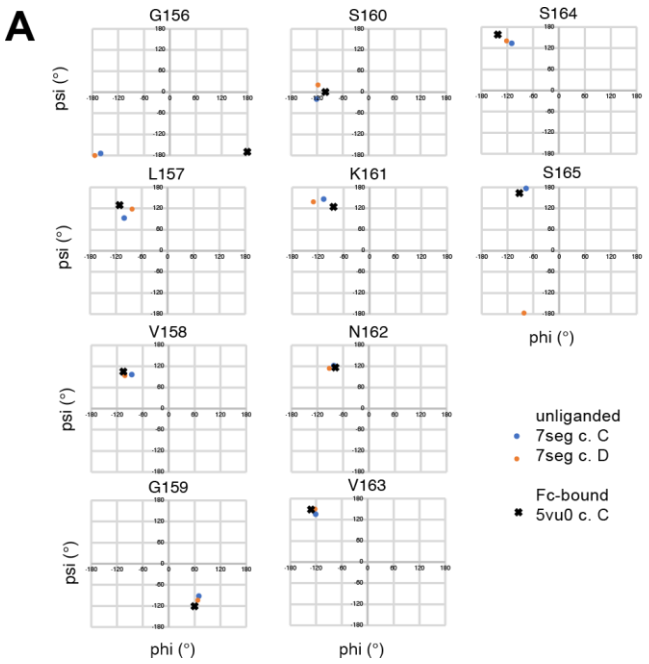

B

	7seg c. C		7seg c. D		5vu0 c. C	
Residue	phi (°)	psi (°)	phi (°)	psi (°)	phi (°)	psi (°)
153	-164	157	-147	166	-153	167
154	-119	157	-128	167	-126	164
155	-144	136	-160	150	-162	160
156	-161	-174	-174	-180	180	-170
157	-101	93	-83	118	-112	130
158	-86	97	-102	94	-105	106
159	70	-92	67	-103	60	-121
160	-121	-19	-118	20	-101	1
161	-107	147	-131	139	-84	124
162	-82	122	-92	115	-78	117
163	-121	136	-122	151	-132	149
164	-110	134	-122	141	-142	159
165	-77	177	-82	-178	-92	164
166	-78	174	-88	157	-74	166
167	-91	140	-82	152	-83	157
168	-127	122	-126	132	-139	147
169	-89	112	-89	108	-102	131
170	-103	128	-102	126	-116	125

Supplemental Figure 3.5. Backbone dihedral angles from two FcγRIIIa X-ray crystallography structures. A. Phi-Psi angle plots for select residues in the FG loop. **B.** Table of Phi-Psi angles for select FcγRIIIa residues. 7seg and 5vu0 are pdb IDs for the two datasets analyzed.

CHAPTER 4

CONCLUSION AND FUTURE DIRECTION

Structural difference between the CD16a 158 allotype

Understanding the mechanism behind the difference in affinity of the CD16a 158 allotype will inform therapeutic treatments involving NK cells. There are no current published structures of F158 CD16a, making it difficult to theorize the impact of this residue position. While some Fc engineering efforts have increased affinity to both 158 allotypes (1), it may be of interest to researchers to target the lower affinity F158 specifically, especially considering our recent evidence showing affinity and ADCC are linked. Improving F158 affinity, and by extension F158 ADCC, could eliminate different 158 allotype responses to antibody therapeutic treatments. This is especially important considering the allelic frequency ratio of F158 to V158 is 1.5:1 (2).

Here we have shown that the F158 substitution changes the backbone structure within the Fc-binding interface of CD16a relative to V158. The 158 residue itself does make direct contacts with Fc (3). Chemical shift perturbations were observed with residues K120 and Y132, which were later determined to be important for Fc-binding (Figure 2.5)(Figure 3.1). It is likely perturbation weakened the interaction of these residues with Fc and consequently lowered binding affinity. A second peak appeared on the HSQC of the N-linked anomeric carbon of the F158 N162 glycan (Figure 2.5). The additional conformation may be sterically prohibited from binding, lowering the average affinity of F158. This explanation falls within our suggested model that CD16a must exchange into a binding-competent form to bind Fc (Figure 3.6).

Lastly, F158 displays faster the binding kinetics. The association rate of fully-glycosylated F158 are greater than 2.5E+06 1/Ms, making it difficult to model (Figure 2.4).

Glycan truncation was used to lower kinetic rates, increasing affinity and allowing for better modeling. Comparison of (3)GlcNAc V/F158 revealed that the F158 kinetic rates were both around 2-fold faster than V158 (Figure 2.4). This is consistent with later measurement of F158 affinity to 4-fold lower than V158 (Figure 3.1). The quicker kinetic rates of F158 may decrease ADCC by lowering the amount of time CD16a is bound to opsonized pathogens.

The N162 glycan controls CD16a affinity

It was thought that the CD16a N162 glycan played an important role in its affinity after it was found that the N162Q mutation eliminated affinity gained between complex-type and oligmannose N-glycans (4). It was a new concept that glycan composition affected CD16a affinity and furthermore, suggesting that this effect was tied to one of the five N-glycan sites. The mechanistic details of this effect and its impact on ADCC were unknown. One possible hypothesis was that intramolecular glycan-protein contact(s) stabilized CD16a, thereby increasing its affinity. Mutagenesis of CD16a surface residues proximal to the N162 glycan did not significantly alter affinity, suggesting that no major stabilizing N162 glycan-protein contacts exist (Figure 3.1). None of these variant affinities were lower than 750 nM. Mass spectrometry of each variant revealed similar glycan composition at each N-glycan site, further discounting stabilizing intramolecular contacts.

Later investigation with solution NMR revealed that CD16a glycan composition changes its backbone environment (Figure 3.5). This experiment provided a full view of glycan processing from large, complex-type glycans to a single GlcNAc, with man5 exhibiting intermediate affinity. Nearly every probed residue had measured CSP's. Although many of these differences were not significant, several significant changes in chemical environment were found

near all five N-glycan sites upon truncation to man5. Truncation to (1)GlcNAc, the highest affinity CD16a form, had CSP's of the largest magnitude, localized near the N45 and N162 glycans. With N162 being in the binding interface, this observation explains the high (1)GlcNAc affinity.

This does not provide quantitative details on the contributions of each sugar residue. The most thorough former investigation of CD16a glycan composition accounted for four CD16a glycoforms (5). We expanded this to six different glycoforms, on both wt and S164A forms. Removal of sialic acid and core α-linked mannose provided large increases in affinity. The negative charge and hydrophilicity of sialic acid may impede the binding of Fc, in addition to the increased conformational entropy and rotamers an additional sugar provides (6). It is possible that the reduction in rotamers provided by core α-linked mannose truncation explains the relatively large increase in affinity. This is supported by the observation that all six glycan truncations resulted in an increased affinity. Comparison of these six truncations to the N162-lacking, S164A form show that this individual glycan is responsible for the majority of the compositional affinity effect. This is emphasized by the similar affinity of the sialylated forms, but a 12-fold affinity difference with the largest truncation, (1)GlcNAc (Figure 3.2).

ADCC assays provide evidence for the role of N162 at a cellular level. CD16a is required for NK cell ADCC (7). S164A YTS NK cells are insensitive to kifunensine treatment that reduces glycan processing in contrast to V158 YTS NK cells that see a 2-fold increase in ADCC with kifunensine treatment (Figure 3.2). The presence of N162 is the sole difference between these two cell lines, thus providing strong evidence for N162 mediating CD16a glycan compositional affinity effects.

ADCC and CD16a affinity are linked

Revealing the nature of the relationship between CD16a affinity and ADCC provides strong rationale for CD16a engineering. Previous studies have focused on the improvement of Fc to improve ADCC response, yet the CD16a side has been understudied (1,8,9). If affinity is linked to ADCC as Fc engineering implies, then engineering both Fc and CD16a would theoretically provide an exponential increase to ADCC. It was previously demonstrated that the 300 nM affinity V158 allotype displayed greater ADCC than the 1μM affinity F158. It was unknown if improvement of CD16a affinity would result in an increase in ADCC, or if V158 was the upper limit. We tested the ADCC of ten different CD16a variants and found a positive correlation with affinity (Figure 3.1). The four variants with the highest affinity had the highest ADCC.

Glycan composition and Fc defucosylation both increase affinity, as well as ADCC, providing further evidence linking ADCC to CD16a affinity. It is well supported herein, that CD16a glycan truncation increases its affinity (Figure 3.2)(Figure 2.3,2.4)(4). Further evidence has been provided showing that CD16a with under processed glycans has higher ADCC (Figure 3.3)(10). Additionally, afucosylated antibodies have higher affinity to CD16a, as well as higher ADCC (Figure 3.3)(11). Together, these data show affinity increases through mutagenesis, glycan composition, and antibody defucosylation lead to higher ADCC.

CD16a engineering as a platform to for NK cell immunotherapy

Having elucidated the mechanism of binding between CD16 and Fc, as well as identifying the important residues in this interaction, this information provides critical insights toward CD16a engineering. Perhaps the main limitation of using yeast display to improve CD16a

affinity is its problem with glycosylated proteins. CD16a having five N-gylcans despite its small 20 kDa size complicated any potential experiment using yeast display. We have known that the N38, N72, N169 glycans do not contribute to affinity, but N45 is critical to stability (12). The role of the N162 glycan was complicated and needed to be addressed before engineering efforts could take place. It lies near the interface of Fc, its removal did not significantly impact affinity however, glycan composition impacted affinity (12). Now that we understand how N162 glycan composition affects affinity, and that a fully processed CD16a has higher affinity without N162, we can use this information for engineering (13).

We have discovered that N162 glycan composition changes the backbone structure of CD16a near the Fc-binding interface (Figures 2.5,3.5). Furthermore, our analysis proposed a conformational change of the N162-containing FG loop to a binding-competent form that eliminates steric clashing of the loop and glycan with Fc, allowing it to bind (Figure 3.6). Using this new information, we can mutagenize target residues within the FG loop in effort to obtain a backbone conformation similar to the binding competent form, but one that will not occupy multiple states. Indeed, preliminary work done in collaboration with Dr. Aarya Venkat utilizes ProteinMPNN and AlphaFold2 to computationally model an engineered FG loop with the desired features. Future studies should utilize SPR for affinity determination and NMR to analyze backbone structure and determine if a binding-competent CD16a form can be stabilized and functional.

In either direction of targeted FG loop engineering or yeast surface display, functional analysis is required to confirm any potential therapeutic use. Promising hits should be transduced into NK cells and sorted for expression. Purified cell lines can be tested in ADCC assays to measure and

compare cytotoxicity to the other CD16a forms. One drawback of my CD16a variant YTS NK cell lines is that their CD16a expression and cytotoxicity is reduced compared to the original YTS- FcγRIIIa cell line. Little information on this cell line is publicly available, leaving improvement of our lines up to speculation. One aspect that should be investigated is the promoter use for CD16a expression. In my cell lines the cytomegalovirus (CMV) promoter was used for CD16a expression while the EF1α promoter was used for GFP. NK cells and CMV have co-evolved defense mechanisms to evade one another (14). It is possible that NK cells have an innate mechanism for downregulating CMV viral infections that would induce from the CMV promoter. Obtaining similar expression and ADCC of our internal YTS-V158 line to the YTS-FcγRIIIa cell line is essential to establish engineered CD16a NK cells as a potential therapy. Once the cell lines are similar, the CD16a gene can be replaced or modified with the engineered high affinity .

References

1. Mossner, E., Brunker, P., Moser, S., Puntener, U., Schmidt, C., Herter, S., Grau, R., Gerdes, C., Nopora, A., van Puijenbroek, E., Ferrara, C., Sondermann, P., Jager, C., Strein, P., Fertig, G., Friess, T., Schull, C., Bauer, S., Dal Porto, J., Del Nagro, C., Dabbagh, K., Dyer, M. J., Poppema, S., Klein, C., and Umana, P. (2010) Increasing the efficacy of CD20 antibody therapy through the engineering of a new type II anti-CD20 antibody with enhanced direct and immune effector cell- mediated B-cell cytotoxicity. *Blood* **115**, 4393-4402

2. Mahaweni, N. M., Olieslagers, T. I., Rivas, I. O., Molenbroeck, S. J. J., Groeneweg, M., Bos, G. M. J., Tilanus, M. G. J., Voorter, C. E. M., and Wieten, L. (2018) A comprehensive overview of FCGR3A gene variability by full-length gene sequencing including the identification of V158F polymorphism. *Sci Rep* **8**, 15983
3. Falconer, D. J., Subedi, G. P., Marcella, A. M., and Barb, A. W. (2018) Antibody Fucosylation Lowers the FcgammaRIIIa/CD16a Affinity by Limiting the Conformations Sampled by the N162- Glycan. *ACS Chem Biol* **13**, 2179-2189
4. Subedi, G. P., and Barb, A. W. (2018) CD16a with oligomannose-type N-glycans is the only "low- affinity" Fc gamma receptor that binds the IgG crystallizable fragment with high affinity in vitro. *J Biol Chem* **293**, 16842-16850
5. Mizushima, T., Yagi, H., Takemoto, E., Shibata-Koyama, M., Isoda, Y., Iida, S., Masuda, K., Satoh, M., and Kato, K. (2011) Structural basis for improved efficacy of therapeutic antibodies on defucosylation of their Fc glycans. *Genes Cells* **16**, 1071-1080
6. Soares, C. O., Grosso, A. S., Ereno-Orbea, J., Coelho, H., and Marcelo, F. (2021) Molecular Recognition Insights of Sialic Acid Glycans by Distinct Receptors Unveiled by NMR and Molecular Modeling. *Front Mol Biosci* **8**, 727847
7. Narvekar, A., Pardeshi, A., Jain, R., and Dandekar, P. (2022) ADCC enhancement: A conundrum or a boon to mAb therapy? *Biologicals* **79**, 10-18
8. Presta, L. G., Shields, R. L., Namenuk, A. K., Hong, K., and Meng, Y. G. (2002) Engineering therapeutic antibodies for improved function. *Biochem Soc Trans* **30**, 487-490
9. Townsend, W., Hiddemann, W., Buske, C., Cartron, G., Cunningham, D., Dyer, M. J. S., Gribben, J. G., Phillips, E. H., Dreyling, M., Seymour, J. F., Grigg, A., Trotman, J., Lin, T. Y., Hong, X. N., Kingbiel, D., Nielsen, T. G., Knapp, A., Herold, M., and Marcus, R.

(2023) Obinutuzumab Versus Rituximab Immunochemotherapy in Previously Untreated iNHL: Final Results From the GALLIUM Study. *Hemasphere* **7**, e919

10. Rodriguez Benavente, M. C., Hughes, H. B., Kremer, P. G., Subedi, G. P., and Barb, A. W. (2023) Inhibiting N-glycan processing increases the antibody binding affinity and effector function of human natural killer cells. *Immunology* **170**, 202-213

11. Shields, R. L., Lai, J., Keck, R., O'Connell, L. Y., Hong, K., Meng, Y. G., Weikert, S. H., and Presta, L.G. (2002) Lack of fucose on human IgG1 N-linked oligosaccharide improves binding to human Fcgamma RIII and antibody-dependent cellular toxicity. J Biol Chem 277, 26733-26740

12. Patel, K. R., Roberts, J. T., Subedi, G. P., and Barb, A. W. (2018) Restricted processing of CD16a/Fc gamma receptor IIIa N-glycans from primary human NK cells impacts structure and function. *J Biol Chem* **293**, 3477-34

13. Reeves, P. J., Callewaert, N., Contreras, R., and Khorana, H. G. (2002) Structure and function in rhodopsin: high-level expression of rhodopsin with restricted and homogeneous N-glycosylation by a tetracycline-inducible N-acetylglucosaminyltransferase I-negative HEK293S stable mammalian cell line. *Proc Natl Acad Sci U S A* **99**, 13419-13424

14. Barnes, S., Schilizzi, O., Audsley, K. M., Newnes, H. V., and Foley, B. (2020) Deciphering the Immunological Phenomenon of Adaptive Natural Killer (NK) Cells and Cytomegalovirus (CMV). *Int J Mol Sci* **21**

APPENDIX A

THE ANTIBODY-BINDING FC GAMMA RECEPTOR IIIA / CD16A IS N-GLYCOSYLATED WITH HIGH OCCUPANCY AT ALL FIVE SITES[1]

[1]Lampros, Elizabeth A., Kremer, Paul G., Aguilar Díaz de León, Jesus S., Roberts, Elijah T., Rodriguez Benavente, Maria C., Amster, I. John., & Barb, Adam W. 2022. Current research in immunology, 3, 128–135.

Abstract

The antibody-binding Fc γ receptors (FcγRs) trigger life-saving immune responses. One proven strategy to improve efficacy of therapeutic monoclonal antibodies that require FcγR engagement for full effect is to increase receptor binding affinity, in particular binding to FcγRIIIa / CD16a. Currently, affinities are measured using recombinantly-expressed soluble extracellular FcγR domains and it is notable that these domains are highly processed with multiple N-glycosylation sites. Multiple groups have demonstrated that CD16a N-glycan composition is variable and composition impacts antibody binding affinity. Despite these observations, it is not known if N-glycans are present at high levels at each site. Here we determined the occupancy of the five CD16a N-glycosylation sites using complementary mass spectrometry-based methods. N-glycans modified four CD16a sites (N38, N45, N162 and N169) at levels >84% for the V158 and F158 allotypes based on MS analyses of peptides following enzymatic N-glycan release. Likewise, N-glycans occupied >93% of the N38, N45 and N162 sites on the V158/T171A variant that lacks the N169-glycosylation site. Peptides containing the N74 site degraded during sample preparation, though specifically blocking this process revealed ~90% N74 occupancy for the V158 allotype. Thus, a proteomics approach demonstrated a high degree of N-glycan modification for three CD16a variants. Orthogonal validation using intact protein mass spectrometry confirmed these results and demonstrated that the predominant species identified by intact protein mass spectrometry corresponded to CD16a with five N-glycans, with a smaller contribution from CD16a with four N-glycans.

Introduction

The interaction of an antibody-coated target with leukocyte-expressed Fc γ receptors (FcγRs) has the potential to stimulate multiple types of protective immune responses (de Taeye, et al. 2019). Several reports indicate that the sensitivity and the strength of FcγR-mediated responses may be increased to improve the treatment of multiple diseases including cancers, infection and autoimmunity (Cartron, et al. 2002, Weng and Levy 2003, Zhang, et al. 2007, Musolino, et al. 2008, Bibeau, et al. 2009). For example, improving the FcγR-binding affinity of select antibodies that require FcγR interactions for full therapeutic effect improved efficacy, including the remarkable doubling of life expectancy in one obinutuzumab trial (Mossner, et al. 2010, Niederfellner, et al. 2011, Salles, et al. 2012, Herter, et al. 2013, Cheson, et al. 2018, Pott, et al. 2020). These observations support the effort to develop antibodies with improved FcγR-binding affinity, largely by engineering either the Fc N-glycan or the Fc polypeptide (Liu, et al. 2020, Gunn, et al. 2021). Among the five cognate activating FcγRs, FcγRIIIa, also known as CD16a, is the primary target for engineered antibodies because it is primarily responsible for eliciting antibody-dependent cell-mediated cytotoxicity (ADCC)(Wu, et al. 2019).

CD16a is heavily processed and contains five N-glycosylation sites. Prior studies showed a high degree of glycan heterogeneity at different N-glycosylation sites using recombinant CD16a or CD16a purified from primary human leukocytes (Zeck, et al. 2011, Patel, et al. 2019, Patel, et al. 2020, Roberts, et al. 2020, Patel, et al. 2021). Furthermore, CD16a with minimally-processed N-glycans increases IgG1 Fc binding affinity (Hayes, et al. 2017, Patel, et al. 2018, Subedi and Barb 2018). Among the five N-glycosylation sites, both N162 and N45 impact antibody binding affinity, and the three remaining sites may contribute to yet undefined properties of CD16a on

the cell surface considering a high degree of processing at N38 and N74 (Drescher, et al. 2003, Shibata-Koyama, et al. 2009, Subedi and Barb 2018, Patel, et al. 2019). However, though the prior glycoproteomics approaches identified the presence of N-glycans at each of the five sites, these data do not distinguish the relative levels of N-glycosylation at each site; it is possible that each site is modified at a different frequency and impacts function.

Carbohydrates reduce the ionization of peptides, thus it is not possible to directly compare the signal intensities of glycosylated peptides to aglycosylated peptides in glycoproteomics experiments without an internal standard for each species (Riley, et al. 2020). Occupancy may be estimated using PNGaseF, an enzyme that cleaves the bond between the Cγ atom and sidechain N of Asn, releasing the N-glycan and generating an Asp residue where an N-glycan was formerly attached (Plummer, et al. 1984). This reaction increases the mass of the peptide by 0.984 Da, and the glycosylation percentage is determined by calculating the individual contribution of Asn and Asp containing peptides to the signal intensity in an MS spectrum (Carr and Roberts 1986). There are a few notable caveats to this approach. First, substitution of an Asp residue changes the retention time for some peptides; this situation may be addressed by carefully selecting the window of retention times included for the calculation. Second, unmodified Asn residues may spontaneously deamidate, forming an Asp residue without N-glycosylation or PNGaseF activity. This outcome is reduced by preparing samples for analysis immediately prior to MS analysis, or by storing samples in a lyophilized state prior to analysis. Furthermore, spontaneous deamidation in the sample may be quantified by comparing isotopologue patterns for non-N-glycosylated Asn-containing peptides in the sample. Third, it is also possible that confounding peaks may obscure the isotopologue patterns and thus deconvolution of the Asp and Asp containing

peptides. This scenario may be addressed by using specialized hardware capable of high-resolution detection, or by incorporating 18O into the Asp residue in place of 16O, and observing a mass increase of 2.988 Da relative to an unmodified Asn residue (Gonzalez, et al. 1992). However, 18O incorporation can be complicated by [18O]-water concentrations below 100% that requires accounting for both 16O and 18O incorporation into Asp and acid catalyzed exchange of 18O atoms at other sites.

Recent advances in intact protein mass spectrometry also provide a route to estimating N-glycan occupancy (Chen, et al. 2021, Rogals, et al. 2021). This approach determines the mass of the intact protein with complete N-glycans, but may be complicated by a high degree of N-glycan heterogeneity. Recombinant expression from a cell line modified to limit N-glycan processing, including Gnt1- HEK293S cells (Reeves, et al. 2002), dramatically reduces heterogeneity. Fully N-glycosylated species may be assigned based on the mass measurement, however, a multiply-glycosylated protein with partial occupancy may generate multiple configurationally-distinct isomers.

We investigated CD16a using multiple mass spectrometry-based approaches to estimate the N-glycan occupancy at each individual site. We compared different single amino acid variants including the naturally occurring high affinity V158 allotype and the low affinity F158 allotype that is more common in the human population to identify any potential differences in N-glycan occupancy (Bruhns, et al. 2009). We also analyzed the V158/T171A variant which disrupts the sequence for N169 glycosylation because the proximity of the site at only five residues from the C-terminus indicates N-glycan occupancy may be low and potentially impact N162 glycosylation (Bano-Polo, et al. 2011).

Experimental Methods

Materials – All materials were purchased from Millipore Sigma unless otherwise noted.

Protein expression and purification – The soluble extracellular antibody-binding domain of CD16a V158 corresponding to residue R1-G174 was prepared as previously described (Subedi, et al. 2014, Subedi and Barb 2015). TEV digestion followed by size exclusion chromatography and EndoF1 digestion were performed as previously described, except that a Superdex75 column was used (Subedi, et al. 2017). Plasmids encoding the soluble CD16a F158, and T171A variants were prepared using fusion PCR (Ho, et al. 1989).

PNGaseF digestion using [16O]water – Sample (20 μg) in 50 μL of 50 mM ammonium carbonate, 10% MeOH, pH 8, was boiled for 5 min. Then, 1 μL of 0.25 M dithiothreitol (DTT) was added to reduce the proteins' disulfide bonds. The samples were then incubated at 37 °C for 1 h. Iodoacetamide (IAM, 1.4 μL of 0.5 M) was then added followed by incubation at RT for 30 min in the dark. The reaction was quenched with an additional 1 μL of 0.25 M DTT and an additional 15 min incubation at RT in the dark. The endoproteases GluC (1 μL of 1 mg/mL; Promega) and chymotrypsin (1.5 μL of 1 mg/mL) were added to the samples, which were then incubated overnight at 37 °C. Some samples were boiled for 5 min following proteolysis. Peptides were isolated using a C18 resin according to the manufacturer's instructions. Fractions eluted from the C18 resin in 80:20:1 acetonitrile:water:formic acid and were frozen and then lyophilized. The lyophilized product was resuspended in 2 μL 50 mM sodium phosphate, pH 7.5

and 17 µL of water. PNGase F (1 µL; New England Biolabs) was added to each sample and then incubated overnight at 37° C. Peptides were lyophilized, resuspended with water, and purified with a C18 step prior to MS. Some samples, as noted, were boiled for 5 min prior to the C18 purification. Efficiency of the PNGase F reaction was monitored with an intact (non-proteolyzed) CD16a V158 sample using an SDS-PAGE and compared to a sample prepared without PNGase F addition.

PNGaseF digestion using [18O]water – Peptides from samples (20 µg) were prepared as described above, except without C18 purification. Lyophilized peptides were resuspended with 19 µL of 97% 1H2-18O. Simultaneously, glycerol-free PNGase F (New England Biolabs) was lyophilized, resuspended in an equal volume of 1H2-18O, lyophilized again, and finally resuspended in an equal volume of 1H2-18O. [18O-exchanged]-PNGase F (1 µL) was added to 19 µL of lyophilized peptides and then incubated overnight at 37° C. Peptides were lyophilized, resuspended with water, and purified with a C18 step prior to MS.

Peptide mass spectrometry – Each sample (0.5 µL) was loaded into an EASY nLC-1200 LC system with PepMap nanocolumn (ThermoFisher) and a Nanospray FlexIon source (ThermoFisher) and analyzed with a Q Exactive Plus Hybrid Quadrupole-Orbitrap Mass Spectrometer (ThermoFisher). Liquid chromatography and mass spectrometry were performed as described (Patel, et al. 2021). Peptides were identified using Byonic (ProteinMetrics). Manual validation of the MS1 spectra including differences in observed and calculated m/z, as well as the presence of expected y and b ions calculated using the Proteomics Toolkit Fragment Ion

Calculator from MS2 spectra for each peptide was performed in XCaliber Qual Browser (ThermoFisher) and is reported in a supplemental table. RAW files for each proteomics sample are deposited in the MASSIVE server (https://massive.ucsd.edu/ProteoSAFe/static/massive.jsp) under the accession number MSV000088222 (massive.ucsd.edu).

The Asn v. Asp content of peptides containing N-glycosylation sites were determined by extracting the MS1 spectra containing both peptides using an R script (Supplemental Methods). Often, these eluted in overlapping retention time windows and a single window that encompassed both species was chosen for analysis. A second R script (Supplemental Methods) fitted the coefficients for the amount of Asn and Asp peptides to the intensity data for each peak. The expected isotope distributions were calculated for each CD16a glycosylation site using ProteinProspector MS-Isotope (Chalkley, et al. 2008). The percentage of N-glycosylation at each site was then determined by dividing the intensity of the Asp-containing peptide by the sum of the intensities for the Asp and Asn containing peptides.

Intact protein mass spectrometry – Protein samples were buffer exchanged using 10 kDa MWCO centrifugal spin filters into 50 mM ammonium acetate (SigmaUltra >98%) in HPLC grade water, and concentrated to a final protein concentration of 1-7 μM. Mass spectra were collected using a SolariX XR 12 T Fourier transform ion cyclotron resonance mass spectrometer (Bruker Scientific). Samples were introduced by direct infusion into an electrospray ionization source at a rate of 120 μL/min, using a capillary inlet voltage of 4200-4500 V. Mass spectra were collected in positive mode in the range of m/z 1000-3000. The transient length was 2.7962 s and 1 M

points were collected. Mass spectra were analyzed using Data Analysis (Bruker Scientific), and protein monoisotopic masses were determined using the SNAPTM algorithm.

Results

Site-specific N-glycan occupancy – We determined N-glycan occupancy at each site using a proteomics-based approach. This approach does not require N-glycan homogeneity because N-glycans are removed during the analysis, providing an opportunity to characterize CD16a N-glycan occupancy with highly heterogeneous N-glycans (Patel, et al. 2021).

The CD16a V158 allotype produced 156 unique peptides covering 94.9% of the protein. The F158 allotype and V158/T171A variant revealed 151 and 145 peptides, respectively, but slightly higher coverages with 99.4% and 98.9%, respectively. The average mass error for all identified peptides was 6.43 ppm. Assigned MS2 spectra unambiguously defined peptides containing N-glycosylation sites to support analyses of N-glycan occupancy. We quantified the intensity of each MS1 peak in the multiplet by fitting a Gaussian line shape function (Figure A.1). Fitting these intensity data with predicted intensities of the Asp- and Asn-containing peptides deconvoluted the relative contribution from each peptide to the observed spectrum, and allowed an estimate of the experimental error by using all peaks from the multiplet. Finally, N-glycan occupancy was determined by dividing the abundance of the Asp-peptide by the total of the Asn- and Asp-peptides.

CD16a V158 peptides containing the N38, N45, N162 and N169 glycosylation sites showed minimal contribution to the observed intensities resulting from masses calculated using Asn residues in the N-glycosylation sequon; peptides with Asp residues at these sites dominated

with a contribution of 91 – 99.8% of the intensities observed in MS1 spectra (Figure A.2). These data indicate high levels of N-glycosylation at N38, N45 N162 and N169 (Table A.1). Two peptides containing the N74 glycosylation site, however, showed no Asp content.

The CD16a F158 allotype revealed comparable N-glycan occupancy with high levels at N38, N45, N162 and N169, though the N38 levels were slightly lower at 84% (Table A.1). The CD16a F158 N74 site likewise showed no Asp content.

We also analyzed a single residue variant of the CD16a V158 allotype, T171A, that disrupts the terminal N-glycan sequon to block N169 modification. The N38, N45 and N162 again showed high levels of N-glycosylation ranging from 92.9 – 100% (Table A.1). The CD16a V158/T171A N74 peptides were likewise devoid of Asp content in the N-glycosylation sequon.

Site specific occupancy using 18O-water – We performed the PNGaseF reaction in [18O]-water to provide greater separation between the Asp and Asn containing peptide products and validate the results from [16O]-water. One factor complicating the PNGaseF reaction is that reagents or impure [18O]-water can introduce [16O]-water, requiring careful separation of peptide peaks containing Asn, [16O]-Asp or [18O]-Asp (Gonzalez, et al. 1992). This may be reduced by introducing [18O]-water following lyophilization of the substrate peptides. To our surprise, PNGaseF retained activity following two lyophilization steps, allowing near complete exchange to [18O]-water and reducing the contribution of [16O]-water to <1% in the reaction (Figure S.A.2).

Peptides containing the N38, N45, N162 and N169 glycosylation sited revealed substantial [18O] incorporation. MS2 spectra of these peptides indicated that the majority of the

Asp residues in the D-X-S/T sequon contained at least one [18O] atom. These results are consistent with measurements performed using [16O]-water (Figure A.2 and Table A.1). The N74 peptides again showed no evidence for [18O]-Asp incorporation.

N74 glycan occupancy – The absence of detectable N74 glycosylation was surprising, and suggests a low occupancy for the N74 glycan. This conclusion is unexpected based on previous characterizations of N74 glycans using the same recombinant protein source, as well as studies of CD16a purified from primary human monocytes and NK cells (Patel, et al. 2019, Roberts, et al. 2020, Patel, et al. 2021).

One possible explanation for low estimates of N74 occupancy is that the presence of residual GluC endoproteinase activity during the PNGaseF glycan removal reaction could cleave peptides if an Asp is formed following N-glycan removal. This cleavage would degrade formerly N-glycosylated peptides, and the data would appear as if no Asp residues, and thus no N-glycan occupancy, were present on a given peptide. Furthermore, the degraded Asp-containing peptides would not be identified by the spectral analysis algorithm that uses the native CD16a sequence as an input.

Identification of the L75 peptide provided evidence for GluC cleavage of the N74-containing peptide and thus underestimation of N-glycan occupancy at N74 (Figure A.4). A small amount of peptide degradation appeared at N38 and N162. It is unclear why the N74 peptide is a more suitable substrate for GluC activity compared to peptides containing the other four sites, perhaps this observation is due to the larger size of the N74 peptide or a potentially optimal amino acid sequence.

To reduce GluC-catalyzed degradation of the N74 peptide following PNGaseF digestion, we repeated the experiment by adding a heat denaturation step following proteolysis and prior to reversed-phase purification. Analysis of these spectra demonstrated clear Asp content in the N74 peptides, and thus a high level of occupancy (Figure A.5). Furthermore, the L75 peptide was present at a low level. Two peptides containing the N74 site showed 92.8 ±2.0% and 89.4 ±0.9% Asp content and thus N-glycan occupancy. This result is consistent with previous MS-based analyses of CD16a glycoproteomics showing diverse glycan species at N74.

Detailed examination of mass spectra generated from reactions in [18O]-water reveals additional [18O] labels incorporated into peptides containing the N74, N162 and N169 glycosylation sites (Figure A.3). An MS2 spectrum of the longer N74 revealed that two additional [18O] atoms were incorporated into the C-terminal Glu residue. Others have noted that auxiliary labeling reactions resulted from the presence of residual protease activity (Alley, et al. 2013, Shajahan, et al. 2017). The same heat treatment to remove protease activity that reduced N74 cleavage following PNGaseF cleavage did not reduce the auxiliary [18O] incorporation into the N74, N162 and N169 peptides, indicating that the auxiliary labeling is not catalyzed by the GluC protease.

Intact CD16a mass spectrometry – Mass spectrometry of an intact glycoprotein provides information regarding N-glycan occupancy, however, compositional heterogeneity resulting from extensive N-glycan processing introduces complexity. To reduce heterogeneity, we expressed the CD16a V158 allotype in HEK293 cells that lack a key N-glycan processing enzyme, Gnt1/MGAT1 (Reeves, et al. 2002). These cells express CD16a with predominantly

Man5 N-glycans at each N-glycosylation site (Subedi and Barb 2018). CD16a is expressed as an N-terminal GFP fusion, that once removed, revealed clear mobility differences on a Superdex75 size exclusion column (Figure A.6A). SDS-PAGE analysis revealed an upper and lower band, of roughly equal intensities, both separated from GFP (Figure A.6B). Selection of fractions 61,62, 67 and 69 included an increasing amount of the smaller CD16a band and GFP (Figure A.6C). Incubation with endoglycosidase F1 (EndoF) efficiently trimmed the CD16a N-glycans to a single GlcNAc residue, collapsing the distinct CD16a bands into a single band with greater mobility (Figure A.6C). By comparison, GFP lacks an N-glycan and showed no change in mobility.

Analyses of both the EndoF-treated and untreated Superdex75 fractions by FT-ICR MS revealed high molecular weight species with multiple charge states. The two highest intensity peaks observed in fraction 61 following EndoF treatment represented a single species with three charge states (Figure A.6D). The observed mass calculated from the major species observed in fraction 61, following deconvolution, proved highly comparable to the calculated mass of CD16a with five GlcNAc residues with a mass error of 0.618 ppm (Table A.2). Fraction 61 prior to EndoF treatment revealed a lower mass error value of 0.176 ppm and corresponded to CD16a with five Man5 N-glycans.

Fraction 69 contained two major species, each with three charge states (Figure A.6D). The most abundant species matched that observed in fraction 61. The observed mass calculated from the second most intense species observed in fraction 69, following deconvolution, proved highly comparable to the calculated mass of CD16a with four GlcNAc residues with a mass error of 0.632 ppm (Table A.2). This same species from the same fraction, prior to EndoF treatment,

revealed a lower mass error value of 0.128 ppm and corresponded to CD16a with four Man5 N-glycans. In total, these results indicate that the two major CD16a species contained five or four N-glycans, and is consistent with the proteomics measurements.

Discussion

These data provide a thorough characterization of CD16a N-glycan occupancy. All CD16a N-glycosylation sites are highly modified. It is somewhat surprising that the CD16a N169 and N162 sites are highly modified; these two sites are close to the C-terminus of this construct (G174) and likely result from a highly efficient STT3B modification because STT3A is expected to modify the C-terminal N-glycosylation sites with very low efficiency (Shrimal, et al. 2013). The high levels of N162 occupancy in the V158/T171A variant indicate that glycosylation at N162 is independent from N169 glycosylation (Table A.1). Previous observations with the highly homologous receptor, CD16b, both found high N-glycan occupancy for most sites but a low level at the N64 site (Washburn, et al. 2019, Wojcik, et al. 2020). Though the N64 site is not found in CD16a, these two receptors share 97.7% amino acid identity for the extracellular domains.

It is notable that the F158 and V158 allotypes reveal statistically indistinguishable N-glycan occupancy at each site (Table A.1). Though the F158 allotype binds with reduced affinity relative to V158 (Bruhns, et al. 2009), glycan occupancy differences are unlikely to account for differences in affinity. The factor(s) contributing to the affinity difference remain undefined.

With respect to future efforts measuring N-glycan occupancy with [18O] incorporation, the preservation of PNGaseF activity following two lyophilization steps allows a significant

reduction of the [16O]-water content when isotope labeling is desired (Figure S.A.1). The spectra for the V158 allotype collected with samples digested in [18O]-water reveal a small amount of peptide corresponding to Asp without [18O] incorporation, which is expected following incorporation of an [16O] atom. This is most notable with the MS1 spectrum of the N45-containing peptide that shows <1% of this peptide (Figure A.3). It is interesting that N38 and N169 show an increased [16O] content that could be explained by deamidation of an unoccupied N169 prior to the PNGaseF reaction.

Finally, there is currently a growing interest in CD16a as a therapeutic, as a target for antibodies to recruit and/or activate NK cells, or for engineering to increase effector response efficiency (Zhao, et al. 2020, Zhu, et al. 2020, Bogen, et al. 2021). A complete description of N-glycan occupancy, like that described here, is essential to identify variables that potentially impact function. Furthermore, the presence of an N-glycan dramatically alters how that portion of the protein surface is perceived by the environment and thus represents an important intrinsic feature of any glycosylated protein.

Acknowledgement

We thank Dr. Elisabet Gas Pascual (UGA) for operating the Q Exactive Plus mass spectrometer.

Funding

Funding to A.W.B. by the National Institutes of Health under Awards No. U01 AI148114 (NIAID). I. J. A. is grateful for funding of the 12 T FTICR mass spectrometer by the National

Institutes of Health, award S10 OD025118. The content is solely the responsibility of the authors and does not necessarily represent the official views of the National Institutes of Health.

Conflict of Interest

The authors declare no conflicts of interest.

References

Alley WR, Jr., Mann BF, Novotny MV. 2013. High-sensitivity analytical approaches for the structural characterization of glycoproteins. Chem Rev, 113:2668-2732.

Bano-Polo M, Baldin F, Tamborero S, Marti-Renom MA, Mingarro I. 2011. N-glycosylation efficiency is determined by the distance to the C-terminus and the amino acid preceding an Asn-Ser-Thr sequon. Protein Sci, 20:179-186.

Bibeau F, Lopez-Crapez E, Di Fiore F, Thezenas S, Ychou M, Blanchard F, Lamy A, Penault-Llorca F, Frebourg T, Michel P, et al. 2009. Impact of Fc{gamma}RIIa-Fc{gamma}RIIIa polymorphisms and KRAS mutations on the clinical outcome of patients with metastatic colorectal cancer treated with cetuximab plus irinotecan. J Clin Oncol, 27:1122-1129.

Bogen JP, Carrara SC, Fiebig D, Grzeschik J, Hock B, Kolmar H. 2021. Design of a Trispecific Checkpoint Inhibitor and Natural Killer Cell Engager Based on a 2 + 1 Common Light Chain Antibody Architecture. Front Immunol, 12:669496.

Bruhns P, Iannascoli B, England P, Mancardi DA, Fernandez N, Jorieux S, Daeron M. 2009. Specificity and affinity of human Fcgamma receptors and their polymorphic variants for human IgG subclasses. Blood, 113:3716-3725.

Carr SA, Roberts GD. 1986. Carbohydrate mapping by mass spectrometry: a novel method for identifying attachment sites of Asn-linked sugars in glycoproteins. Anal Biochem, 157:396-406.

Cartron G, Dacheux L, Salles G, Solal-Celigny P, Bardos P, Colombat P, Watier H. 2002. Therapeutic activity of humanized anti-CD20 monoclonal antibody and polymorphism in IgG Fc receptor FcgammaRIIIa gene. Blood, 99:754-758.

Chalkley RJ, Baker PR, Medzihradszky KF, Lynn AJ, Burlingame AL. 2008. In-depth analysis of tandem mass spectrometry data from disparate instrument types. Mol Cell Proteomics, 7:2386-2398.

Chen S, Wu D, Robinson CV, Struwe WB. 2021. Native Mass Spectrometry Meets Glycomics: Resolving Structural Detail and Occupancy of Glycans on Intact Glycoproteins. Anal Chem, 93:10435-10443.

Cheson BD, Chua N, Mayer J, Dueck G, Trneny M, Bouabdallah K, Fowler N, Delwail V, Press O, Salles G, et al. 2018. Overall Survival Benefit in Patients With Rituximab-Refractory Indolent Non-Hodgkin Lymphoma Who Received Obinutuzumab Plus Bendamustine Induction and Obinutuzumab Maintenance in the GADOLIN Study. J Clin Oncol, 36:2259-2266.

de Taeye SW, Rispens T, Vidarsson G. 2019. The Ligands for Human IgG and Their Effector Functions. Antibodies (Basel), 8.

Drescher B, Witte T, Schmidt RE. 2003. Glycosylation of FcgammaRIII in N163 as mechanism of regulating receptor affinity. Immunology, 110:335-340.

Gonzalez J, Takao T, Hori H, Besada V, Rodriguez R, Padron G, Shimonishi Y. 1992. A method for determination of N-glycosylation sites in glycoproteins by collision-induced dissociation analysis in fast atom bombardment mass spectrometry: identification of the positions of carbohydrate-linked asparagine in recombinant alpha-amylase by treatment with peptide-N-glycosidase F in 18O-labeled water. Anal Biochem, 205:151-158.

Gunn BM, Lu R, Slein MD, Ilinykh PA, Huang K, Atyeo C, Schendel SL, Kim J, Cain C, Roy V, et al. 2021. A Fc engineering approach to define functional humoral correlates of immunity against Ebola virus. Immunity, 54:815-828 e815.

Hayes JM, Frostell A, Karlsson R, Muller S, Martin SM, Pauers M, Reuss F, Cosgrave EF, Anneren C, Davey GP, et al. 2017. Identification of Fc Gamma Receptor Glycoforms That Produce Differential Binding Kinetics for Rituximab. Mol Cell Proteomics, 16:1770-1788.

Herter S, Herting F, Mundigl O, Waldhauer I, Weinzierl T, Fauti T, Muth G, Ziegler-Landesberger D, Van Puijenbroek E, Lang S, et al. 2013. Preclinical activity of the type II CD20 antibody GA101 (obinutuzumab) compared with rituximab and ofatumumab in vitro and in xenograft models. Mol Cancer Ther, 12:2031-2042.

Ho SN, Hunt HD, Horton RM, Pullen JK, Pease LR. 1989. Site-directed mutagenesis by overlap extension using the polymerase chain reaction. Gene, 77:51-59.

Liu R, Oldham RJ, Teal E, Beers SA, Cragg MS. 2020. Fc-Engineering for Modulated Effector Functions-Improving Antibodies for Cancer Treatment. Antibodies (Basel), 9.

Mossner E, Brunker P, Moser S, Puntener U, Schmidt C, Herter S, Grau R, Gerdes C, Nopora A, van Puijenbroek E, et al. 2010. Increasing the efficacy of CD20 antibody therapy through the

engineering of a new type II anti-CD20 antibody with enhanced direct and immune effector cell-mediated B-cell cytotoxicity. Blood, 115:4393-4402.

Musolino A, Naldi N, Bortesi B, Pezzuolo D, Capelletti M, Missale G, Laccabue D, Zerbini A, Camisa R, Bisagni G, et al. 2008. Immunoglobulin G fragment C receptor polymorphisms and clinical efficacy of trastuzumab-based therapy in patients with HER-2/neu-positive metastatic breast cancer. J Clin Oncol, 26:1789-1796.

Niederfellner G, Lammens A, Mundigl O, Georges GJ, Schaefer W, Schwaiger M, Franke A, Wiechmann K, Jenewein S, Slootstra JW, et al. 2011. Epitope characterization and crystal structure of GA101 provide insights into the molecular basis for type I/II distinction of CD20 antibodies. Blood, 118:358-367.

Patel KR, Nott JD, Barb AW. 2019. Primary Human Natural Killer Cells Retain Proinflammatory IgG1 at the Cell Surface and Express CD16a Glycoforms with Donor-dependent Variability. Mol Cell Proteomics, 18:2178-2190.

Patel KR, Roberts JT, Barb AW. 2020. Allotype-specific processing of the CD16a N45-glycan from primary human natural killer cells and monocytes. Glycobiology, 30:427-432.

Patel KR, Roberts JT, Subedi GP, Barb AW. 2018. Restricted processing of CD16a/Fc gamma receptor IIIa N-glycans from primary human NK cells impacts structure and function. J Biol Chem, 293:3477-3489.

Patel KR, Rodriguez Benavente MC, Lorenz WW, Mace EM, Barb AW. 2021. Fc gamma receptor IIIa/CD16a processing correlates with the expression of glycan-related genes in human natural killer cells. J Biol Chem, 296:100183.

Plummer TH, Jr., Elder JH, Alexander S, Phelan AW, Tarentino AL. 1984. Demonstration of peptide:N-glycosidase F activity in endo-beta-N-acetylglucosaminidase F preparations. J Biol Chem, 259:10700-10704.

Pott C, Sehn LH, Belada D, Gribben J, Hoster E, Kahl B, Kehden B, Nicolas-Virelizier E, Spielewoy N, Fingerle-Rowson G, et al. 2020. MRD response in relapsed/refractory FL after obinutuzumab plus bendamustine or bendamustine alone in the GADOLIN trial. Leukemia, 34:522-532.

Reeves PJ, Callewaert N, Contreras R, Khorana HG. 2002. Structure and function in rhodopsin: high-level expression of rhodopsin with restricted and homogeneous N-glycosylation by a tetracycline-inducible N-acetylglucosaminyltransferase I-negative HEK293S stable mammalian cell line. Proc Natl Acad Sci U S A, 99:13419-13424.

Riley NM, Bertozzi CR, Pitteri SJ. 2020. A Pragmatic Guide to Enrichment Strategies for Mass Spectrometry-Based Glycoproteomics. Mol Cell Proteomics, 20:100029.

Roberts JT, Patel KR, Barb AW. 2020. Site-specific N-glycan Analysis of Antibody-binding Fc gamma Receptors from Primary Human Monocytes. Mol Cell Proteomics, 19:362-374.

Rogals MJ, Yang JY, Williams RV, Moremen KW, Amster IJ, Prestegard JH. 2021. Sparse isotope labeling for nuclear magnetic resonance (NMR) of glycoproteins using 13C-glucose. Glycobiology, 31:425-435.

Salles G, Morschhauser F, Lamy T, Milpied N, Thieblemont C, Tilly H, Bieska G, Asikanius E, Carlile D, Birkett J, et al. 2012. Phase 1 study results of the type II glycoengineered humanized anti-CD20 monoclonal antibody obinutuzumab (GA101) in B-cell lymphoma patients. Blood, 119:5126-5132.

Shajahan A, Heiss C, Ishihara M, Azadi P. 2017. Glycomic and glycoproteomic analysis of glycoproteins-a tutorial. Anal Bioanal Chem, 409:4483-4505.

Shibata-Koyama M, Iida S, Okazaki A, Mori K, Kitajima-Miyama K, Saitou S, Kakita S, Kanda Y, Shitara K, Kato K, et al. 2009. The N-linked oligosaccharide at Fc gamma RIIIa Asn-45: an inhibitory element for high Fc gamma RIIIa binding affinity to IgG glycoforms lacking core fucosylation. Glycobiology, 19:126-134.

Shrimal S, Trueman SF, Gilmore R. 2013. Extreme C-terminal sites are posttranslocationally glycosylated by the STT3B isoform of the OST. J Cell Biol, 201:81-95.

Subedi GP, Barb AW. 2015. The Structural Role of Antibody N-Glycosylation in Receptor Interactions. Structure, 23:1573-1583.

Subedi GP, Barb AW. 2018. CD16a with oligomannose-type N-glycans is the only "low-affinity" Fc gamma receptor that binds the IgG crystallizable fragment with high affinity in vitro. J Biol Chem, 293:16842-16850.

Subedi GP, Falconer DJ, Barb AW. 2017. Carbohydrate-Polypeptide Contacts in the Antibody Receptor CD16A Identified through Solution NMR Spectroscopy. Biochemistry, 56:3174-3177.

Subedi GP, Hanson QM, Barb AW. 2014. Restricted motion of the conserved immunoglobulin G1 N-glycan is essential for efficient FcgammaRIIIa binding. Structure, 22:1478-1488.

Washburn N, Meccariello R, Duffner J, Getchell K, Holte K, Prod'homme T, Srinivasan K, Prenovitz R, Lansing J, Capila I, et al. 2019. Characterization of Endogenous Human FcgammaRIII by Mass Spectrometry Reveals Site, Allele and Sequence Specific Glycosylation. Mol Cell Proteomics, 18:534-545.

Weng WK, Levy R. 2003. Two immunoglobulin G fragment C receptor polymorphisms independently predict response to rituximab in patients with follicular lymphoma. J Clin Oncol, 21:3940-3947.

Wojcik I, Senard T, de Graaf EL, Janssen GMC, de Ru AH, Mohammed Y, van Veelen PA, Vidarsson G, Wuhrer M, Falck D. 2020. Site-Specific Glycosylation Mapping of Fc Gamma Receptor IIIb from Neutrophils of Individual Healthy Donors. Anal Chem, 92:13172-13181.

Wu J, Mishra HK, Walcheck B. 2019. Role of ADAM17 as a regulatory checkpoint of CD16A in NK cells and as a potential target for cancer immunotherapy. J Leukoc Biol, 105:1297-1303.

Zeck A, Pohlentz G, Schlothauer T, Peter-Katalinic J, Regula JT. 2011. Cell type-specific and site directed N-glycosylation pattern of FcgammaRIIIa. J Proteome Res, 10:3031-3039.

Zhang W, Gordon M, Schultheis AM, Yang DY, Nagashima F, Azuma M, Chang HM, Borucka E, Lurje G, Sherrod AE, et al. 2007. FCGR2A and FCGR3A polymorphisms associated with clinical outcome of epidermal growth factor receptor expressing metastatic colorectal cancer patients treated with single-agent cetuximab. J Clin Oncol, 25:3712-3718.

Zhao Y, Li Y, Wu X, Li L, Liu J, Wang Y, Liu Y, Li Q, Wang Z. 2020. Identification of anti-CD16a single domain antibodies and their application in bispecific antibodies. Cancer Biol Ther, 21:72-80.

Zhu H, Blum RH, Bjordahl R, Gaidarova S, Rogers P, Lee TT, Abujarour R, Bonello GB, Wu J, Tsai PF, et al. 2020. Pluripotent stem cell-derived NK cells with high-affinity noncleavable CD16a mediate improved antitumor activity. Blood, 135:399-410.

Table A.1. N-glycosylation site occupancy of three CD16a variants (n.o.= not observed, n.a. = not applicable, *- presence of more than two species)

variant (to the right)		V158		F158	V158/T171A
peptide (below)	site	^{16}O (%)	^{18}O (%)	^{16}O (%)	^{16}O (%)
DNSTQWF	N38	91 ± 33	n.o.	84 ± 6	n.o.
DNSTQW	N38	n.o.	n.o.	n.o.	94 ± 11
NSTQWF	N38	n.o.	99 ± 13	n.o.	n.o.
STQWFHNE	N45	93.6 ± 0.9	>95*	93.6 ± 0.9	92.9 ± 0.9
HNESL	N45	n.o.	93 ± 4	n.o.	n.o.
GLVGSKNVSSE	N162	99.8 ± 0.9	n.o.	n.o.	n.o.
VGSKNVSSE	N162	n.o.	n.o.	n.o.	100 ± 1
CRGLVGSKNVSSE	N162	97 ± 13	100*	n.o.	n.o.
FGSKNVSSE	N162	n.o.	n.o.	99 ± 4	n.o.
TVNITITQG	N169	99.5 ± 0.8	99*	99.4 ± 0.9	n.a.
TVNIAITQG	N169	n.a.	n.a.	n.a.	0 ± 0.2

Table A.2. Mass accuracy of intact CD16a measurements using FT-ICR MS

Species	Observed $[M+H]^+$ (Da)	Observed neutral mass (Da)	Calculated mass (Da)	mass error (ppm)
CD16a w/ 5xMan5	26127.0390	26126.0317	26126.0271	0.176
CD16a w/ 4xMan5	24910.6084	24909.6011	24909.6043	0.128
CD16a w/ 5xGlcNAc	21060.3039	21059.2967	21059.3097	0.618
CD16a w/ 4xGlcNAc	20857.2508	20856.2435	20856.2303	0.632
GFP form1	28032.9850	28031.9772	28032.0056	1.013
GFP form2	28736.3098	28735.3020	28735.3233	0.741

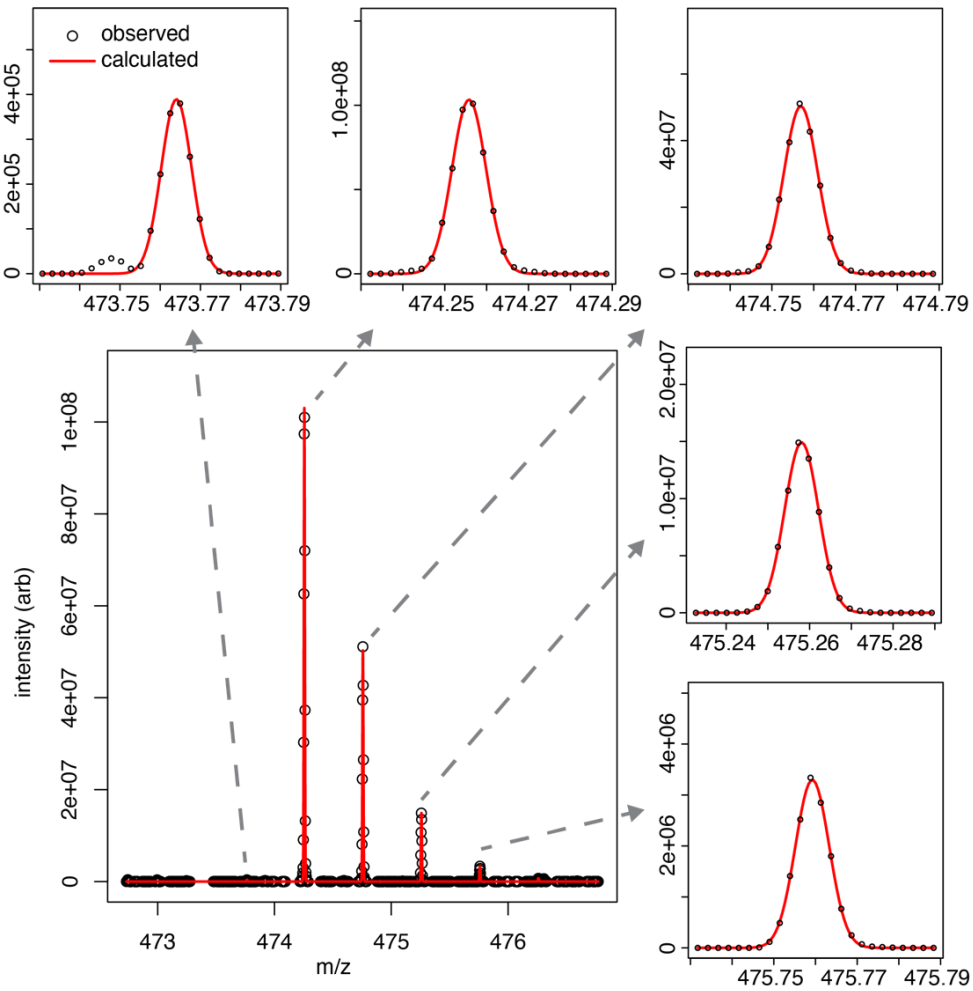

Figure A.1. A Gaussian line shape fitted to the individual isotopologue peaks to determine N-glycan occupancy. This MS1 spectrum shows the N169-containing peptide from the CD16a V158 allotype, following PNGaseF-catalyzed N-glycan removal. The peak at the left of the spectrum contains only an unglycosylated Asn at position 169. The second peak contains contributions for both Asn and Asp (formed by PNGaseF digestion of an N-glycosylated peptide) at this position, with the Asp-containing peptide predominant in this example.

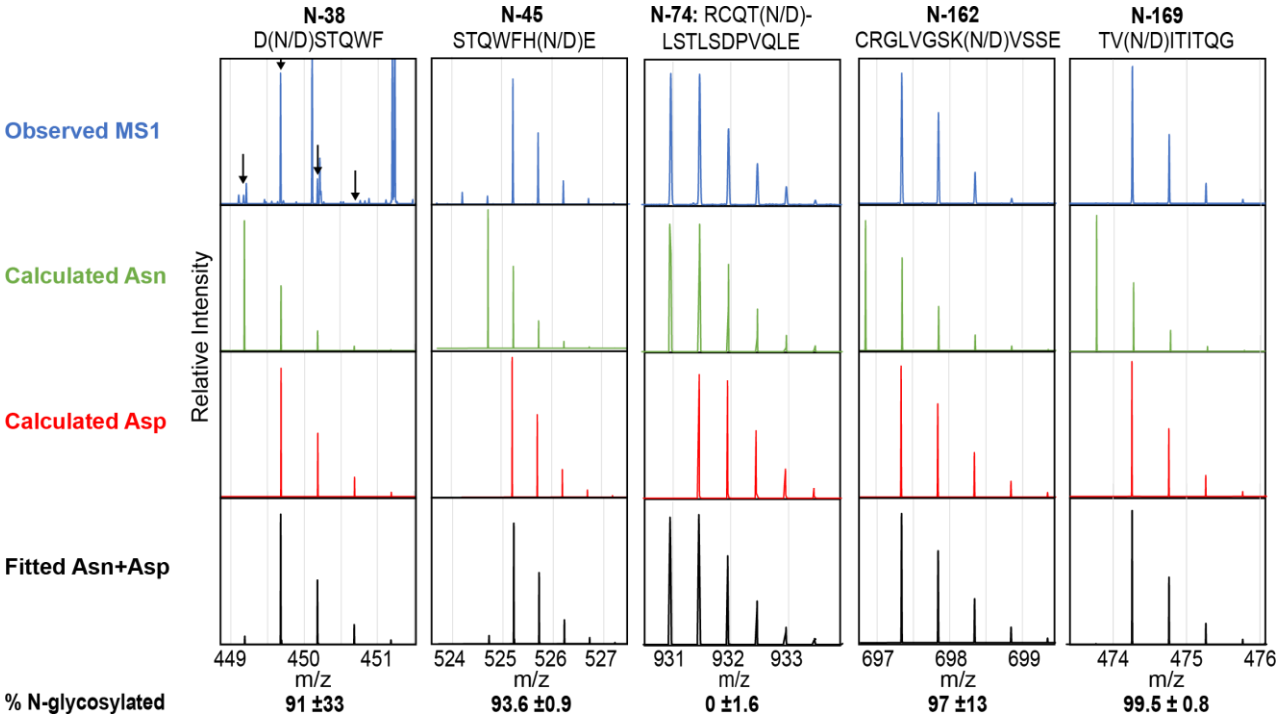

Figure A.2. N-glycosylation of CD16a V158 determined by treating with PNGaseF in [^{16}O]-water. Recorded spectra corresponding to each peptide are shown in the top row. The calculated isotope distributions for Asn- and Asp-containing peptides are shown in the second and third rows, respectively. The final row shows the fitted Asn + Asp data to determine the percentage of peptides that showed N-glycosylation.

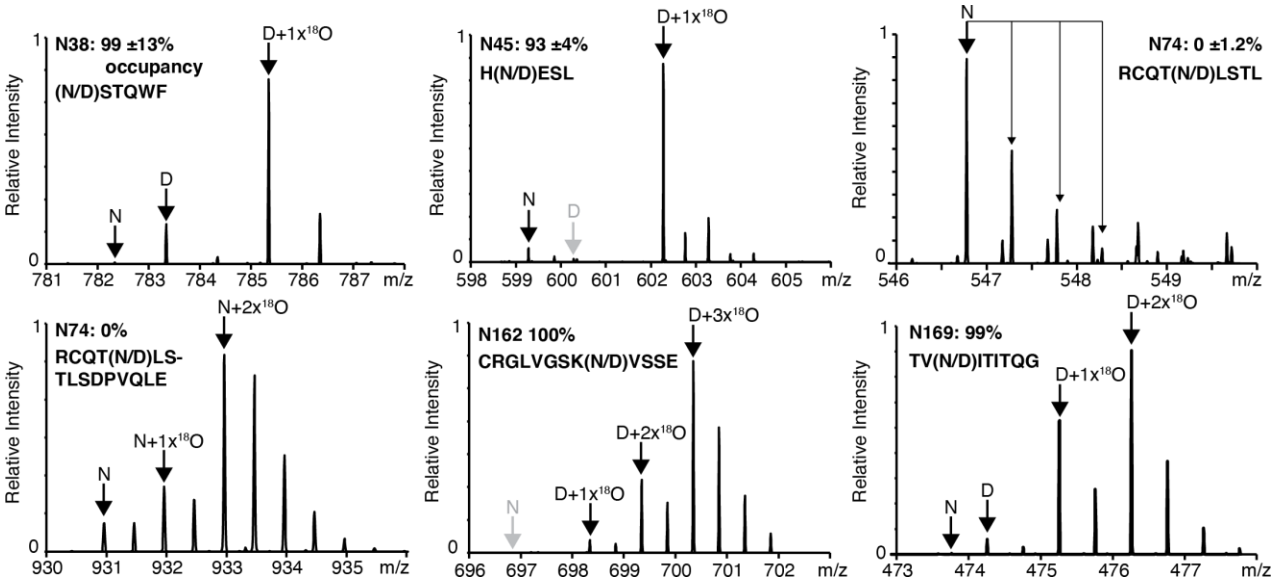

Figure A.3. N-glycosylation of CD16a V158 determined by treating with PNGaseF in [^{18}O]-water. Monoisotopic peaks for major species contributing to the observed spectra are indicated with large black arrows. Small black arrows denote members of the peak multiplet, where appropriate. N-glycan occupancy at each site as estimated from these spectra is indicated in the upper left of each panel. Apparent N74-glycan occupancy is reduced by peptide cleavage following N-glycan hydrolysis.

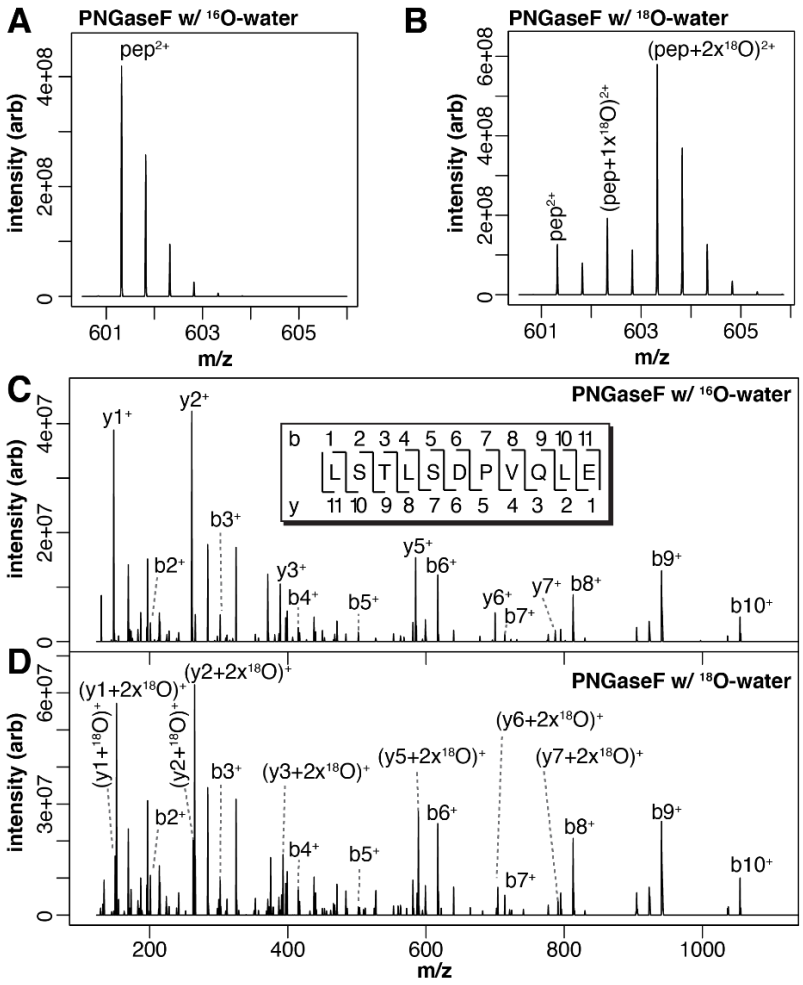

Figure A.4. The L75 peptide is only expected to result from GluC-digestion following PNGaseF-digestion of a glycosylated N74-containing peptide. MS1 spectra of the L75 peptide identified in spectra collected using CD16a V158 following PNGaseF digestion in either ^{16}O (**A**) or ^{18}O (**B**) water. The positions of monoisotopic peaks for each species are indicated. (C & D) MS2 spectra of the major species from panels **A** and **B**, respectively, indicate the ion composition as well as demonstrate ^{18}O incorporation in the C-terminal Glu residue.

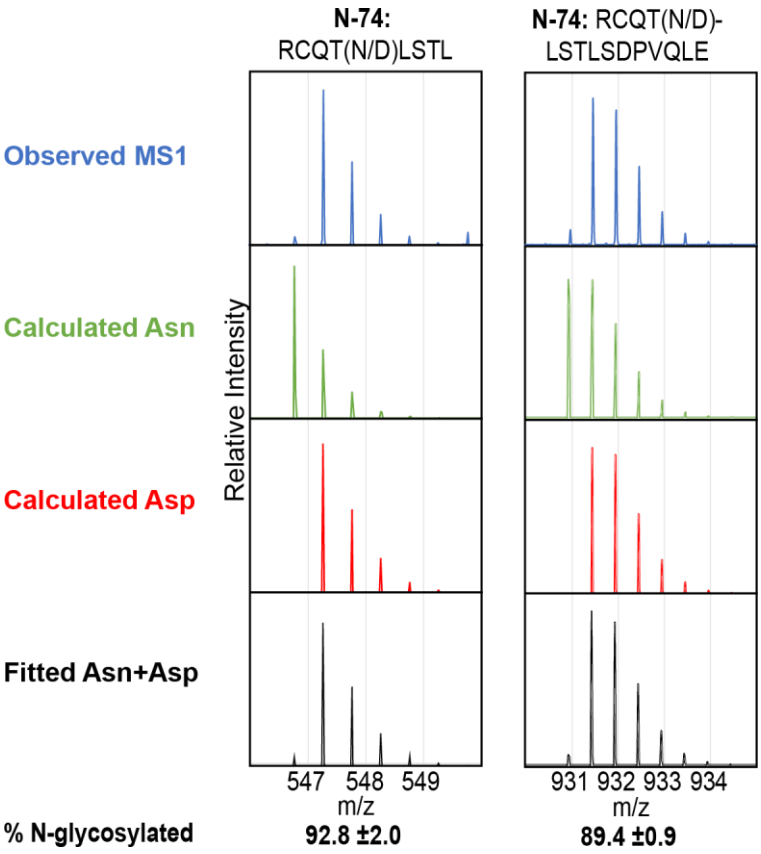

Figure A.5. N-glycan occupancy for the N74 site of CD16a V158 as observed with two peptides in [^{16}O]-water. Recorded spectra corresponding to each peptide are shown in the top row. The calculated isotope distributions for Asn- and Asp-containing peptides are shown in the second and third rows, respectively. The final row shows the fitted Asn + Asp data to determine the percentage of peptides that showed N-glycosylation.

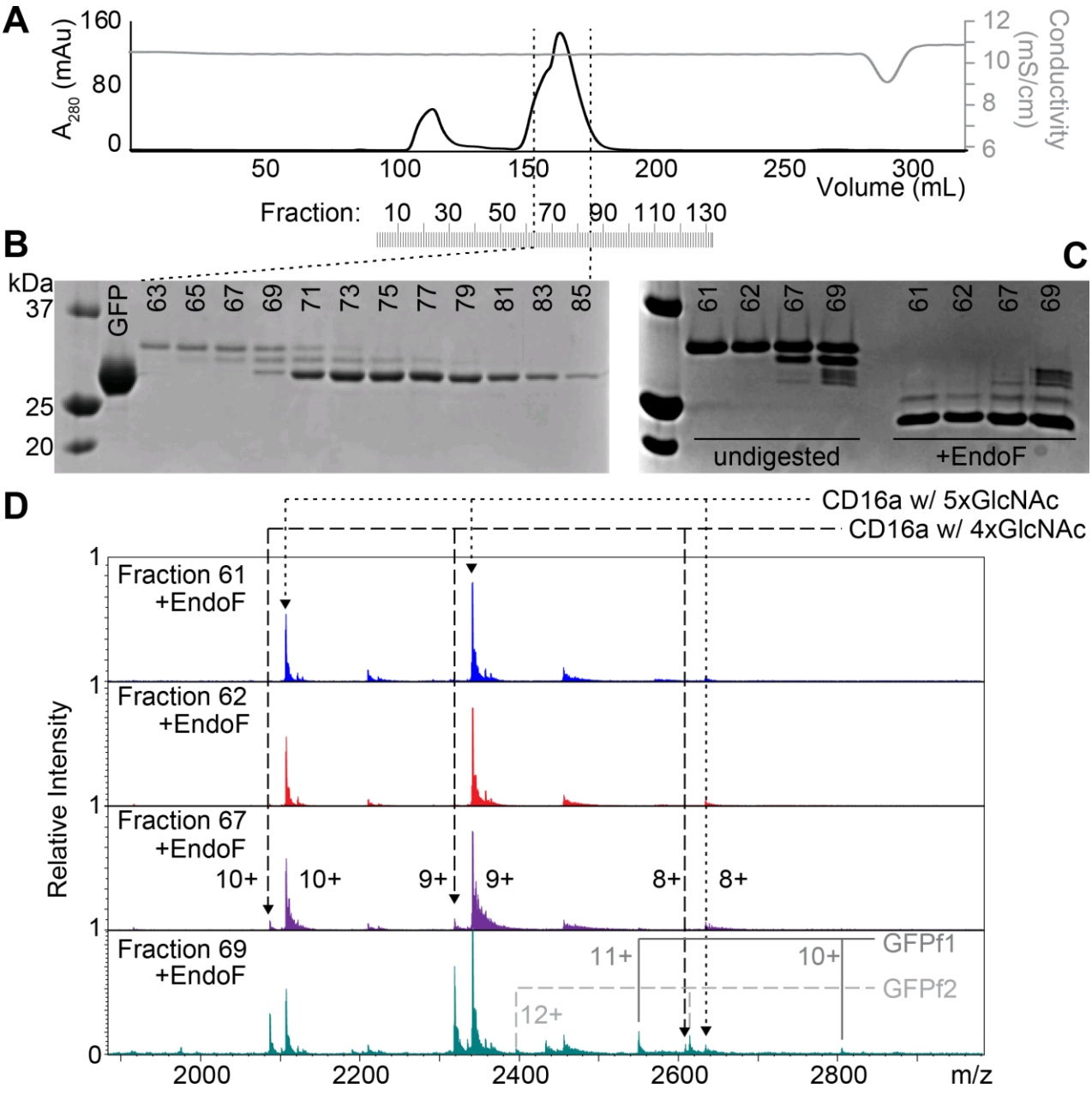

Figure A.6. Analysis of intact CD16a V158. **A.** Gel filtration of CD16a using a Superdex 75 gel filtration column following TEV digestion. **B.** SDS-PAGE analysis of the central peak. **C.** SDS-PAGE analysis of select CD16a fractions before and after treatment with EndoF. **D.** FT-ICR MS analysis of EndoF-treated CD16a fractions. The observed masses are reported in Table 2. GFP

form 1 includes residues KIEW through the TEV cleavage site, and GFP form 2 starts with DIFEA and ends with the TEV cleavage site.

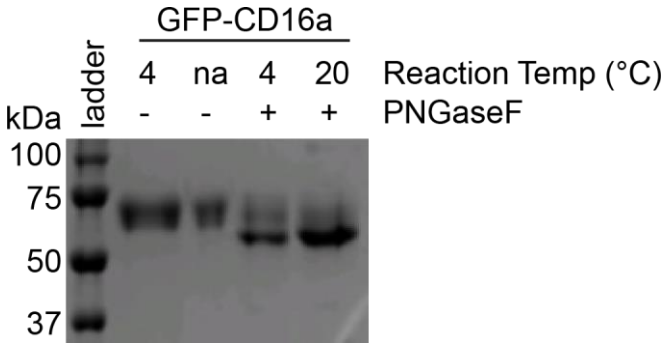

Figure SA.1. PNGaseF retains activity at 4 ℃ and 20 ℃ following two rounds of resuspension and lyophilization.

Appendix B

DECODING HUMAN-MACAQUE INTERSPECIES DIFFERENCES IN FC-EFFECTOR FUNCTIONS: THE STRUCTURAL BASIS FOR CD16-DEPENDENT EFFECTOR FUNCTION IN RHESUS MACAQUE[1]

[1]Tolbert, Willam D., Gohain, Neelakshi, Kremer, Paul G., Hederman, Andrew P., Nguyen, Dung N., Van, Verna, Sherburn, Rebekah, Lewis, George K., Finzi, Andres, Pollara, Justin, Ackerman, Margaret E., Barb, Adam W., & Pazgier, Marzena. 2022. Frontiers in immunology, 13, 960411.

Abstract

Fc mediated effector functions of antibodies play important roles in immunotherapies and vaccine efficacy but assessing those functions in animal models can be challenging due to species differences. Rhesus macaques, Macaca mulatta (Mm) share approximately 93% sequence identity with humans but display important differences in their adaptive immune system that complicates their use in validating therapeutics and vaccines that rely on Fc effector functions. In contrast to humans, macaques only have one low affinity FcγRIII receptor, CD16, which shares a polymorphism at position 158 with human FcγRIIIa with Ile^{158} and Val^{158} variants. Here we describe structure-function relationships of the Ile/Val^{158} polymorphism in Mm FcγRIII. Our data indicate that the affinity of the allelic variants of Mm FcγRIII for the macaque IgG subclasses vary greatly with changes in glycan composition both on the Fc and the receptor. However, unlike the human Phe/Val^{158} polymorphism in FcγRIIIa, the higher affinity variant corresponds to the larger, more hydrophobic side chain, Ile, even though it is not directly involved in the binding interface. Instead, this side chain appears to modulate glycan-glycan interactions at the Fc/FcγRIII interface. Furthermore, changes in glycan composition on the receptor have a greater effect for the Val^{158} variant such that with oligomannose type glycans and with glycans only on Asn45 and Asn162, Val^{158} becomes the variant with higher affinity to Fc. These results have implications not only for the better interpretation of nonhuman primate studies but also for studies performed with human effector cells carrying different FcγRIIIa alleles.

Results

The N-glycosylation of the Val158 and Ile158 proteins proved highly comparable, with no remarkable differences apparent from the MS data. The majority (>83%) of the N-glycan species observed at each site of both Mm FcγRIII allotypes were complex-type (Figure B.1A). Notably, the Asn45 site contained ~10% of hybrid N-glycoforms, which is much lower than a similar recombinant HEK293-expressed human FcγRIIIa that contained >50% of hybrid types (40). The predominant Asn45 glycoforms were not extensively branched and relatively few were modified with a terminal sialic acid (Figure B.1B). Asn64 likewise contained many complex-type glycoforms and was the most processed among the three glycosylation sites examined, with a complex-type, biantennary di-sialylated glycans among the top forms present. The Asn162 glycoforms were highly comparable to the Asn45 forms, although they included a smaller percentage of hybrid forms (5-6%). Surprisingly, we observed truncated Asn64 (5-15%) and Asn162 (3%) glycopeptides. The predominant truncated form only contained a single HexNAc residue. These truncated species are not normally observed for N-glycans, and could be representative of an O-linked residue. Closer examination of the Asn64 and Asn162 MS2 spectra showed the clear presence of a single HexNAc residue attached to Asn64 or Asn162, eliminating a Ser or Thr-linked O-glycan as a possible explanation. Thus, these glycans potentially resulted from truncation during protein expression or purification.

The Mm FcγRIII(Val158) variant shows greater glycan mobility than the Mm FcγRIII(Ile158) as determined by NMR.

Next, we analyzed the mobility of glycans attached to the Mm FcγRIII(Val158) and Mm FcγRIII(Ile158) variants using solution NMR spectroscopy to identify possible differences in conformational heterogeneity (41-44). Uniform amino acid labeling through adding biosynthetic precursors like ammonium chloride for the NMR analysis of glycoproteins, including Mm FcγRIII, is not feasible, but individual [15N]-amino acids are readily incorporated from the complex culture medium. We expressed Mm FcγRIII variants as used in structural studies (with Asn45, Asn64, and Asn162 glycosylation sites) in medium supplemented with [15N]-glycine and [15N]-lysine. Glycine readily converts to serine and lysine does not convert to other amino acids in this system (data not shown).

The 1H-15N HSQC-TROSY spectrum of Mm FcγRIII(Val158) was well dispersed and showed 31 strong peaks and ~10 weaker peaks for the 44 expected Gly, Ser and Lys residues (Figure B.2A). This pattern is consistent with a folded protein that contains a mix of α-helices, β-sheets and loop regions. The differences in peak intensities within this spectrum indicate that it is likely that these residues experience different motion regimes. A spectrum of the Mm FcγRIII(Ile158) allotype showed a highly comparable pattern of peaks, though some of the weaker peaks did not appear in this spectrum due to a lower sample concentration (240 μM v. 180 μM; Figure B.2A). Although Val158 and Ile158 proteins only differ by a single methyl group, there are substantial differences in multiple peak positions that are visible in an overlay of the spectra. There are 9 backbone Lys/Gly/Ser NH moieties within 10 Å of Val158 and Ile158 including Gly159-Ser160-Lys161 that may account for the three largest deviations (noted with arrows in Figure B.2A). Unlike amino acids, it is possible to uniformly incorporate [13C] labels into the glycoprotein carbohydrates by adding [13C]-glucose to the expression medium (45, 46). The most notable

spectral feature visible with this strategy is the correlation between the 1H1-13C1 nuclei of the GlcNAc residue that is bonded (through C1) to the Asn sidechain with one peak expected for each N-glycan in an HSQC spectrum. Observation of these correlations using human FcγRIII identified the presence of contacts that stabilized the Asn45 and Asn162 glycans, but not the three remaining N-glycans (47). It is notable that it is the Asn45 and Asn162 glycans that can impact antibody binding affinity (34, 48).

Mm FcγRIII contains three N-glycosylation sites at Asn45, Asn64 and Asn162. A 13C-HSQC spectrum reveals three distinct peaks that can be assigned by comparison to a highly comparable spectrum of human FcγRIIIa (47) (Figure B.2B). The peak corresponding to the Asn64 glycan is sharp and intense. The peak position and line shape indicates this N-glycan experiences the least restriction due to contacts with the polypeptide backbone, based on characterizations of human FcγRIIIa and other glycoproteins (43, 47, 49, 50). This behavior is likewise consistent with the MS data showing Asn64 as the most highly modified site, including the higher-than-expected abundance of truncated forms which likely requires the glycan to be readily accessible to a glycan hydrolyzing enzyme. The displaced position and broad shape of the Asn45 peak likely results from intimate contacts formed between the N-glycan and amino acids. Furthermore, this peak position is consistent with the higher level of hybrid and oligomannose N-glycoforms present in the MS data compared to Asn64 and Asn162. It is notable that the Asn45 peak is considerably broader in spectra collected using the Ile158 protein (Figure B.2B).

Intriguingly, the Asn162 peak from an Mm FcγRIII(Ile158) spectrum is displaced further from the Asn64 peak when compared to Mm FcγRIII(Val158). This result indicates that the attachment point of the Asn162 glycan experiences slightly different chemical environments in

each protein. It is not clear if these differences result from the magnetic influence of the extra methyl in Ile158 or from differences in protein mobility, though the former explanation is considered less likely due to the ~11 Å distance separating the Ile158 methyl and the glycan bond to Asn162. These differences were minimized but still present once the glycans were replaced with a minimally-remodeled form (Figure A.2C). Proteins expressed from the HEK293S (GnT1-) cell line contain predominantly Man5 oligomannose-type N-glycans and nearly homogeneous compositions (34, 51). Based on the differences in spectra collected using 15N and 13C-labeled samples, we believe it is likely that the Ile158 stabilizes the motion of the amino acid and carbohydrate residues proximal to the Asn162-glycan more than Val158, which could provide an explanation for its greater affinity to IgG.

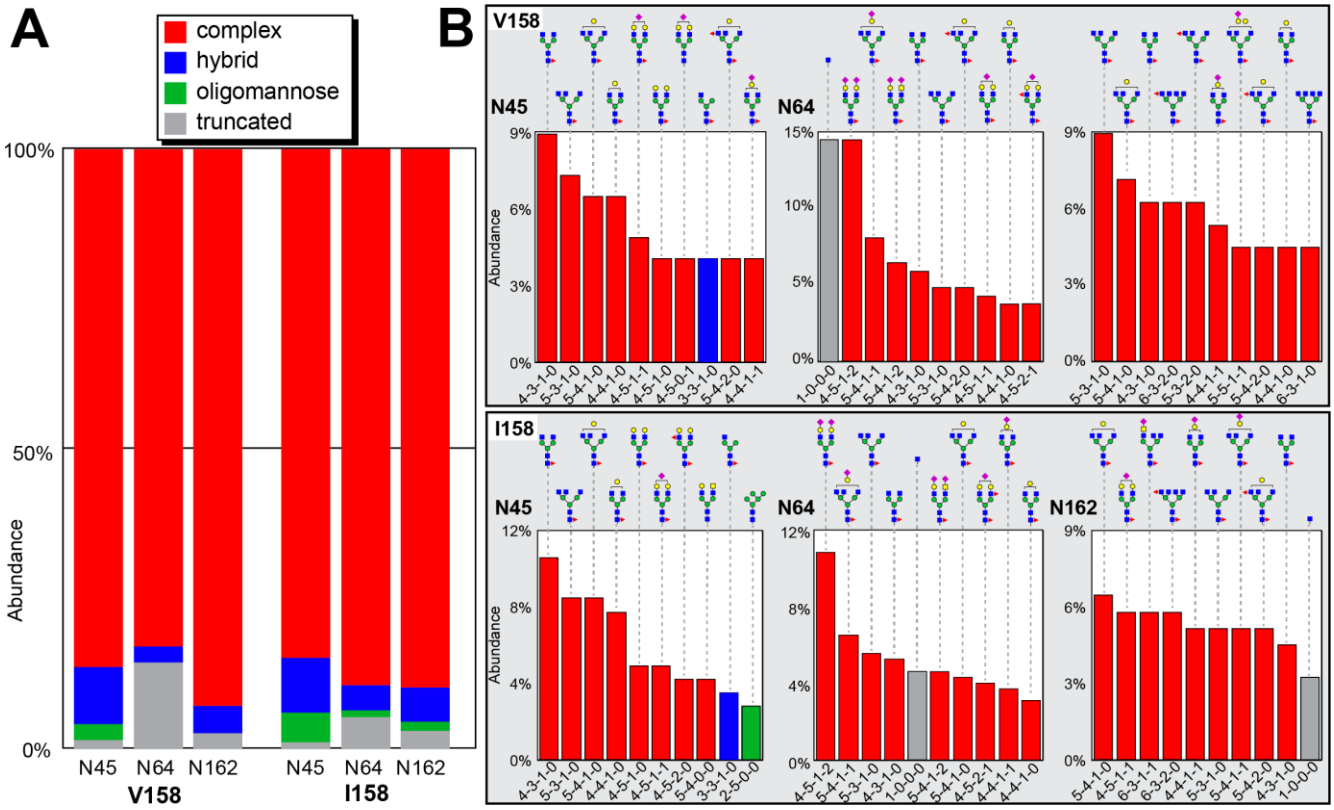

Figure B.1. Glycan composition of Mm FcγRIII Val[158] and Ile[158]. (**A**) Glycoforms identified at each site. (**B**) The top ten most abundant N-glycans at each site. Cartoon diagrams represent one possible configuration and utilize the SNFG convention for monosaccharides; isobaric ions were not distinguished. The composition of each N-glycan is provided below the chart with numbers of N-acetylhexosamine, hexose, deoxyhexose, and N-acetylneuraminic acid residues, respectively.

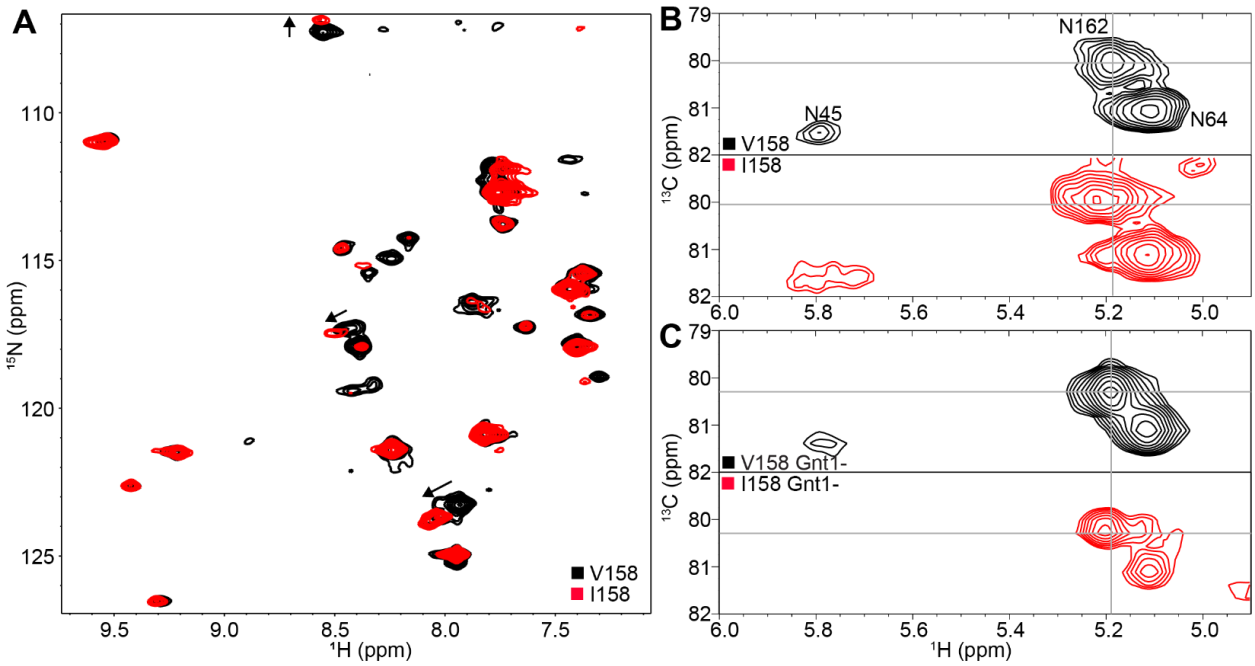

Figure B.2. Solution NMR spectroscopy revealed subtle differences between the MmFcgRIII Val^{158} and Ile^{158} proteins. (**A**) ^{1}H-^{15}N TROSY-HSQC with [^{15}N-Gly,Ser,Lys] labeling. (**B**) HSQC showing (1)GlcNAc $^{1}H_1$-$^{13}C_1$ correlations for Mm FcgRIIIa with heterogeneous complex-type N-glycans or (**C**) homogeneous Man5 oligomannose-type N-glycans.

Appendix C

INHIBITING N-GLYCAN PROCESSING INCREASES THE ANTIBODY BINDING AFFINITY AND EFFECTOR FUNCTION OF HUMAN NATURAL KILLER CELLS[1]

[1]Rodriguez Benavente, Maria C., Hughes, Harrison B., Kremer, Paul G., Subedi, Ganesh P., Barb, Adam W. (2023). Immunology, 170(2), 202–213.

Abstract

Antibody-dependent cell-mediated cytotoxicity (ADCC) is an immune response performed by natural killer (NK) cells that clears infected or cancerous tissue. Because the potency of human NK cell responses is highly variable across the population, increasing NK cell activity is expected to increase the efficacy of many treatments. Both cytokine treatment and NK cell receptor engineering are being explored to increase ADCC response. Here we demonstrate that manipulating NK cell post-translational modification is an alternative strategy to increase ADCC. Treating cultured YTS-CD16a cells or primary human NK cells with kifunensine, an inhibitor of asparagine-linked (N-)glycan processing, nearly doubled ADCC. This increase required CD16a as blocking CD16a eliminated ADCC. Furthermore, afucosylated antibodies acted synergistically with kifunensine-treated NK cells to further increase ADCC by an additional 33%. We also demonstrated that kifunensine treatment increased the antibody-binding affinity of CD16a on the NK cell surface. Lastly, we determined that inhibiting N-glycan processing perturbs a single region of the CD16a structure proximal to the N162 glycan, one of five CD16a N-glycans and the only N-glycan found near the antibody-binding surface. These results identify N-glycan processing as an important factor that limits NK cell ADCC.

Results

To confirm the 3G8 binding site on CD16a, we examined a panel of CD16a proteins containing mutations to residues forming the antibody-binding surface (Table S.C.1). The K161A mutant provided the largest affinity reduction (~200 fold), and the 3G8 binding site mapped to the area surrounding K161 (Figure C.1D). This CD16a region also binds IgG1 Fc, though the binding sites are not perfectly aligned (Figures C.1B and C). These analyses indicate 3G8 is minimally

sensitive to CD16a N-glycan composition and confirms that IgG1 Fc competes with 3G8 to bind a shared CD16a surface.

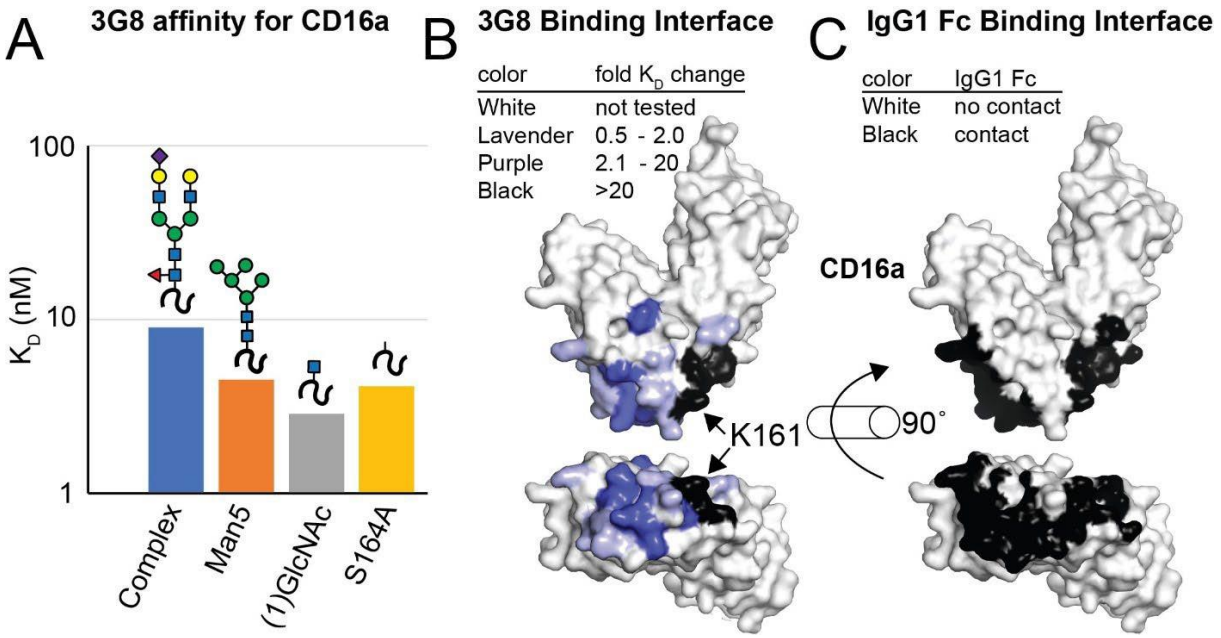

Figure C.1. Binding affinities of 3G8 binding various CD16a glycoforms and sequence variants. Cartoon diagrams of N-glycan structure follow the SNFG convention and illustrate expected composition of the N162 glycans (A). CD16a amino acid substitutions affected 3G8 binding affinity, and the effect of these mutations are mapped onto a structure of CD16a (B). The 3G8 interface overlaps with the IgG1 Fc binding interface identified with x-ray crystallography (C).

CD16a Variant	3G8 K_D (nM)	error	3G8 Fab K_D (nM)	error
V158-Complex-type	6.61	0.04	13.66	0.11
V158-Man5	3.21	0.03	4.56	0.06
V158-(1)GlcNAc	2.87	0.05	3.34	0.06
V158 mutation				
N162Q	3.31	0.03	6.00	0.06
S164A	4.13	0.03	4.56	0.05
S160A	3.67	0.00	4.52	0.03
H134A	4.51	0.02	4.38	0.03
I88A	4.77	0.02	5.07	0.06
K131A	5.26	0.04	4.62	0.03
T122A	12.3	0.1	11.4	0.1
T167Y	13.8	0.1	11.4	0.1
K120A	16.9	0.2	17.4	0.2
R155S	22.5	0.3	23.3	0.5
L157S	23.5	0.2	23.4	0.9
H119A	30.07	0.05	31.5	0.2
W113A	136	2	97	4
W90A	154	85	53	7
K161A	1234	14	1149	50

Supplemental Table C.1. 3G8 binding affinities measured by SPR. Errors represent errors of least-squares curve fitting.